3D FINITE ELEMENT ANALYSIS AND EXPERIMENTAL STUDY OF STABILITY OF SLOTTED LINERS

A Dissertation

by

XIAODA LIU

Submitted to the Office of Graduate and Professional Studies of
Texas A&M University
in partial fulfillment of the requirements for the degree of

DOCTOR OF PHILOSOPHY

Chair of Committee,	Nobuo Morita
Committee Members,	Theofanis Strouboulis
	Jihoon Kim
	Kan Wu
Head of Department,	Jeff Spath

August 2018

Major Subject: Petroleum Engineering

ABSTRACT

Slotted liners are widely used in horizontal wells because of the abilities to ensure wellbore integrity and sand control. During installation and operations, the slotted liners have to be strong enough to hold axial loads and radial compression to prevent excessive buckling and deformation of slots.

In this work, past papers about casing/liner failure are reviewed, and a comprehensive FEM analysis of various slotted liner failure mechanisms, including axial compression, bending, and collapse is studied. Experiments are carried out to compare with simulation.

Experiments were designed to select the grades of materials, diameter/thickness of pipes, and slot pattern. For the base pipe, the maximum strain is associated with more uniform deformation. In contrast, the maximum distortion of the slotted liner is concentrated around the slots. As a result, the depletion limit needs to be reduced to avoid casing/liner failure.

Finite element models were developed to decide the slotted liner design under various load conditions. A 3D nonlinear finite element method (FEM) model was developed for simulating stress changes related to rock mechanics and depletion in the formation, including overburden, reservoir section and underburden to evaluate the effect of stress change on casing stability. Various lithology and rock failure theories can be considered in the model.

The study showed considerations for slotted liner design and analyzed how much material grades, casing/tubing dimension and slot patterns can be expected to evaluate the risk of slotted liner failure. The numerical and experimental results in this work can help engineers understand mechanisms of slotted liner failure and optimize the slotted liner design. A series of

simulation steps can be followed to simulate deformation and failure mechanisms of many more complex downhole tools.

DEDICATION

This dissertation is gratefully dedicated to my parents, Zhuwang Liu and Xuezhi Yang, my sister, Xinqi Liu. Without their continuous support and love, my work would never have been completed.

ACKNOWLEDGEMENTS

I would like to express my greatest acknowledgements to my supervisor Dr. Nobuo Morita. He offered me great help and I will always remember him as the best mentor. Also thanks to his encouragement and patience which greatly impacted my life.

Thanks to Dr. Jihoon Kim, Dr. Kan Wu, Dr. Theofanis Strouboulis for providing valuable advice. Thanks also go to Geomechanics JIP research program provided by Petroleum Engineering Department at Texas A&M University, for providing the financial support for this study.

I would also like to express my thanks to Dr. Hiroko Kitajima, for her help in my experiments and enlightened me on research ideas.

I also appreciate my research group team members: Mohit Dholi, Naoto Araki, Takuma Kaneshima, Tan Tran and Kexin Cui for the valuable discussions and good time together during my PhD.

Thanks to Jinrong Yu for supporting me through ups and downs during my PhD.

CONTRIBUTORS AND FUNDING SOURCES

Great thanks to the financial support from Geomechanics JIP (Joint Industry Program).

This work was supported by a dissertation committee consisting of Professor Nobuo Morita from Petroleum Engineering Department, Dr. Jihoon Kim and Dr. Kan Wu from Petroleum Engineering Department., and Dr. Theofanis Strouboulis from Aerospace Engineering Department. All work for the dissertation was completed independently by the student.

The results in Chapter 2 and 3 were published in 2018 (Liu and Liu) in articles listed in reference.

NOMENCLATURE

OD	casing outer diameter
ID	casing inner diameter
T	wall thickness
L	length
E	Young's modulus
E_t	tangential Young's modulus
E_s	secant Young's modulus
F	force
ν	Poisson's ratio
A	area
σ	stress
ε	strain
$\sigma_c^{nominal}$	nominal (engineering) stress
$\varepsilon_c^{nominal}$	nominal compressive strain
$\nu^{nominal}$	nominal Posson's ratio and
σ_c	true compressive stress
ε_c	true compressive strain, and
ε_c^P	true compressive plastic strain. The compressive stress and strain are negative values.
σ_{cr}^e	critical stress based on elastic limit

σ_{cr}^{def}	critical stress based on plastic deformation
σ_{cr}^{inc}	critical stress based on incremental plastic theory
p_{out}	external pressure on casing/liner
p_{in}	internal pressure on casing
p_c	confining pressure (psi)
L80L	L80 grade steel with thin wall (light)
L80H	L80 grade steel with thick wall (heavy)
N8L2	slotted liner with 8 slots/ft and slot length of 2 inches
N16L1	slotted liner with 16 slots/ft and slot length of 1 inch

TABLE OF CONTENTS

Page

ABSTRACT ii

DEDICATION iv

ACKNOWLEDGEMENTS v

CONTRIBUTORS AND FUNDING SOURCES vi

NOMENCLATURE vii

TABLE OF CONTENTS ix

LIST OF FIGURES xi

LIST OF TABLES xv

1. INTRODUCTION 1

1.1 Background 1
1.2 Literature Review 8
1.3 Objectives 15

2. METHOD 16

2.1 FEM Simulation 20
2.1.1 Model Description 20
2.1.2 Model Validation 22
2.1.3 Axial Compression Simulation 25
2.1.4 Line Load Collapse Test Simulation 31
2.2 Experiments 37
2.2.1 Compression Test 37
2.2.2 Line Load Collapse Test 50
2.2.3 Triaxial Collapse Test 61

3. RESULTS 67

3.1 Axial Compression Test 67
3.2 Line Load Collapse Test 81

4. CONCLUSIONS 83

REFERENCES 85

LIST OF FIGURES

Page

Figure 1 3D normal and shear stresses 2

Figure 2 Displacement and deformation of a square structure, ... 3

Figure 3 Sand control mechanism of slotted liners..... 7

Figure 4 Whole joint of slotted liners 7

Figure 5 Three different slot patterns. A:Single staggered pattern. B: Straight pattern. C: Gang pattern (multiple staggered). 10

Figure 6 Typical Slotted Liner..... 12

Figure 7 Structure of Borehole and Slotted Liner..... 12

Figure 8 Load Force vs. Radial Displacement (Placido, Pasqualino, and Fonseca 2005)..... 13

Figure 9 Critical strain in compression test 14

Figure 10 3D 20-node quadratic isoparametric element..... 17

Figure 11 Basic slotted liner design: N=8/ft (0.3048 m), L=2" (50.8 mm) on left, N=16/ft (0.3048 m), L=1" (25.4 mm) on right 22

Figure 12 Base pipe for 2 7/8" thin wall L80L 24

Figure 13 Model Validation for 2 7/8" thin wall L80..... 25

Figure 14 3D slotted liner mesh..... 26

Figure 15 3D model for slotted liners in experiments, deformed slotted liner on right 26

Figure 16 simulation with axial tension and radial compression..... 27

Figure 17 Simulation of slotted liner with single slot..... 28

Figure 18 Simulation of slotted liner with 8 slots..... 28

Figure 19 Maximum stress concentrated at the slot ends 29

Figure 20 2 7/8" heavy L80 with N16L1 pattern, top left: 3D mesh, top right: Von Mises stress simulation, lower left: horizontal displacement simulation, lower right: experiment sample..... 30

Figure 21 Load and Boundary Conditions for Line Load Collapse Simulation 31
Figure 22 View from z direction for line load collapse simulation 32
Figure 23 Displacement on x direction 33
Figure 24 Displacement on y direction 33
Figure 25 Displacement on z direction 34
Figure 26 Magnitude of displacement 34
Figure 27 Comparison of slotted liner before and after line load test 35
Figure 28 Plastic strain after deformation 36
Figure 29 Strength reduction due to slots (George E. King 2009) 37
Figure 30 Plastic and elastic behavior under different D/t 39
Figure 31 Experiment set up and sample under axial compression 40
Figure 32 Axial Compression Test for Slort (1 ft) Samples, N8L2 on left, N16L1 on right 41
Figure 33 Axial Compression Test for Long (2ft) Base Pipes 42
Figure 34 Axial compression test for long (2ft) slotted liners 43
Figure 35 Pipe deformation when the load increases 45
Figure 36 2 3/8" P110 under compression at yield point, peak strength, 10% axial strain 46
Figure 37 2 7/8” J55 under compression at yield point, peak strength, 10% axial strain 47
Figure 38 2 7/8" J55 N8L2 slotted liners under compression at yield point, peak strength, 10% axial strain 47
Figure 39 2 7/8” J55 N16L1 slotted liners under compression at yield point, peak strength, 10% axial strain 48
Figure 40 2 7/8" light L80 at yield point, peak strength, 10% axial strain 49
Figure 41 2 7/8" heavy L80 at yield point, peak strength, 10% axial strain 49
Figure 42 3 1/2" L80 at yield point, peak strength, 10% axial strain 50
Figure 43 Sketch for line load test 51

Figure 44 Samples used for line load test 51

Figure 45 Experimental setup for line load test 52

Figure 46 2 7/8" J55 samples after line load test 54

Figure 47 2 7/8" thin wall L80 samples after line load test 55

Figure 48 2 7/8" L80 thick wall samples after line load test 56

Figure 49 Slot opening on the side of the load comparing with original slot 57

Figure 50 Slot closing under the load on the loading direction comparing with original slot 58

Figure 51 Experiment: slot deformation after line load collapse test. Load direction on the left, horizontal cross-section on the right. 59

Figure 52 Slot deformation after line load collapse test 60

Figure 53 Deformation on load direction: experiment vs. simulation 60

Figure 54 GCTS RTX - 1500 Triaxial Load Frame 62

Figure 55 Control Panel for GCTS Triaxial Load Frame 63

Figure 56 Triaxial Collapse Equipment and Sample Setup 64

Figure 57 Sample for Triaxial Collapse Test 65

Figure 58 Steel grade effect on base pipes 69

Figure 59 Steel grade effect for N8L2 slotted liners 70

Figure 60 Grade effect for N16L1 slotted liners 71

Figure 61 Slot pattern effect on 2 3/8” N80 slotted liners 73

Figure 62 Slot pattern effect on 2 3/8” P110 slotted liners 74

Figure 63 Slot pattern effect on 2 7/8" J55 slotted liners 75

Figure 64 Slot pattern effect on 2 7/8” L80 (both light and heavy) slotted liners 76

Figure 65 Slot pattern effect on 3 1/2” L80 slotted liners 77

Figure 66 Comparison of slot opening. Left: original slot. Center: Simulation- at 5% axial strain, Deformed Slot under Axial Compression, Right: Experiment- at 5% axial strain 79

Figure 67 Results of Line Load Collapse Test.. 81

LIST OF TABLES

Page

Table 1 Line Load Collapse Test Samples 53

Table 2 Triaxial Collapse Test Samples 66

Table 3 All results for compression tests 67

1. INTRODUCTION

1.1 Background

Finite element method is numerical method for solving complex engineering and mathematical problems. It is especially useful when dealing with complicated geometries, loadings and material properties where analytical solutions is limited. The FEM can divide a whole body into an equivalent system of many smaller bodies or finite elements that are interconnected at nodal points which are shared by two or more elements or boundary lines. The field variables are dependent variables of interest governed by differential equations. And boundary conditions can be specified on the boundary of the field.

The displacement of any point within an element is a function of the nodal displacements and of the position of the point. This is expressed by shape function, which is usually expressed by N_i.

Stiffness matrix is contains primary characteristics of a finite element. For a structural finite element, the stiffness matrix includes the geometric and material behavior information that indicates the resistance of the element to deformation when subject to loading. Different deformation types can be represented such as axial, bending, shear and torsional deformation.

For 3D problems, the normal stresses are expressed by σ and shear stresses are expressed by τ. Figure 1 shows the directions of all the normal stresses and shear stresses on a 3D cube. The planes perpendicular to x, y and z coordinate ae called x, y, and z plane, respectively. The stresses are represented by the following nine stress components.

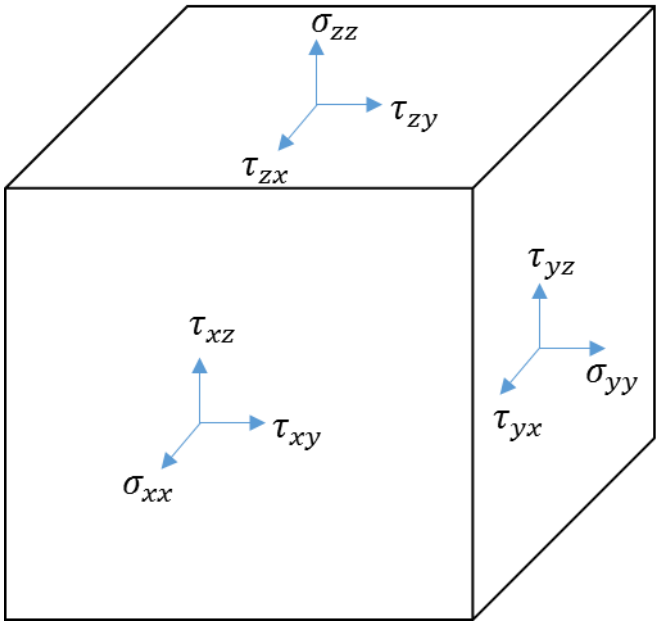

Figure 1 3D normal and shear stresses

The normal strain is defined as the change in length per unit length and the shear strain is defined as the change in angle between two original orthogonal directions. The normal strain is expressed by ε and shear strain is expressed by γ.

$$\varepsilon = \frac{\Delta L}{L}$$

$$\gamma = \theta$$

Figure 2 shows displacement and deformation of a square structure.

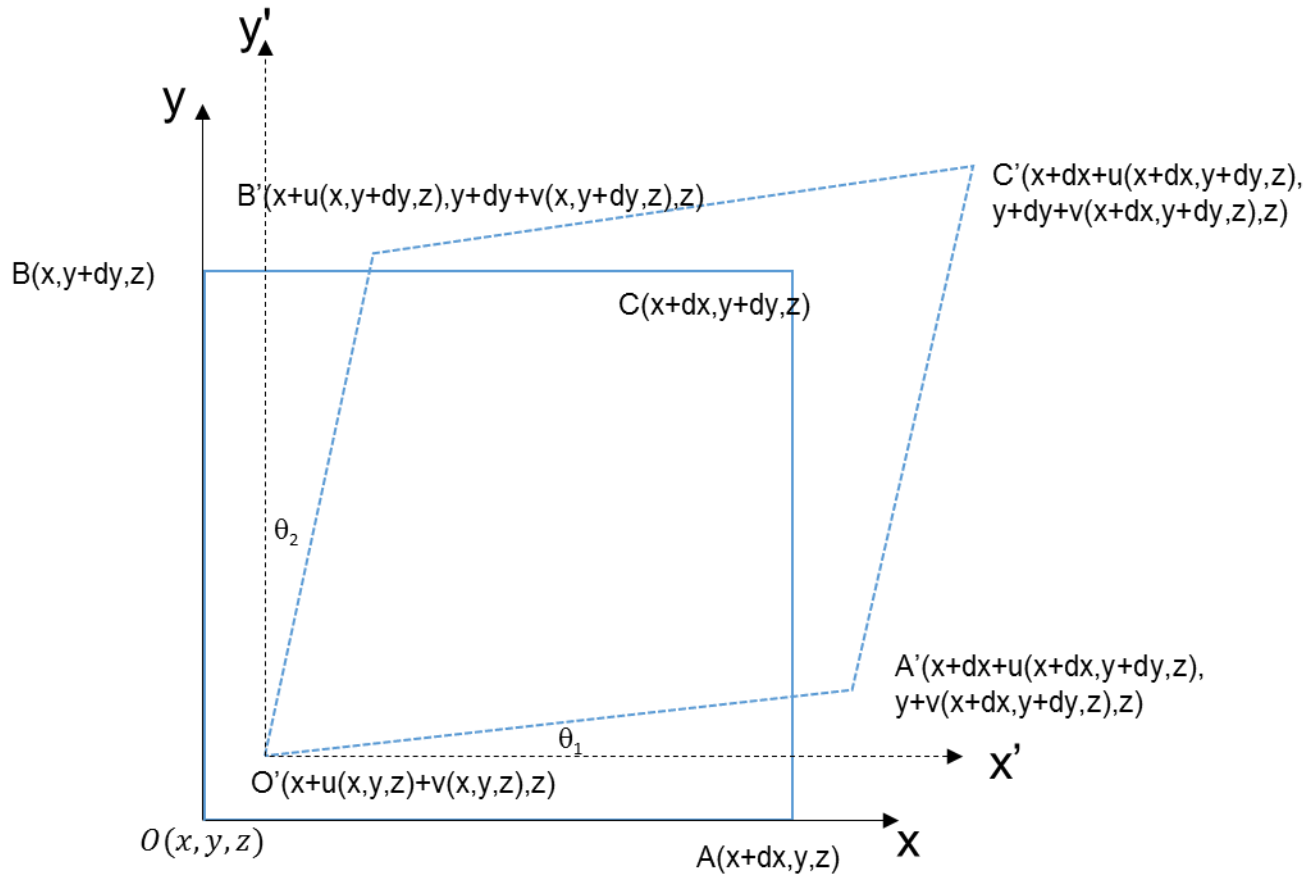

Figure 2 Displacement and deformation of a square structure

Displacement and strain relations are shown in equations below:

$$\varepsilon_x = \frac{u(x+\Delta x) - u(x)}{x + \Delta x - x} = \frac{\partial u}{\partial x}$$

$$\varepsilon_y = \frac{\partial v}{\partial y}$$

$$\varepsilon_z = \frac{\partial w}{\partial z}$$

$$\theta_1 = \frac{\partial v}{\partial x}$$

$$\theta_2 = \frac{\partial u}{\partial y}$$

$$\gamma_{xy} = \frac{\partial v}{\partial x} + \frac{\partial u}{\partial y}$$

$$\gamma_{yz} = \frac{\partial v}{\partial z} + \frac{\partial w}{\partial y}$$

$$\gamma_{zx} = \frac{\partial w}{\partial x} + \frac{\partial u}{\partial z}$$

Equation of equilibrium are given by

$$\frac{\partial \sigma_x}{\partial x} + \frac{\partial \tau_{yx}}{\partial y} + \frac{\partial \tau_{zx}}{\partial z} + F_x = 0$$

$$\frac{\partial \sigma_y}{\partial y} + \frac{\partial \tau_{xy}}{\partial x} + \frac{\partial \tau_{zy}}{\partial z} + F_y = 0$$

$$\frac{\partial \sigma_z}{\partial z} + \frac{\partial \tau_{zy}}{\partial y} + \frac{\partial \tau_{zx}}{\partial x} + F_z = 0$$

Stress strain relations are shown below

$$\varepsilon_x = \frac{1}{E}(\sigma_x - v\sigma_y - v\sigma_z)$$

$$\varepsilon_y = \frac{1}{E}(\sigma_y - v\sigma_z - v\sigma_x)$$

$$\varepsilon_z = \frac{1}{E}(\sigma_z - v\sigma_x - v\sigma_y)$$

$$\tau_{xy} = 2G\gamma_{xy}$$

$$\tau_{yz} = 2G\gamma_{yz}$$

$$\tau_{zx} = 2G\gamma_{zx}$$

Matrix expression is often used to develop equations for finite element method. The displacement strain relation is

$$\varepsilon = \begin{bmatrix} \frac{\partial}{\partial x} & 0 & 0 \\ 0 & \frac{\partial}{\partial y} & 0 \\ 0 & 0 & \frac{\partial}{\partial z} \\ \frac{\partial}{\partial y} & \frac{\partial}{\partial x} & 0 \\ 0 & \frac{\partial}{\partial z} & \frac{\partial}{\partial y} \\ \frac{\partial}{\partial z} & 0 & \frac{\partial}{\partial x} \end{bmatrix} \begin{bmatrix} u \\ v \\ w \end{bmatrix}$$

Equation of equilibrium is given by

$$\nabla\sigma + F = 0$$

Where

$$\nabla = \begin{bmatrix} \frac{\partial}{\partial x} & 0 & 0 & \frac{\partial}{\partial y} & 0 & \frac{\partial}{\partial z} \\ 0 & \frac{\partial}{\partial y} & 0 & \frac{\partial}{\partial x} & \frac{\partial}{\partial z} & 0 \\ 0 & 0 & \frac{\partial}{\partial z} & 0 & \frac{\partial}{\partial y} & \frac{\partial}{\partial x} \end{bmatrix}$$

$$\sigma = [\sigma_x \quad \sigma_y \quad \sigma_z \quad \tau_{xy} \quad \tau_{yz} \quad \tau_{zx}]^T$$

$$F = F_x + F_y + F_z$$

The stress strain relations are shown by

$$\sigma^e = D\varepsilon - (1 - c_m)Ip_o$$

$$\sigma^e = \left[\sigma_x^e \quad \sigma_y^e \quad \sigma_z^e \quad \tau_{xy}^e \quad \tau_{yz}^e \quad \tau_{zx}^e\right]^T$$

Where e means element, and m means matrix.

$$\varepsilon = [\varepsilon_x \quad \varepsilon_y \quad \varepsilon_z \quad \gamma_{xy} \quad \gamma_{yz} \quad \gamma_{zx}]^T$$

$$I = [1 \quad 1 \quad 1 \quad 0 \quad 0 \quad 0]^T$$

$$D = \frac{E(1-\nu)}{(1+\nu)(1-2\nu)} \begin{bmatrix} 1 & \frac{\nu}{1-\nu} & \frac{\nu}{1-\nu} & 0 & 0 & 0 \\ & 1 & \frac{\nu}{1-\nu} & 0 & 0 & 0 \\ & & 1 & 0 & 0 & 0 \\ & & & \frac{1-2\nu}{2(1-\nu)} & 0 & 0 \\ & \text{Symmetry} & & & \frac{1-2\nu}{2(1-\nu)} & 0 \\ & & & & & \frac{1-2\nu}{2(1-\nu)} \end{bmatrix}$$

$$C_m = \frac{1-2\nu_m}{E_m} / (\frac{1-2\nu}{E})$$

Slotted liners are widely used worldwide. Functions of slotted liners include Sand control with low cost and enhance wellbore stability, thus prevent borehole collapse. Slotted liners are designed in a way that the slots will allow smaller hydrocarbon particles to flow into the wellbore, but on the other hand, prevent the larger sand particles from entering the wellbore. The slot width is designed based on the formation sand particle size, to effectively achieve sand control functionality as shown in figure 3 below. Figure 4 shows whole joints of slotted liners. Slotted liners are connected together, and then put into the formation along wellbore.

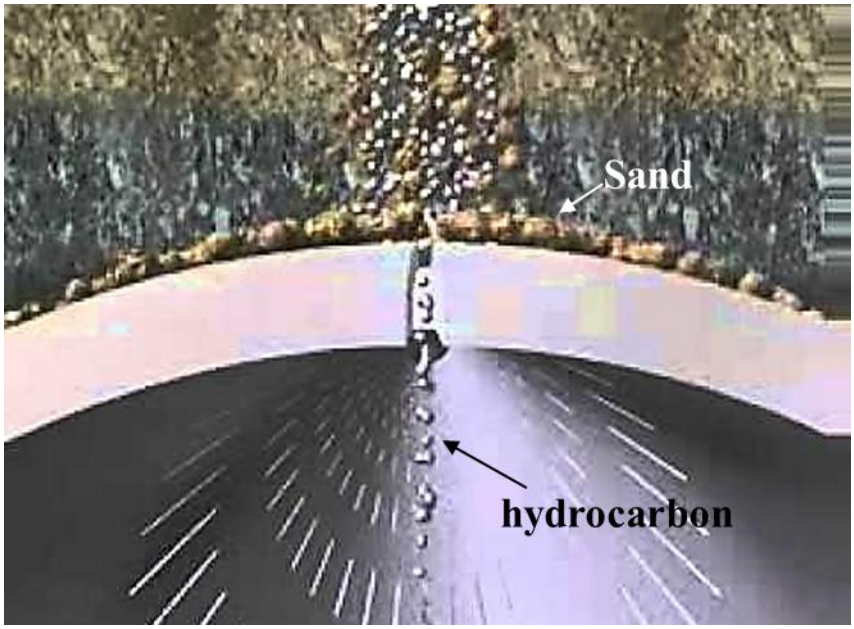

Figure 3 Sand control mechanism of slotted liners

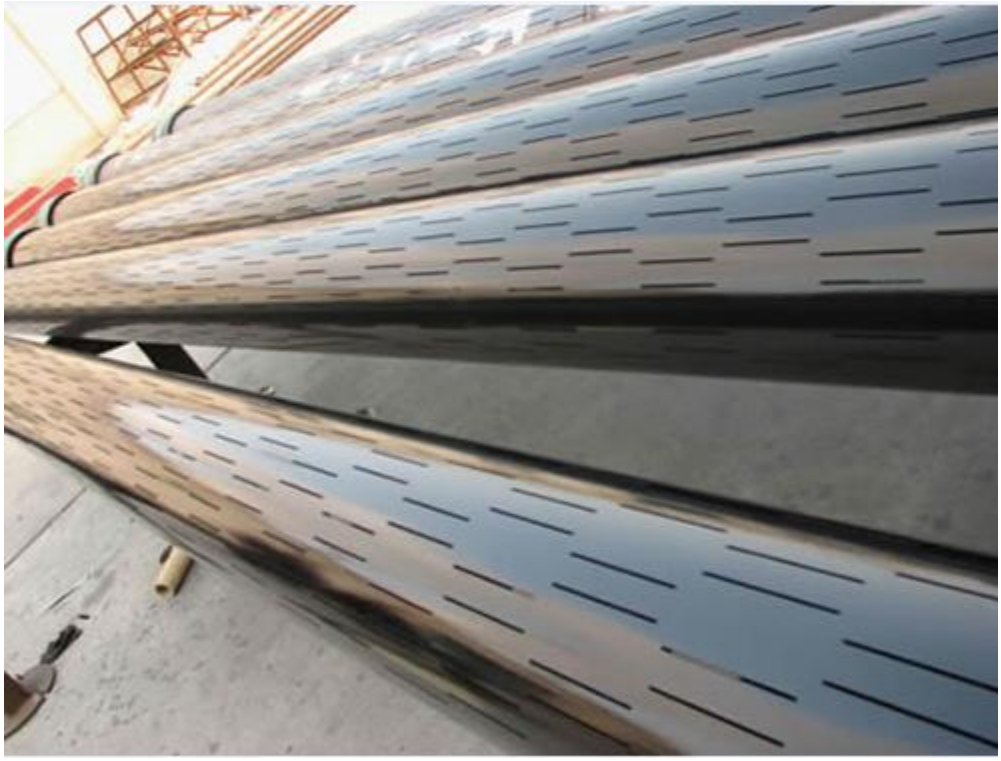

Figure 4 Whole joint of slotted liners

Slotted liners design are different based on formations. Usually for heavy oil, sandstone formation, slots are wider to allow effective production of heavy oil. But for light oil formations, such as limestone, slots are usually thinner but number of slots is larger.

The key issue is that slots will reduce the strength of the original pipes, which will induce stability issue. The goal of the research is to find the optimum design to maintain productivity while minimize the instability issue.

1.2 Literature Review

Slotted liners are widely used to improve the performance of horizontal wells. They are mainly used for sandstone (Furui 2012), limestone reservoirs. There are also applications in shale reservoir. However, the openings on the casing/liner can reduce the strength under geotectonic loading, such as axial compression, bending, and radial compression. The structural integrity of these slotted liners should be properly studied to ensure the safety.

Different plain casing/liner were studied by (Morita 2014, Furui 2012). According to Furui, axial-compression collapse is a major liner-deformation mechanism, and in horizontal sections, failure is induced by increased axial loading because of cavity deformation.

Slotted liners are manufactured by cutting several rows of slots with width ranging from 0.012in to 0.15in, and length ranging from 1in to 3in depending on the formation's grain size. But if the slots are too long, cause overlapping between offset slots, the structural capacity will be the lowest. (Xie 2015) In this way, sand production can be prevented while keeping oil/gas production. Although bigger and more slots can ensure maximum production, structural capacity

will be reduced. So slotted liner design needs to balance sand prevention, open flow area (OFA) and structural capacity.

Abbassian (Abbassian and Parfitt 1998) described a simple method of evaluating the collapse strength and post-collapse behavior of oil field tubulars subjected to external pressure. The method is based on elastic ovalization and subsequent plastic collapse by formation of a four-hinge mechanism. He also mentioned that due to long lengths of tubulars used in wells, unduly conservative design can bring an undesirable penalty on well cost. But on the opposite, under-design increases risk of failure. The design guidelines such as those published by API, are semiempirical which need various assumptions and restrictions which may not be readily applied to slotted liners.

Extensive sand production occurred in many wells, means slots deformed a lot. Slot opening can be due to various mechanisms including buckling under axial compression, bending, collapse under external pressure (formation touching).

The primary objective of slotted liner is to assure the structural capacity, sufficient sand prevention, while maintaining enough open flow area (OFA). In addition to base pipe parameters including materials grades, weight, diameter, wall thickness, properties of slotted liners are impacted by slot length, width, slot pattern and density.

The goal of this paper is to review the existing slotted liner designs, and come up with optimized slotted liner designs including selection of material grades, ratio of diameter and thickness, slot pattern, slot length, width. Finally, through data analysis and field case study, come up with an analytical solution which is easy to use. And a series of simulation methods to capture the deformation more accurately for various kinds of tools under formation.

Slotted liner pattern are shown in figure 5:

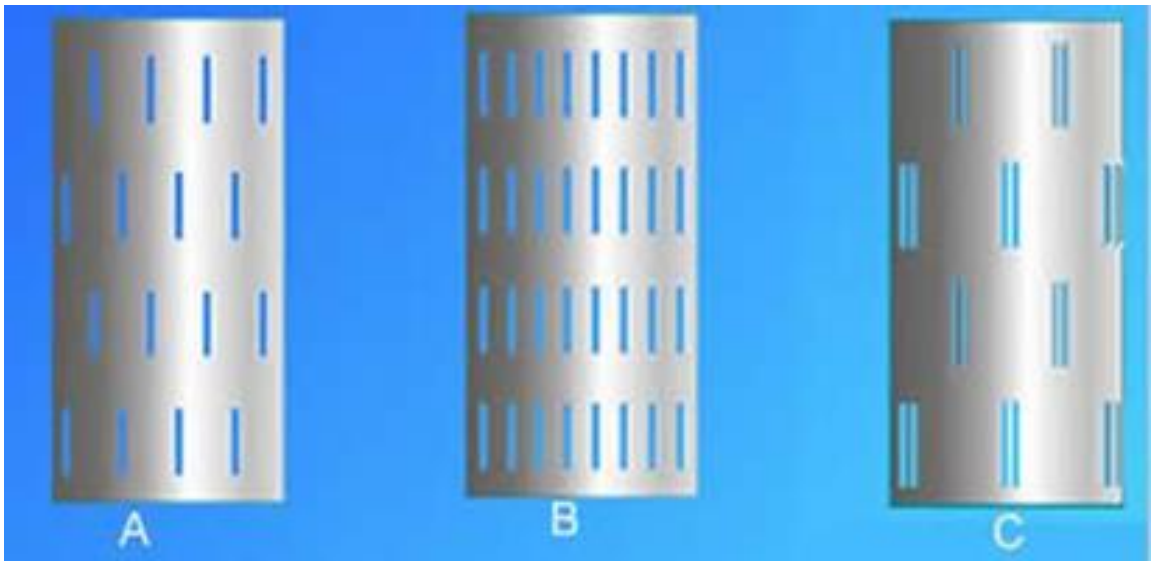

Figure 5 Three different slot patterns. A:Single staggered pattern. B: Straight pattern. C: Gang pattern (multiple staggered).

In the line pattern, slots are placed evenly in identical bands around the pipe, forming straight lines of slots across the length of the slotted liner. In the single-slot staggered pattern, bands of evenly spaced slots are placed around the pipe. Slots in different bands are offset (staggered) to each other. The single-slot staggered pattern preserves the strength of the pipe and provides an even distribution of the slots over the area of the pipe. Gang Pattern (Multiple Staggered Pattern), while having the same overall layout as the single-slot staggered pattern, the gang pattern places two slots, cut at close proximity, instead of just one slot at each position.

Slotted liner with a multiple staggered pattern has been shown to withstand higher torque during installation and provide better resistance to deformation under thermal load compared to the single-slot staggered pattern, making it well suited for application in steam assisted gravity drainage (SAGD) applications.

$$N = \frac{12 \times 3.14 \times D \times C}{100 \times W \times L} \quad (1)$$

N = the number of slots per foot.

D = Outside diameter of the liner (in inches).

C = Open area percentage.

W = selected slot width (in inches).

L = Length of slot (inches).

Functions of slotted liners include Sand control with low cost and enhance wellbore stability. However, the opening slots can reduce the strength of casing/liner, Enhance wellbore stability, help prevent borehole collapse (Morita, 1994). It is widely used in ~90% SAGD (Steam Assisted Gravity Drainage) applications employ slotted liners as the sand control method (RPS Energy Canada, 2009), Monterey Shale in California (Michael F. Morea. 1997), and Limestone (Kumar, Srivastava, and Kumar 2010), deepwater reservoir in Gulf of Mexico (Guo, Blanford, and Candella 2015). But challenges also exist, maintain well productivity requires large open flow area, but on the opposite, large open area will cause stability issue. So, achieve high Open Flow Areas (OFA) while maintain sufficient axial and radial collapse resistance and compression strength is the goal of optimized slotted liner design.

A typical single staggered slotted liner is shown in figure 6. Single staggered slots keep the original strength of the pipe and give more uniform distribution to the stress, hence maintain the structural integrity.

Figure 7 shows the case when wellbore is touching liner, if the wellbore touches liner, the support is very good. But if there is a gap between wellbore and slotted liner, wellbore maybe easier to collapse.

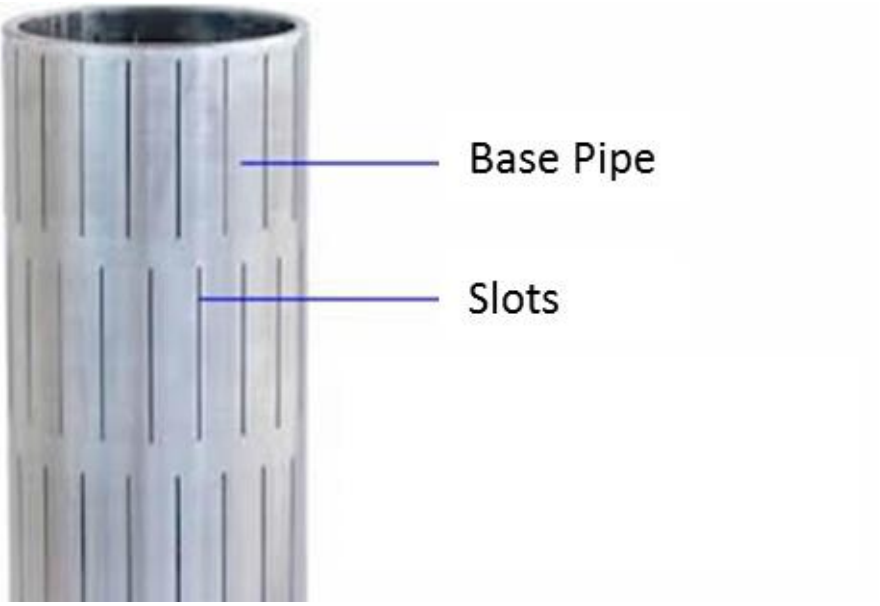

Figure 6 Typical Slotted Liner

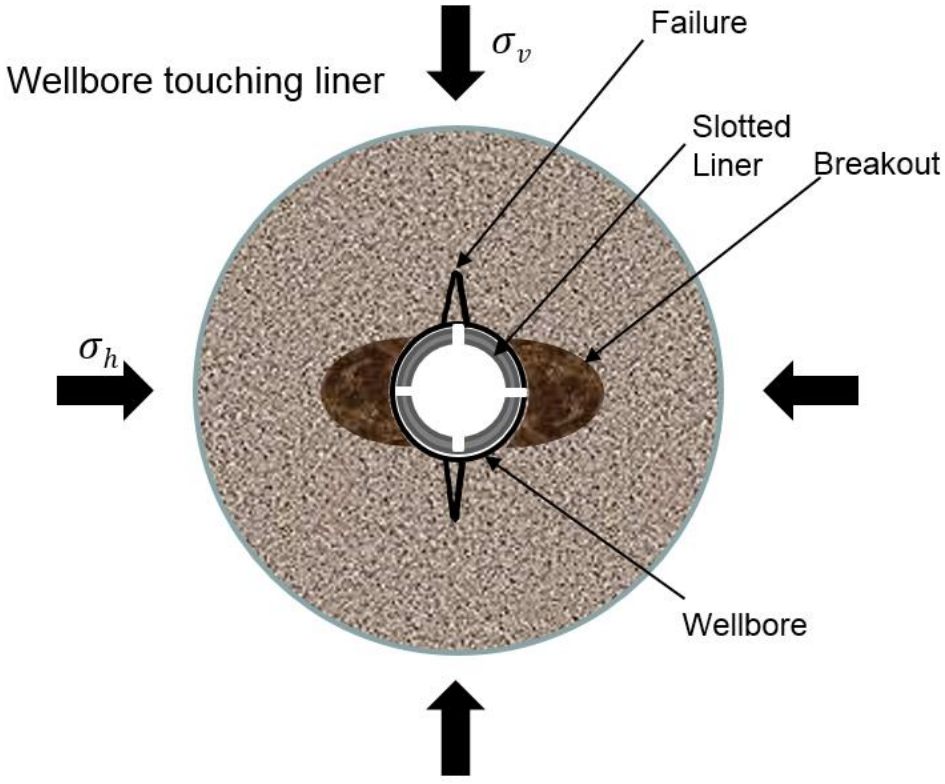

Figure 7 Structure of Borehole and Slotted Liner

Selection of proper grade and thickness of casings/liners is key for mitigating casing failure according to Morita et al (Morita and Shiozawa 2014, Morita 2014). By their observations, casing design for high porosity reservoirs should include the steel properties beyond the yield strength while the API casing design criterion is strictly based on the steel properties up to the yield strength. The tests showed the casings were uniformly deformed until the maximum load so that they were usable up to the maximum strength without significant distortion.

Joao Carlos Ribeiro Placido (Placido, Pasqualino, and Fonseca 2005) showed good match for load-radial displacement curves of simulation and experiments in figure 8. But they only considered one level of slots, it is too ideal to separate out one level without consideration of interaction between other slots. So further analysis needs to be carried out to simulate more realistic cases.

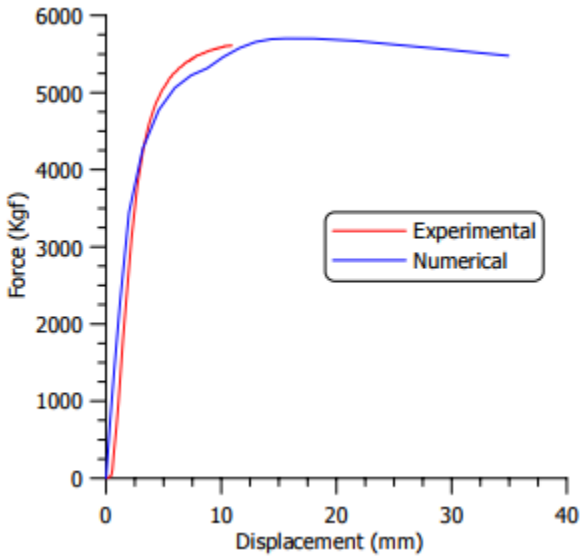

Figure 8 Load Force vs. Radial Displacement (Placido, Pasqualino, and Fonseca 2005)

Critical strain is an important factor to keep the slotted liner from unstable issues. As axial compression builds up on the casing/liner, there exists a peak load beyond which the structure will be unstable. The axial strain at the peak load is called critical strain. As mentioned by Chartier (Chartier 2016), design of slotted liners should consider this critical strain as a safety factor to make sure the critical strain is larger than the maximum strain expected in the installation and production period, a design margin also needs to be considered to account for possible strain localization.

As shown in Figure 9, when the axial strain is smaller than the critical strain, the stability of slotted liner can be maintained, whereas if the axial strain is larger than the critical strain, the structure becomes unstable, and the slotted liner will lose the support capability tremendously, which will cause serious unstable issue in the field.

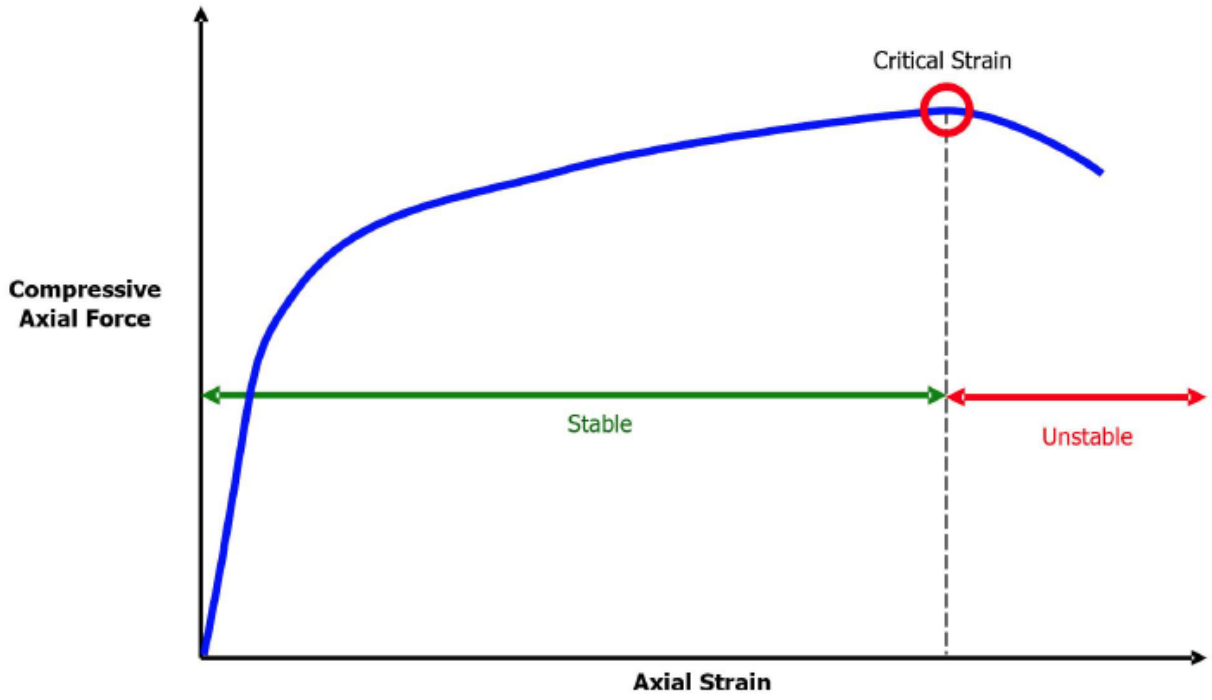

Figure 9 Critical strain in compression test (Chartier 2016)

1.3 Objectives

Using experiment and FEM simulation, we want to achieve:

1. Maximum well productivity without causing unstable problems of well
2. Numerical (FEM) and experimental approach to optimize slotted liner geometries.
3. Derive a correlation for optimum design, help engineers understand possible liner deformation and failure mechanisms, develop completion design criteria to reduce the risk of casing/liner failure, also control sand production effectively
4. Previous study by Xie didn't consider effect of grades, pipe length and pipe diameter/thickness. And there was no experiment. In our study, we will consider selection of grades and pattern with aid of both simulation and experiments

2. METHOD*

In this study, both numerical FEM model and experiments are performed to validate the results. We studied the elastic-plastic behavior of steel slotted liners both numerically and experimentally. For the global reservoir model, Drucker-Prager failure mechanism is applied to simulate the rock failure after depletion.

In figure 10, a 3D 20-node quadratic isoparametric element is shown. 20-node cube element is used because it is accurate. The node sequence may change from theory to theory, it is important to check the node sequence before applying the shape functions.

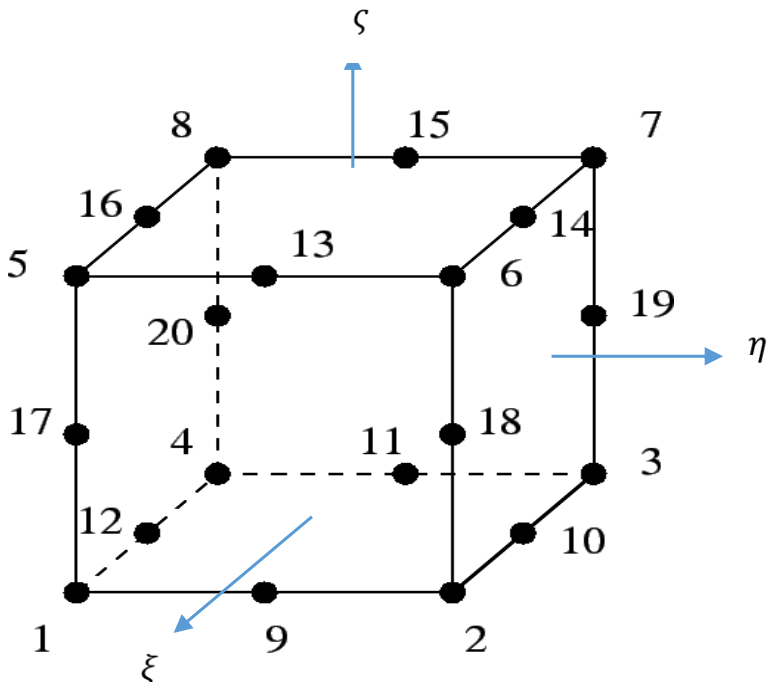

* Part of this dissertation is reprinted with permission from "3D Finite Element Analysis and Experimental Study of Stability of Slotted Liners." by X. Liu, N. Morita. ARMA- 2018-269 presented at 52nd US Rock Mechanics/Geomechanics Symposium, 17-20 June 2018 in Seattle, WA. Copyright 2018 by American Rock Mechanics Association.

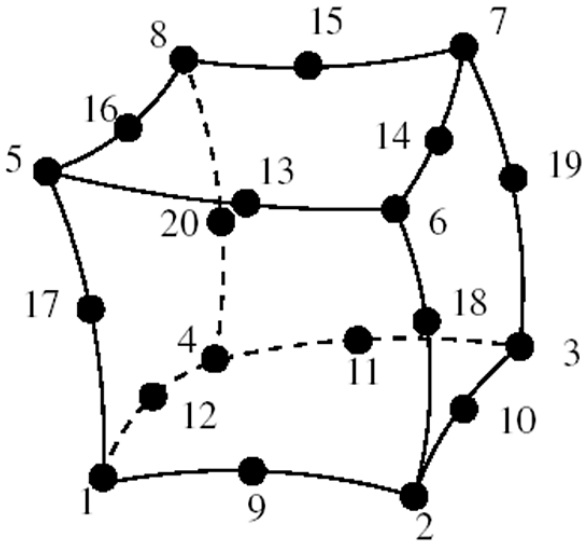

Figure 10 3D 20-node quadratic isoparametric element

Shape functions for the 20 node brick element are listed as following:

$$N1 = \frac{1}{8}(1-\xi)(1-\eta)(-\xi-\eta-\varsigma-2)$$

$$N2 = \frac{1}{4}(1-\xi\times\xi)(1-\eta)(1-\varsigma)$$

$$N3 = \frac{1}{8}(1+\xi)(1-\eta)(1-\varsigma)(\xi-\eta-\varsigma-2)$$

$$N4 = \frac{1}{4}(1+\xi)(1-\eta\times\eta)(1-\varsigma)$$

$$N5 = \frac{1}{8}(1+\xi)(1+\eta)(1-\varsigma)(\xi+\eta-\varsigma-2)$$

$$N6 = \frac{1}{4}(1-\xi\times\xi)(1+\eta)(1-\varsigma)$$

$$N7 = \frac{1}{8}(1-\xi)(1+\eta)(1-\varsigma)(-\xi+\eta-\varsigma-2)$$

$$N8 = \frac{1}{4}(1-\xi)(1-\eta\times\eta)(1-\varsigma)$$

$$N9 = \frac{1}{4}(1-\xi)(1-\eta)(1-\varsigma\times\varsigma)$$

$$N10 = \frac{1}{4}(1+\xi)(1-\eta)(1-\varsigma\times\varsigma)$$

$$N11 = \frac{1}{4}(1+\xi)(1+\eta)(1-\varsigma\times\varsigma)$$

$$N12 = \frac{1}{4}(1-\xi)(1+\eta)(1-\varsigma\times\varsigma)$$

$$N13 = \frac{1}{8}(1-\xi)(1-\eta)(1+\varsigma)(-\xi-\eta+\varsigma-2)$$

$$N14 = \frac{1}{4}(1-\xi\times\xi)(1-\eta)(1+\varsigma)$$

$$N15 = \frac{1}{8}(1+\xi)(1-\eta)(1+\varsigma)(\xi-\eta+\varsigma-2)$$

$$N16 = \frac{1}{4}(1+\xi)(1-\eta\times\eta)(1+\varsigma)$$

$$N17 = \frac{1}{8}(1+\xi)(1+\eta)(1+\varsigma)(\xi+\eta+\varsigma-2)$$

$$N18 = \frac{1}{4}(1-\xi\times\xi)(1+\eta)(1+\varsigma)$$

$$N19 = \frac{1}{8}(1-\xi)(1+\eta)(1+\varsigma)(-\xi+\eta+\varsigma-2)$$

$$N20 = \frac{1}{4}(1-\xi)(1-\eta\times\eta)(1+\varsigma)$$

Since $N_i(\xi_\alpha, \eta_\alpha, \varsigma_\alpha) = \delta_{i\alpha}$, the condition of shape functions is satisfied.

The coordinate transformation is shown as

$$x = \sum_{i=1}^{20} x_i N_i$$

$$y = \sum_{i=1}^{20} y_i N_i$$

$$z = \sum_{i=1}^{20} z_i N_i$$

The volume and area integrations are shown as

$$dV = dxdydz = |J|d\xi d\eta d\varsigma$$

$$d\Gamma = \left|\frac{\partial r}{\partial \xi} \times \frac{\partial r}{\partial \eta}\right| d\xi d\eta$$

Where direction of $d\Gamma$ is perpendicular to the boundary surface.

$$J = \begin{bmatrix} \frac{\partial x}{\partial \xi} & \frac{\partial y}{\partial \xi} & \frac{\partial z}{\partial \xi} \\ \frac{\partial x}{\partial \eta} & \frac{\partial y}{\partial \eta} & \frac{\partial z}{\partial \eta} \\ \frac{\partial x}{\partial \varsigma} & \frac{\partial y}{\partial \varsigma} & \frac{\partial z}{\partial \varsigma} \end{bmatrix}$$

$$d\Gamma = \left|\frac{\partial r}{\partial \xi} \times \frac{\partial r}{\partial \eta}\right| d\xi d\eta = \begin{bmatrix} i & j & k \\ \frac{\partial x}{\partial \xi} & \frac{\partial y}{\partial \xi} & \frac{\partial z}{\partial \xi} \\ \frac{\partial x}{\partial \eta} & \frac{\partial y}{\partial \eta} & \frac{\partial z}{\partial \eta} \end{bmatrix}$$

The finite element equation is given by

$$K^e u^e = F^e + T^e$$

Where

$$K^e = \int_{V^e} (B^T D B)|J|d\xi d\eta d\varsigma$$

$$F^e = \int_{V^e} (N^T N)|J| d\xi d\eta d\varsigma \, F^e$$

$$T^e = \int_{S^e} (N^T T) d\Gamma = \begin{bmatrix} T_1 \\ T_2 \\ \vdots \\ T_{19} \\ T_{20} \end{bmatrix}$$

Where

$$B = [B_1 \; B_2 \; B_3 \; B_4 \; B_5 \; B_6 \; B_7 \; B_8 \;]$$

$$B_i = \begin{bmatrix} \frac{\partial N_i(x,y,z)}{\partial x} & 0 & 0 \\ 0 & \frac{\partial N_i(x,y,z)}{\partial y} & 0 \\ 0 & 0 & \frac{\partial N_i(x,y,z)}{\partial z} \\ \frac{\partial N_i(x,y,z)}{\partial y} & \frac{\partial N_i(x,y,z)}{\partial x} & 0 \\ 0 & \frac{\partial N_i(x,y,z)}{\partial z} & \frac{\partial N_i(x,y,z)}{\partial y} \\ \frac{\partial N_i(x,y,z)}{\partial z} & 0 & \frac{\partial N_i(x,y,z)}{\partial x} \end{bmatrix}$$

Von Mises yield criteria was used.

$$\sigma_v = \sqrt{\frac{1}{2}[(\sigma_{11} - \sigma_{22})^2 + (\sigma_{22} - \sigma_{33})^2 + (\sigma_{33} - \sigma_{11})^2 + 6(\sigma_{12}^2 + \sigma_{23}^2 + \sigma_{31}^2)]}$$

2.1 FEM Simulation

2.1.1 Model Description

Two different basic designs of slotted liners are shown in Figure 11. The design is based on practical manufacturing method, which is a row of circular saws. Between each saw, the length is 6 inches. So in one column of slots, the interval between two slots are 6 inches.

Sample length will include 1 ft (0.3048 m) and 2 ft (0.6096 m), the density of slots can be 8/ft (0.3048 m) (or 16/ft (0.3048 m). Different parameters will be studied including materials grades, wall thickness, length of pipe, length of slots, density of slots, and width of slots.

Slotted liners with three different outer diameters are studied. To ensure the validity of the comparison, open flow area needs to be the same for slotted liners with the same OD. The open flow area are 2.23%, 1.85%, 1.52% for 2.375" OD, 2.875" OD, 3.5" OD liner respectively. The number of slots per foot required to obtain a certain open flow area can be calculated based on Eq. (1).

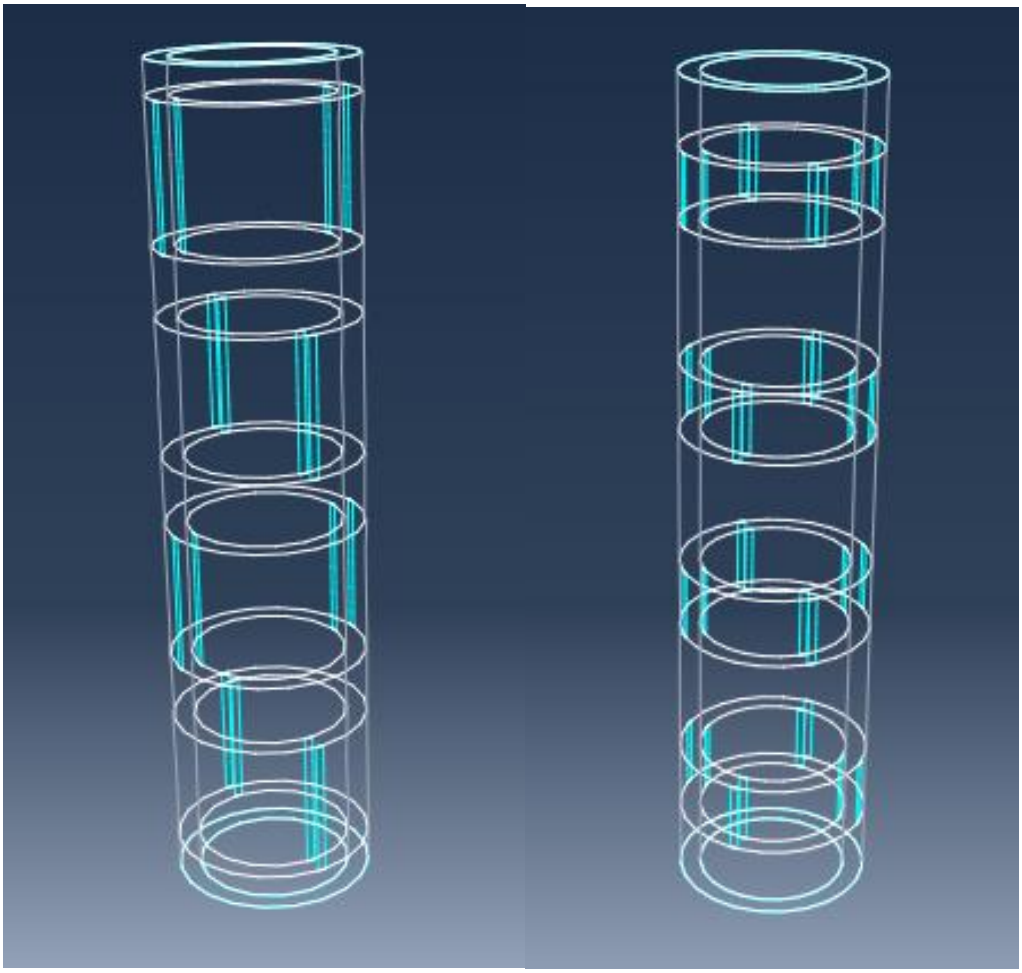

Figure 11 Basic slotted liner design: N=8/ft (0.3048 m), L=2" (50.8 mm) on left, N=16/ft (0.3048 m), L=1" (25.4 mm) on right

2.1.2 Model Validation

True stress and true strain will be used as input in Abaqus. The equations of converting from nominal stress and strain to true stress and strain are listed below:

True compressive stress,

$$\sigma_c = \frac{\sigma_c^{nominal}}{\left(1 - \nu^{nominal}\varepsilon_c^{nominal}\right)^2}$$

True compressive strain,

$$\varepsilon_c = \ln(1 + \varepsilon_c^{nominal})$$

True compressive plastic strain,

$$\varepsilon_c^P = \varepsilon_c^{nominal} - \frac{\sigma_c}{E}$$

Where $\sigma_c^{nominal}$ is nominal (engineering) stress, $\varepsilon_c^{nominal}$ is nominal compressive strain, $\nu^{nominal}$ is nominal Posson's ratio and E is Young's modulus.

σ_c is true compressive stress, ε_c is true compressive strain, and ε_c^P is true compressive plastic strain. The compressive stress and strain are negative values.

For compression test, engineering stress is based on experimental data. After peak point, the curve ascends because of the load bearing ability of sample increased due to increase in area.

The boundary conditions and load conditions are shown in figure 12.

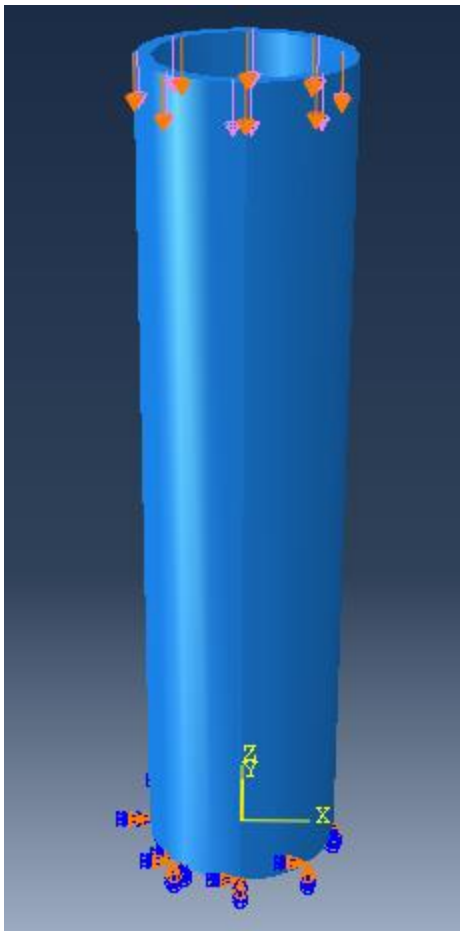

Figure 12 Base pipe for 2 7/8" thin wall L80L

At the bottom, as shown in Figure 12, since the bottom is restricted by bottom plate, encastre boundary condition was applied on the bottom surface of pipe. And axial compression was applied on the top surface by a constant rate of 0.24 in/min. Load was applied on the top surface uniformly.

Simulation model was validated by using true stress and true strain calculated from experimental data. As shown in Figure 13, the simulation matched well with the experimental results. In this way, we can continue to perform simulation for all other cases.

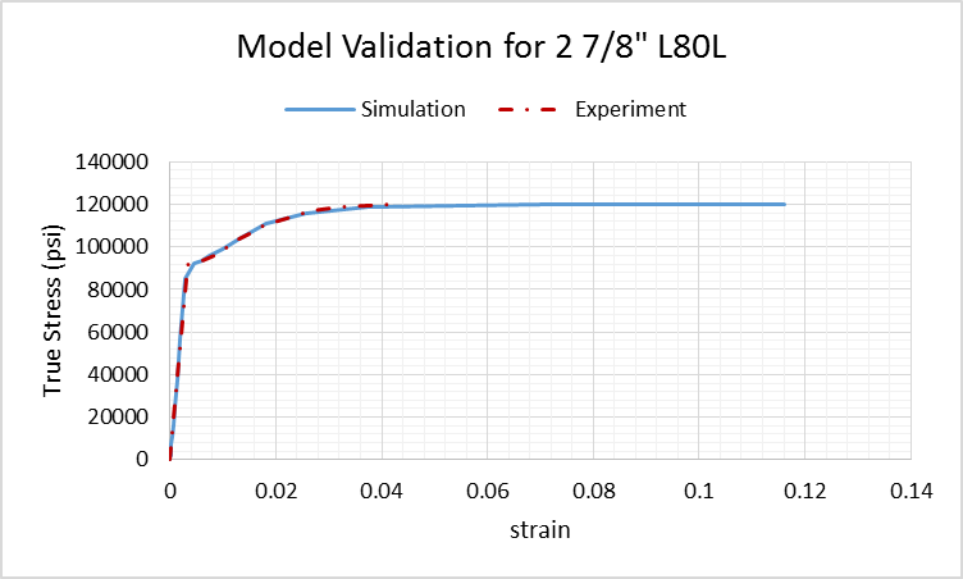

Figure 13 Model Validation for 2 7/8" thin wall L80

2.1.3 Axial Compression Simulation

The numerical simulation will be tested in three ways:

1. Simulate slotted liner with axial compression load only
2. Simulate slotted liner with axial tension and radial compression
3. Simulate slotted liner with axial compression and radial compression.

Figure 14 shows the mesh for 3D slotted liners. The mesh size effect is tested to ensure accurate simulation.

As shown in figure 15, with axial compression only, and bottom surface fixed on z direction, the deformation occurred from top to bottom gradually. In the middle of figure 15, it is the 3D mesh model before deformation, on the right, after deformation, local buckling occurs on the slots band, and slots become wider under axial load.

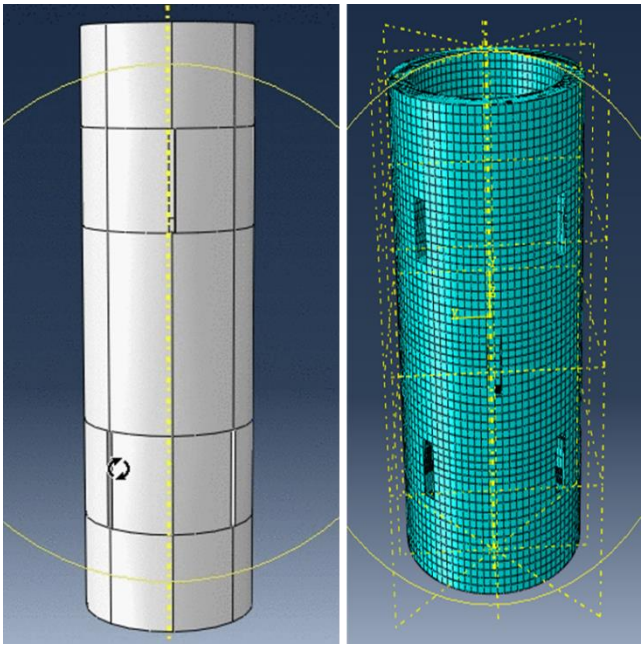

Figure 14 3D slotted liner mesh

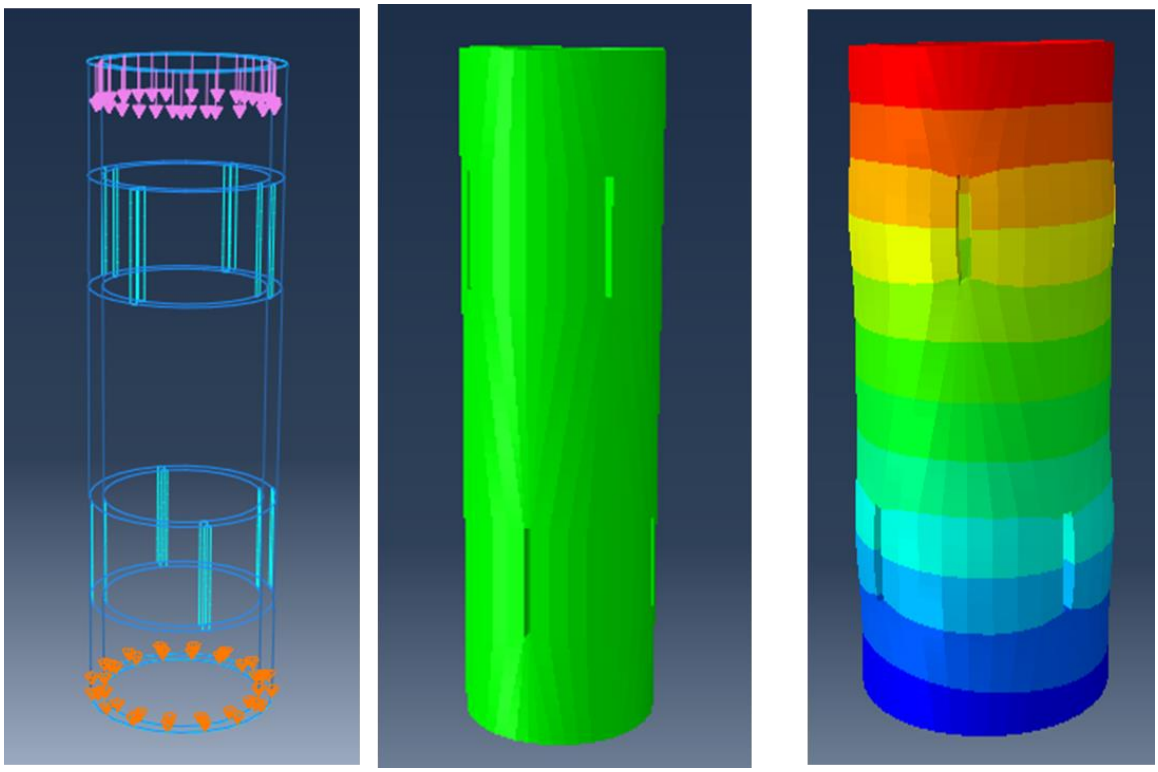

Figure 15 3D model for slotted liners in experiments, deformed slotted liner on right

As we can tell from figure 16, if the axial tension = 1000 psi, and radial compression = 5000 psi, the maximum deformation of the slotted liner with 8 slots is larger than slotted liner with single slot as shown in figures 17 and 18. Which means that more slots will bring stability issue. Figure 19 is a magnified plot showing the maximum stress occurs at the end of slots. As getting far away from the slot ends, the stress becomes smaller.

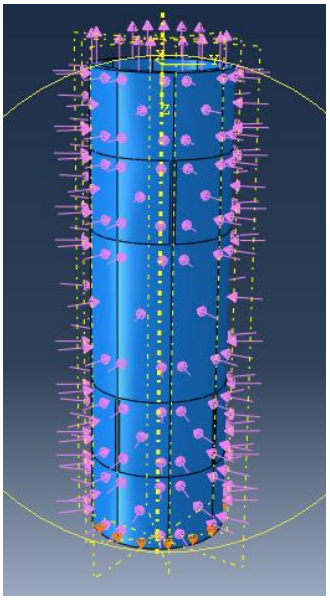

Figure 16 simulation with axial tension and radial compression

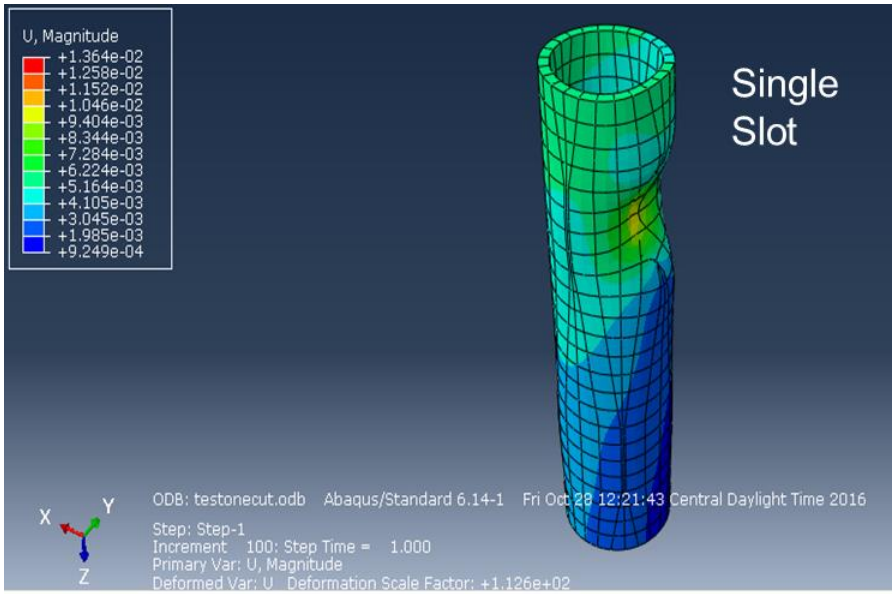

Figure 17 Simulation of slotted liner with single slot

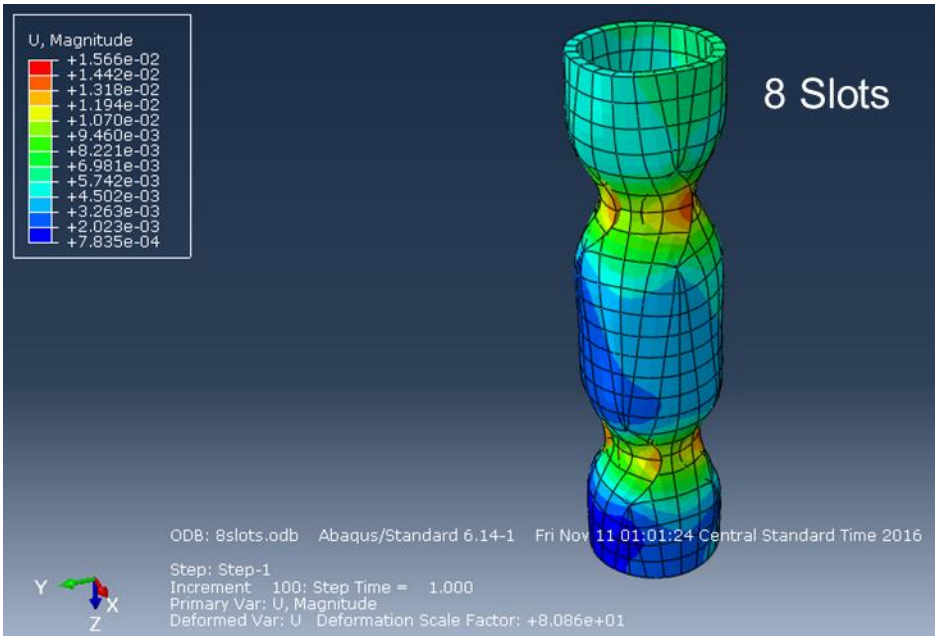

Figure 18 Simulation of slotted liner with 8 slots

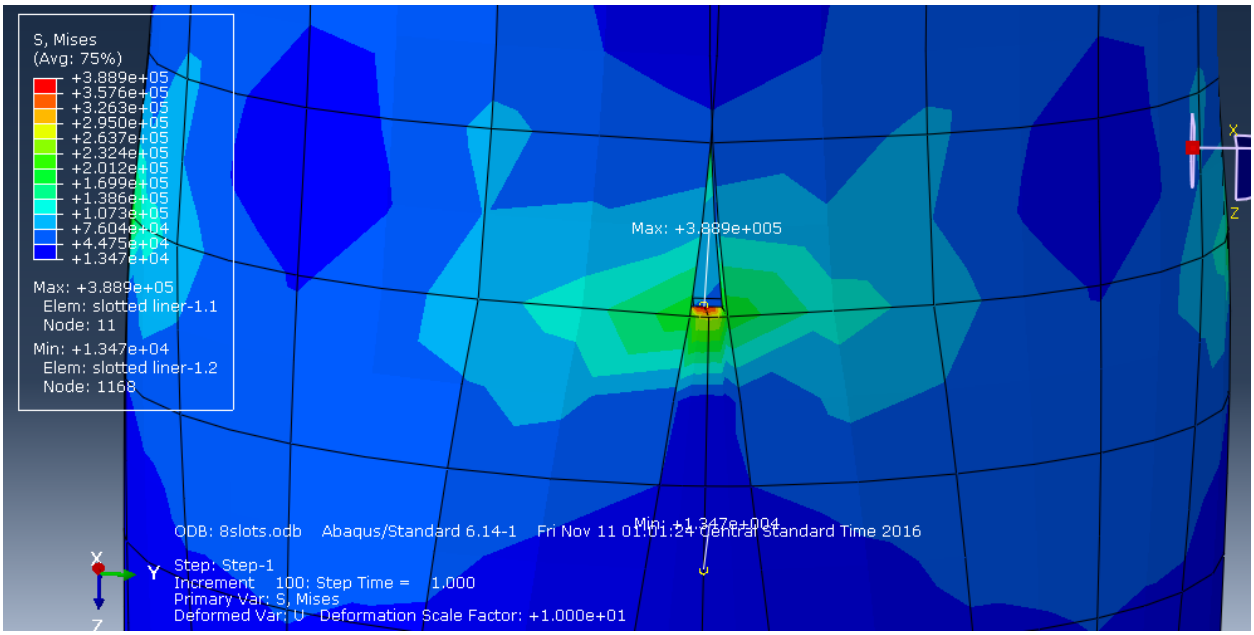

Figure 19 Maximum stress concentrated at the slot ends

In figure 20, a slotted liner model with axial compression is shown. The load is applied on the top surface, and the bottom surface is fixed on all direction due to the restriction of bottom loading plate. The Von Mises stress distribution is shown on the right. It is clear that maximum stress focus on the ends of slots, which will bring in the slot width expansion, and also local buckling is shown. From the plot of displacement, we can see larger deformation occurs around the slots, which will exaggerate the slot width. It matches well with the experimental samples shown on the right of figure 20.

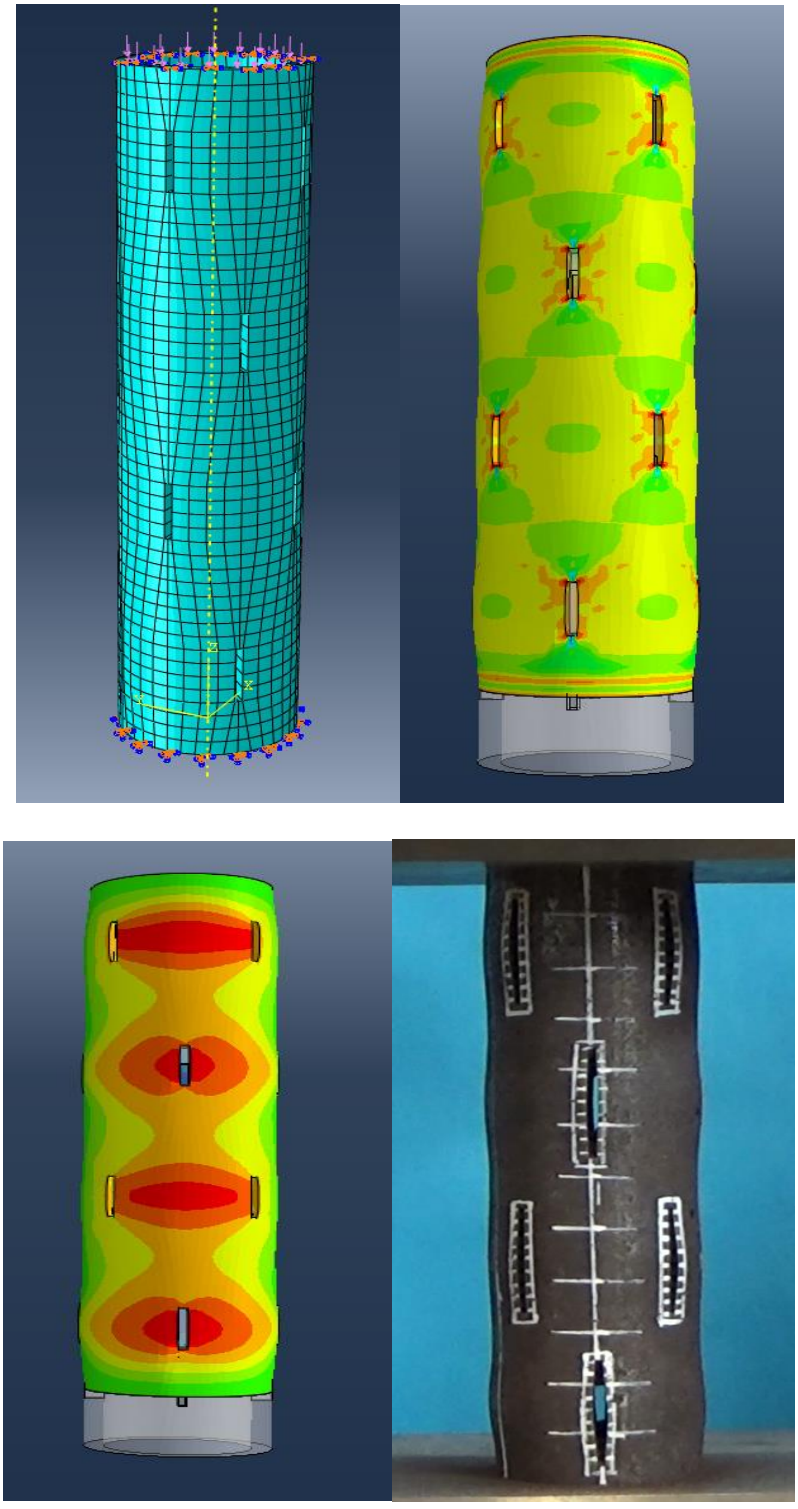

Figure 20 2 7/8" heavy L80 with N16L1 pattern, top left: 3D mesh, top right: Von Mises stress simulation, lower left: horizontal displacement simulation, lower right: experiment sample

In the global reservoir model, Drucker-Prager yield criterion is employed to simulate the rock mechanics behavior.

$$F = [\tau + G(\sigma_m)] - \left[s_0^y + \int \exp(\beta_1 + \beta_2 K + \beta_3 K^2 + \ldots) dK\right]$$

$$\tau = \sqrt{\frac{1}{2} S_{ij} S_{ij}}$$

$$K = \int \sigma_{ij} d\varepsilon \quad \text{for work hardening}$$

$$K = \sqrt{\frac{2}{3} (\varepsilon^p)^T (\varepsilon^p)} \quad \text{for strain hardening}$$

2.1.4 Line Load Collapse Test Simulation

The line load collapse is set up as shown in figures 21 and 22. As we can tell from the sketch, the line load was applied on the top edge of the pipe, and the direction of the load is pointed to the negative y direction. The bottom edge was fixed in all directions due to friction of the bottom plate. There is no restriction on top and bottom cutting surfaces.

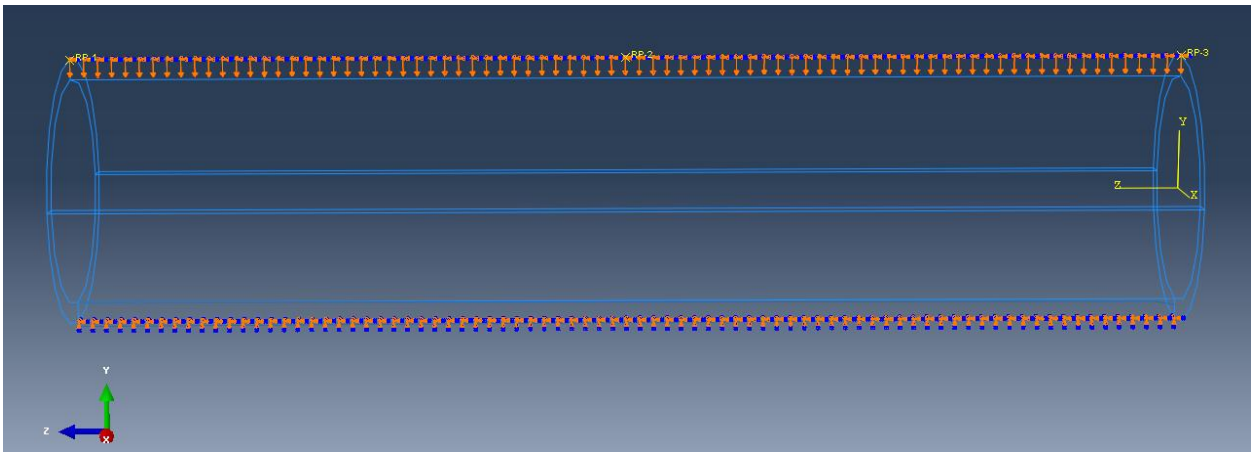

Figure 21 Load and Boundary Conditions for Line Load Collapse Simulation

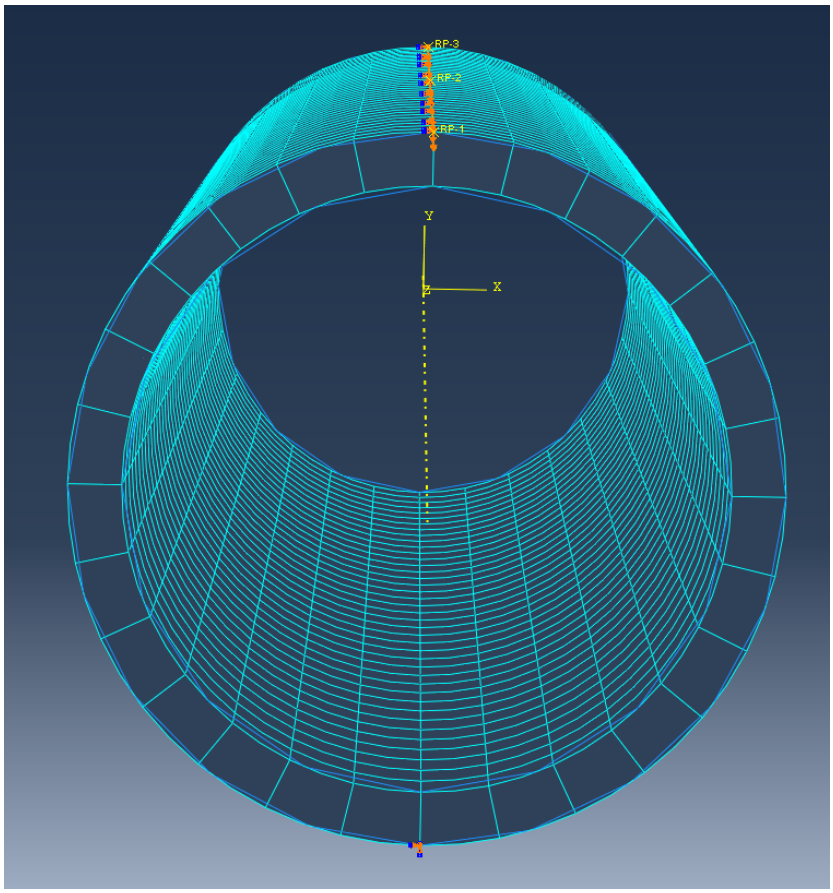

Figure 22 View from z direction for line load collapse simulation

After simulation, from figures 23-25, we can find the displacement on x, y and z direction, respectively. Figure 26 shows the magnitude of displacement.

It is straightforward to see from figure 27, that the sample becomes eclipse shape after line load, since the bottom edge is fixed on all directions, it is still symmetric after deformation.

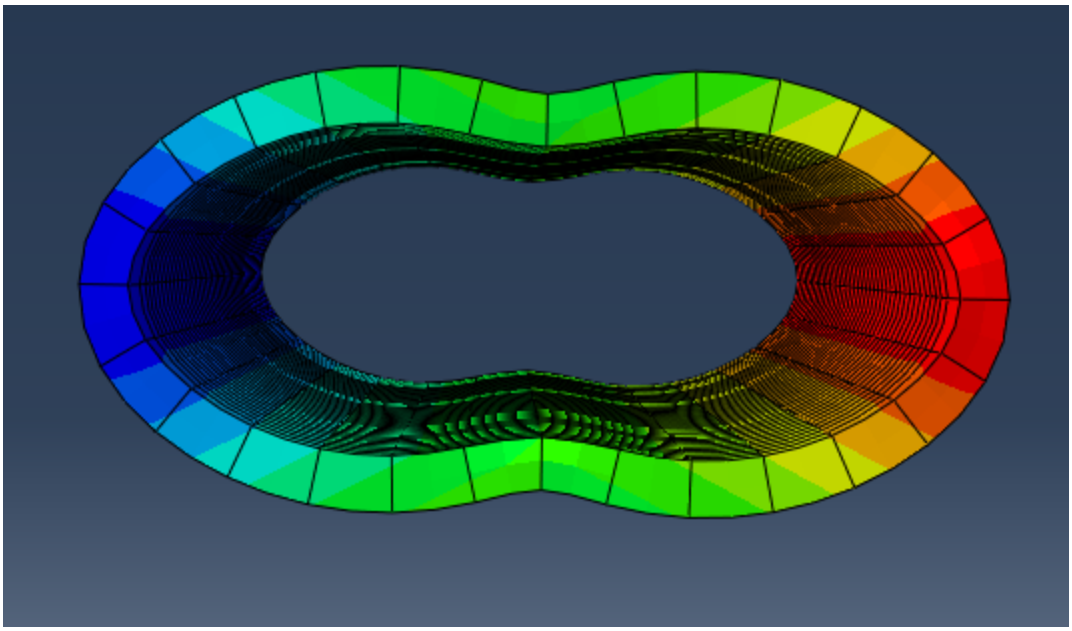

Figure 23 Displacement on x direction

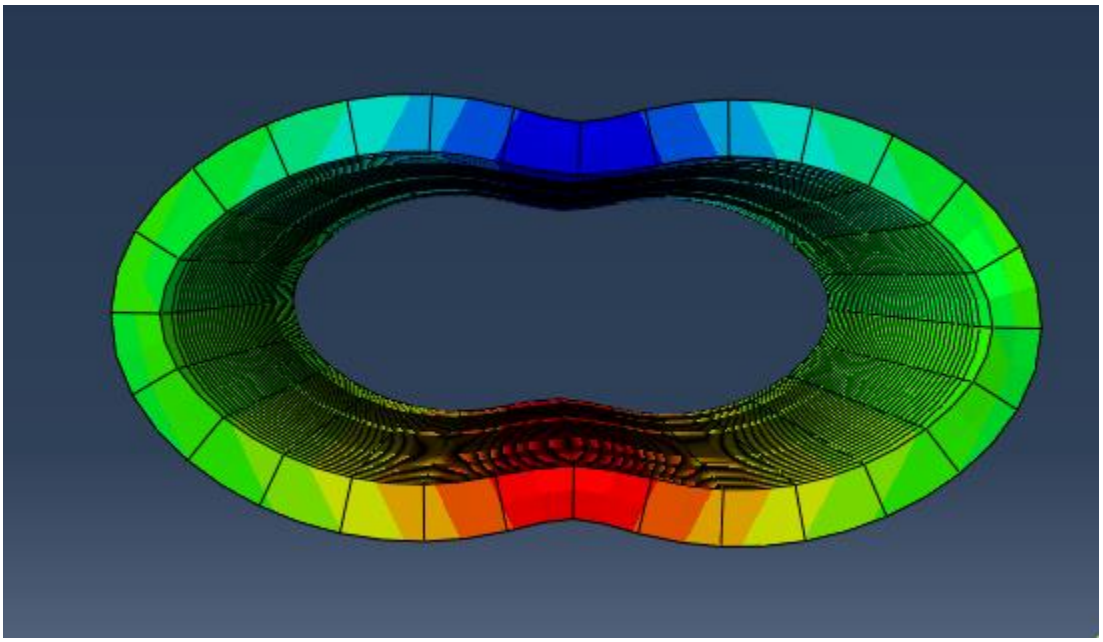

Figure 24 Displacement on y direction

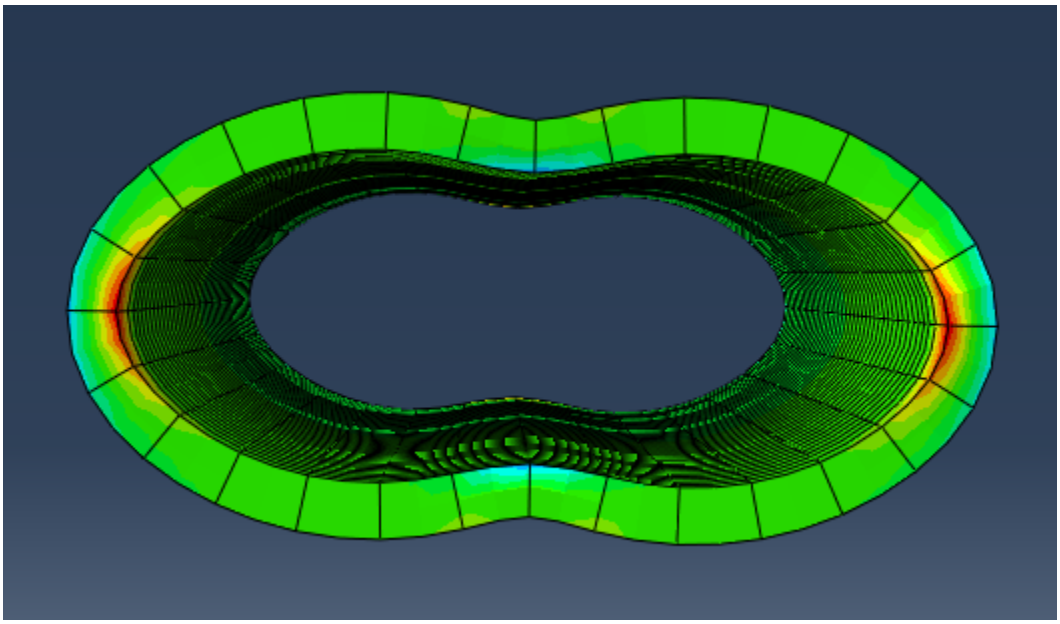

Figure 25 Displacement on z direction

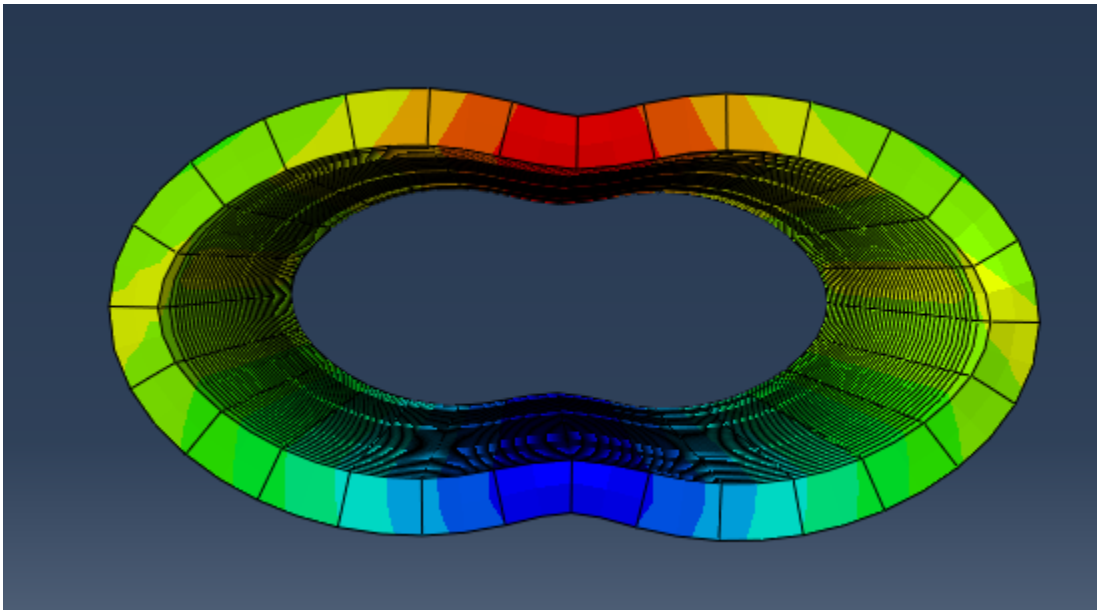

Figure 26 Magnitude of displacement

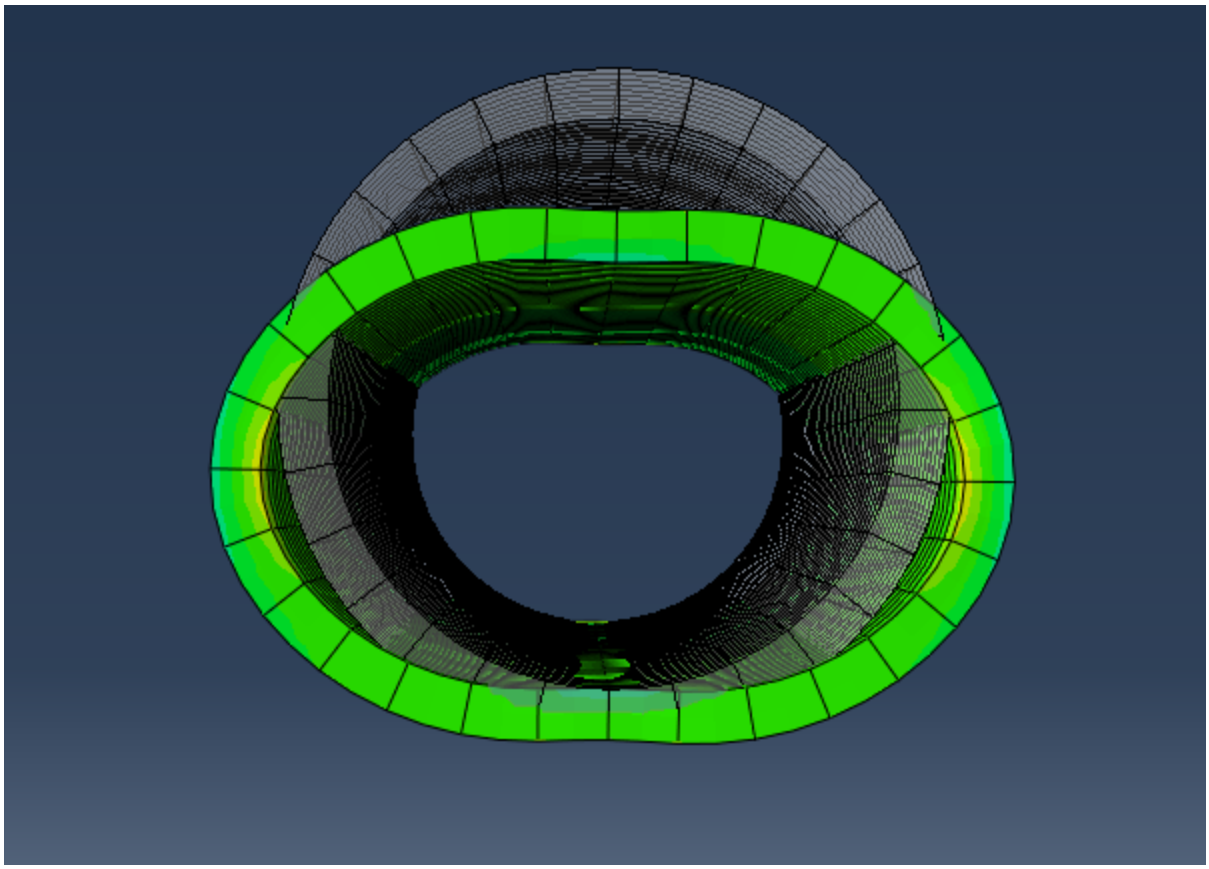

Figure 27 Comparison of slotted liner before and after line load test

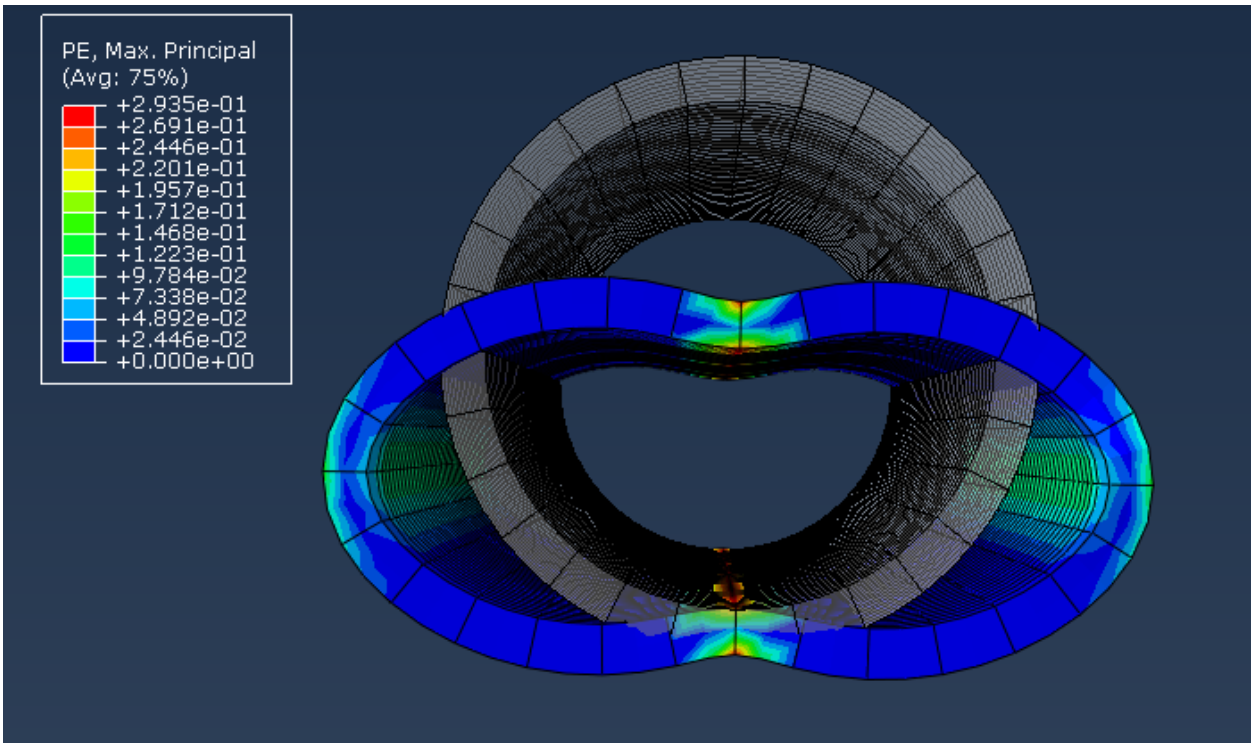

Figure 28 Plastic strain after deformation

Line load test were carried out by displacement control on the same load frame with axial compression test. Plastic region appears after the point where curve convert from linear to nonlinear. From Figure 28, it is obvious to view the plastic deformation happens first at both edges where the load applied, and then both sides on the horizontal direction followed. Maximum plastic strain appeared to be at the both ends of slots that are on the load directions.

Before plastic behavior, the pipe can hold most of the load. But after plastic regions forms, the pipe started to deform quickly.

2.2 Experiments

2.2.1 Compression Test

To ensure safety, we need to calculate the load limit of the load frame. Load limit is calculated based on

$$Load\ (lbs) = Stress * A = Stress * \frac{\pi}{4}(OD^2 - ID^2) \quad (6)$$

In our study, 9.5 lb/ft L-80 with 3.5" OD is the strongest casing. The maximum load will be calculated based on it.

OD=3.5 inch, ID= 2.992 inch,

Assume the maximum stress for L80 is 130,000 psi, the load limit is **336725** lbs.

But slots will reduce the strength as shown in Figure 29.

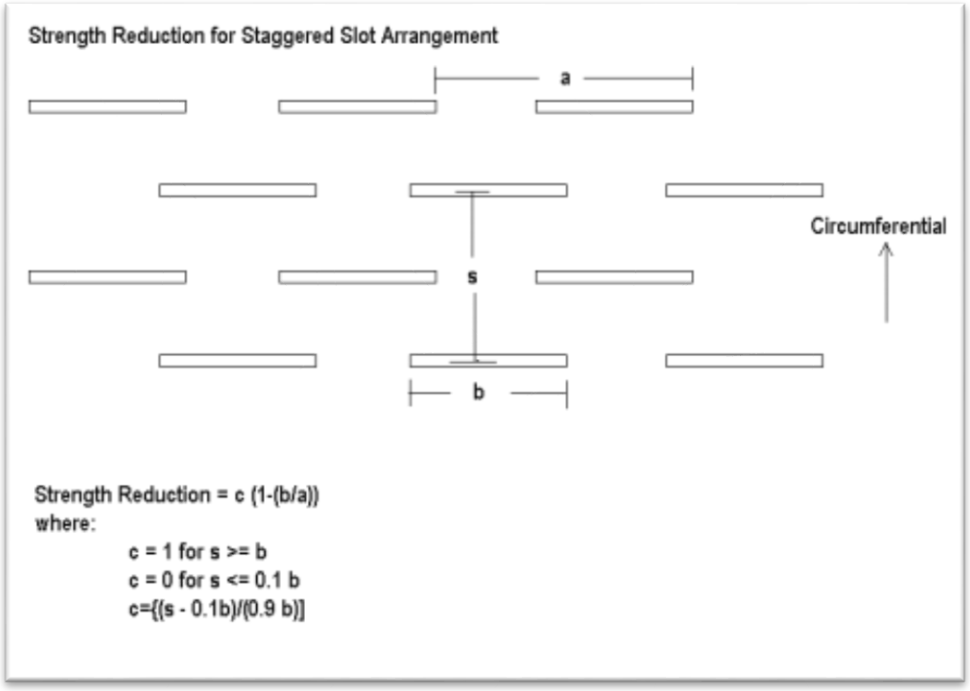

Figure 29 Strength reduction due to slots (George E. King 2009)

According to (George E. King 2009), the strength reduction can be calculated from the equation above. In our case, the strength should be 66.7% of the plain pipe. We'll improve the correlation taken materials grades, and other stuff into consideration. And make an easy to use correlation for quick field application.

To predict the limit load of tubular thin shells, the following equations can be used:

Elastic buckling:

$$\sigma_{cr}^{e} = \frac{2E}{\sqrt{3(1-\nu^2)}}\frac{t}{D}$$

Where E, ν is Young's modulus and Poisson's ratio of steel.

Plastic deformation theory:

$$\sigma_{cr}^{def} = \frac{4}{3}\sqrt{E_t E_S}\frac{t}{D}$$

Where E_t, E_s are tangential and secant Young's modulus.

Incremental plastic theory:

$$\sigma_{cr}^{inc} = \frac{\sqrt{E_t E_S}}{0.845}\frac{t}{D}$$

For plain pipes, these equations are applicable if t/D is smaller than 1/30. But they are not applicable to thick wall pipes. Because when pipes with thick wall induce the local buckling, the tangential Young's modulus becomes close to 0.

Empirical way to determine critical strain is shown as below:

$$\varepsilon_{critical} = \varepsilon\left(\frac{t}{D}, Deformation\ Properties,\ p_{out} - p_{in}, BoundaryCondition\right)$$

When t/D $\rightarrow$ 0,

$$\varepsilon_{critical} = a_1\left(Deformation\ Properties,\ p_{out} - p_{in}, BoundaryCondition\right) * \frac{T}{D}$$

$$+ Higher\ order\ terms$$

As shown in Figure 30, elastic buckling only occurs for large D/t>250, but for my experiments, the maximum D/t = 3.5/0.254=13.8, which is much smaller than 250, so plastic behavior must be considered for my experiments and simulation.

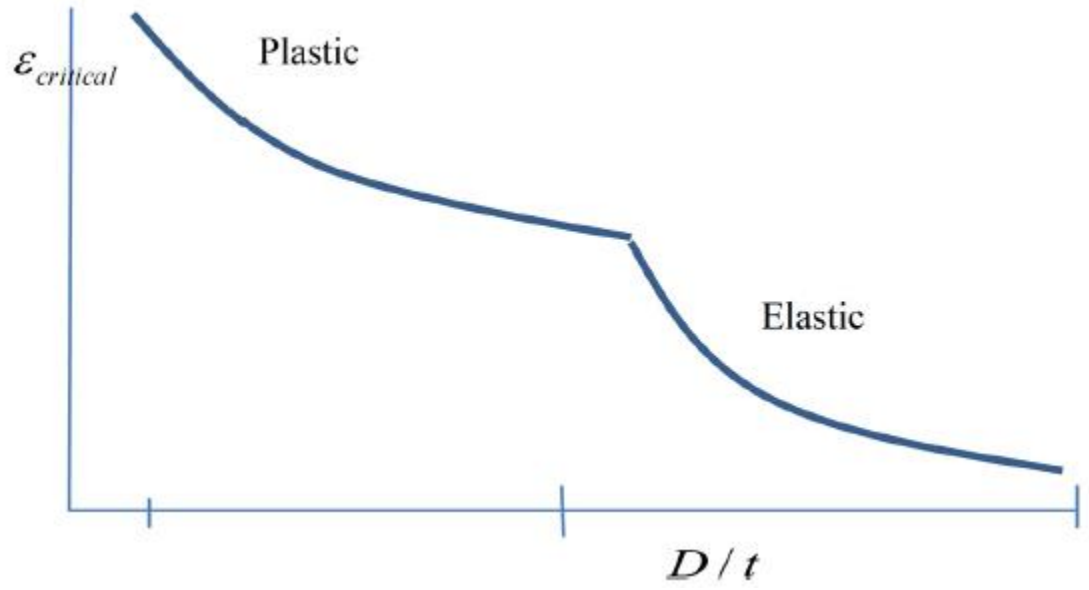

Figure 30 Plastic and elastic behavior under different D/t

According to (Spivak and Horne, 1983), length of slots is not significant from flow point of view. So we design N8L2 and N16L1 to keep the open flow area the same.

As Figure 31 shows, a MTS load frame with 500,000 lb load capacity with data acquisition system. Video camera is set up to monitor the whole process and analyze the local deformation.

Displacement rate is controlled to be constant at 0.24 in/min. For 15% strain, axial displacement = 12*15% = 1.8”. Total load time is 1.8”/0.24 = 7.5 minutes.

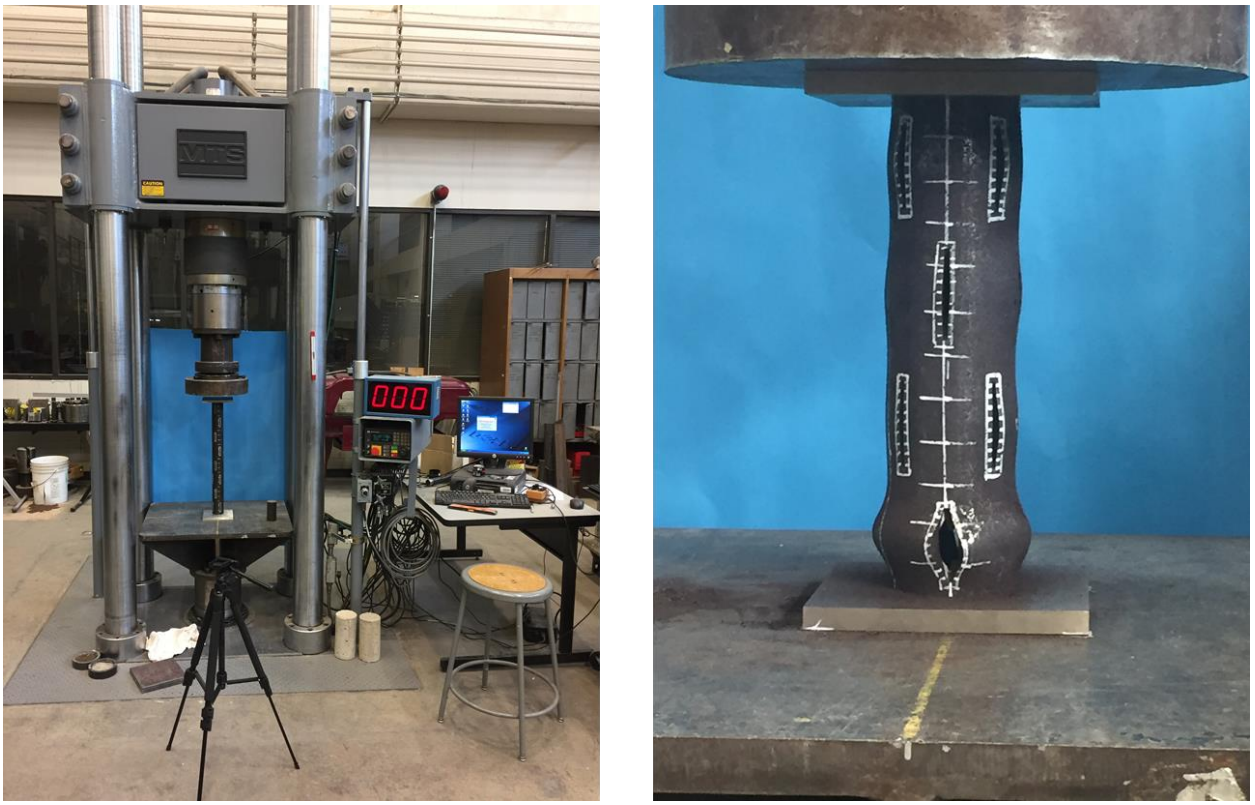

Figure 31 Experiment set up and sample under axial compression

From Figure 32, we can see that slotted liner with 8 slots and slot length of 2 inches (N8L2) deforms more uniformly than slotted liners with 16 slots and slot length of 1 inch (N16L1). The N16L1 sample tends to find a weak level, and once the weak level starts to expand, the load capacity starts to decrease much faster than N8L2 sample. This phenomena can explain why the N8L2 shows stronger properties than N16L1 slotted liners in the following results.

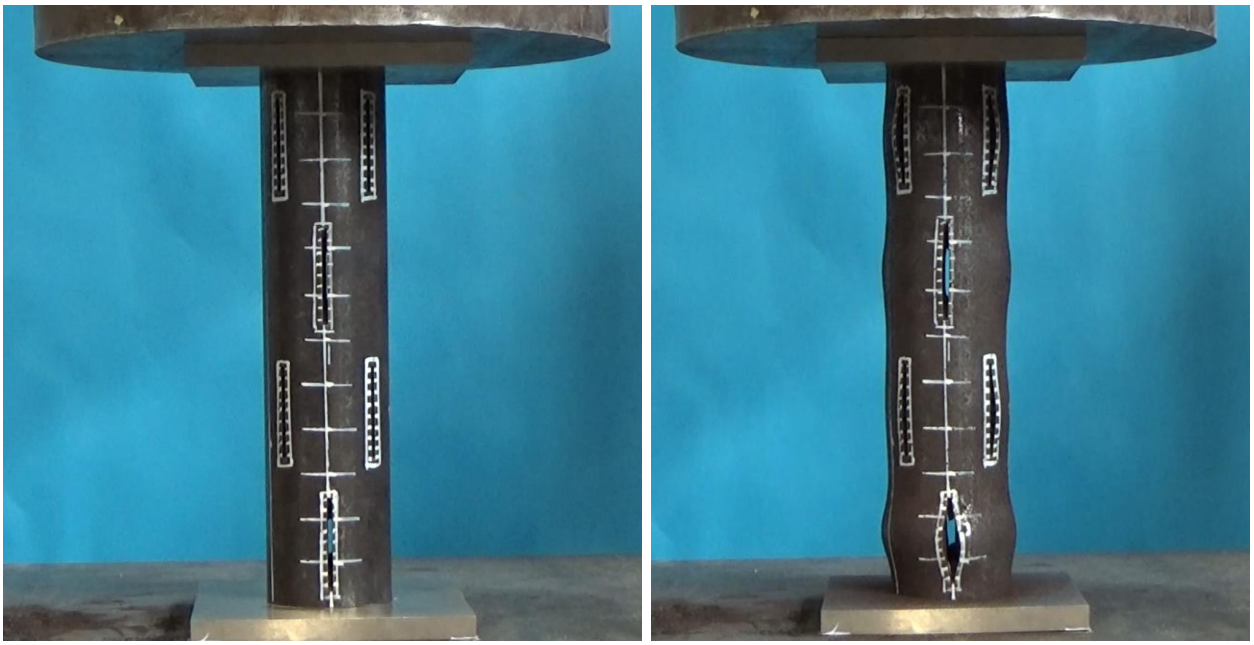

Figure 32 Axial Compression Test for Slort (1 ft) Samples, N8L2 on left, N16L1 on right

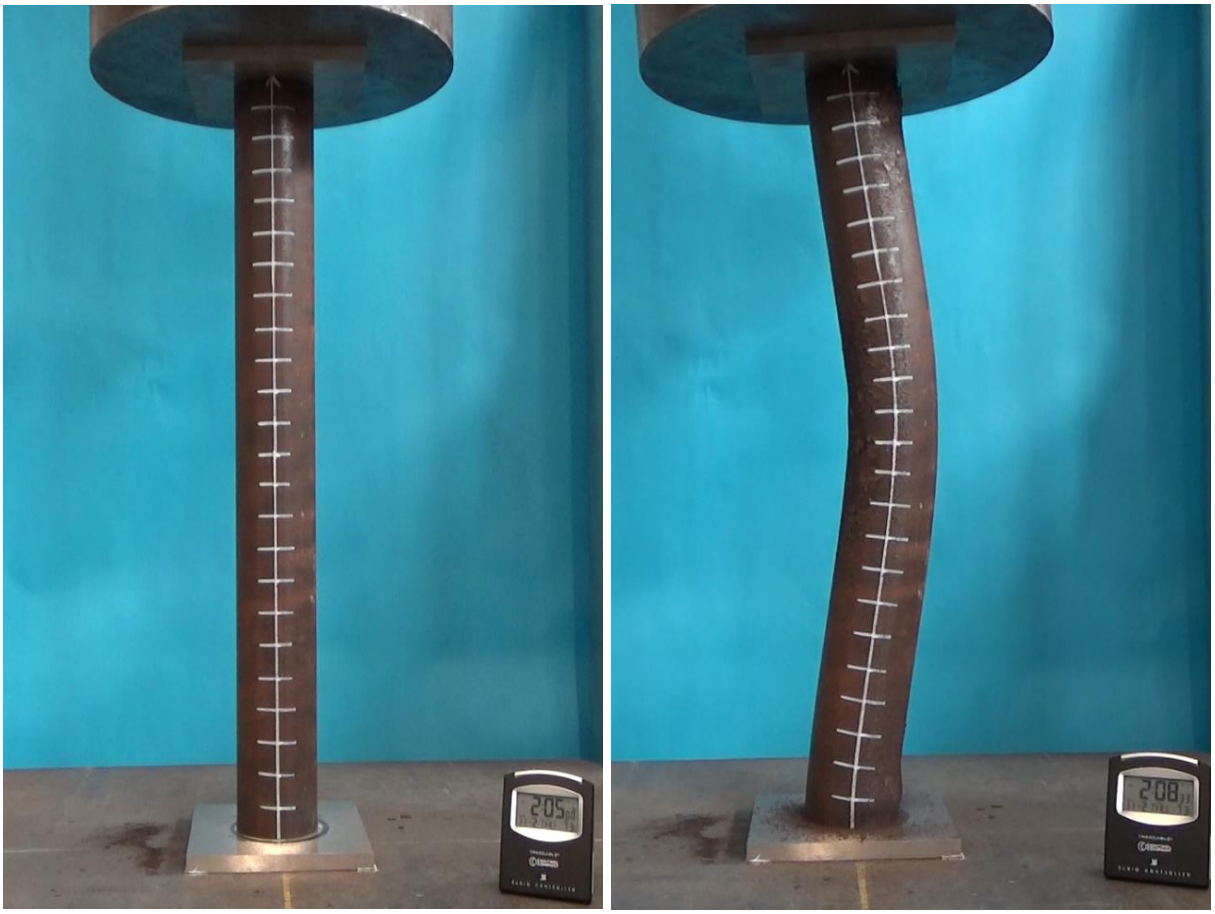

Figure 33 Axial Compression Test for Long (2ft) Base Pipes

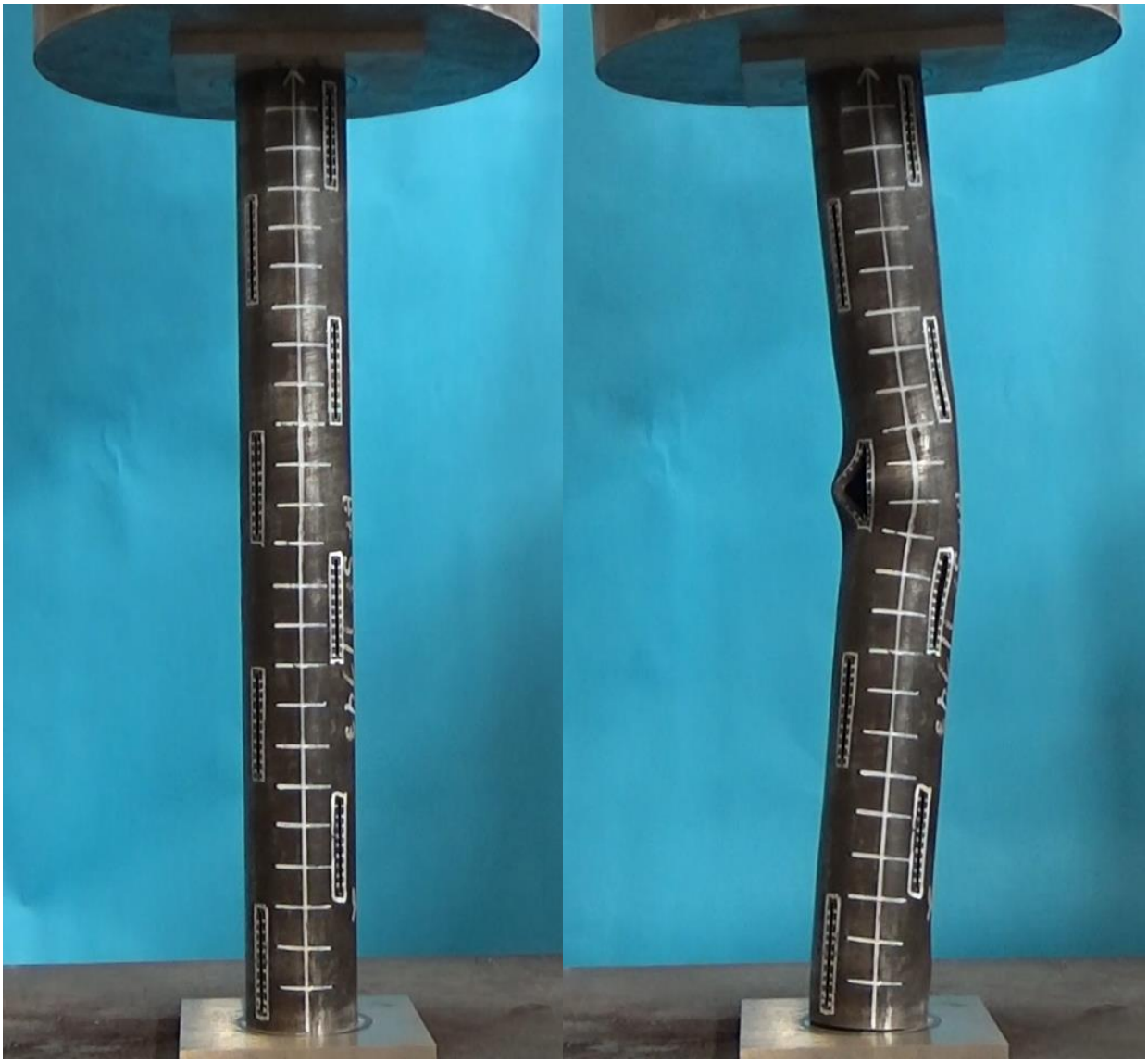

Figure 34 Axial compression test for long (2ft) slotted liners

From figure 33, a long (2 ft) sample is compressed. Since the pipe is long, it is more likely to have global buckling than local buckling. As compared to figure 32, in which shorter (1 ft) samples are shown, shorter samples are more likely to have local buckling at the bottom since the restriction of the bottom plate.

From figure 34, long (2ft) slotted liner sample of L80 is shown. Comparing with shorter samples, the long pipe tends to have lateral buckling. Due to the bending and buckling, the slot in the middle area is open much wider, which will reduce the functionality of the sand control. On the other hand, if the compression continues, the slot may crack from the ends, which will cause severe stability and safety issue. But if the slotted liner is in contact with the wellbore, support from the formation will prevent severe deformation.

The figure 35 shows a typical deformation curve of 3.5'' L80. At the yield point, the pipe didn't show obvious buckling. After the yield point, strain hardening resulted in increased strength till the peak strength. The pipe shows local buckling at both ends. At 10% axial strain, the local buckling becomes obvious at the ends. Because both ends are restricted by the loading plates, they can not expand freely. This explains the local buckling at both ends of the pipe.

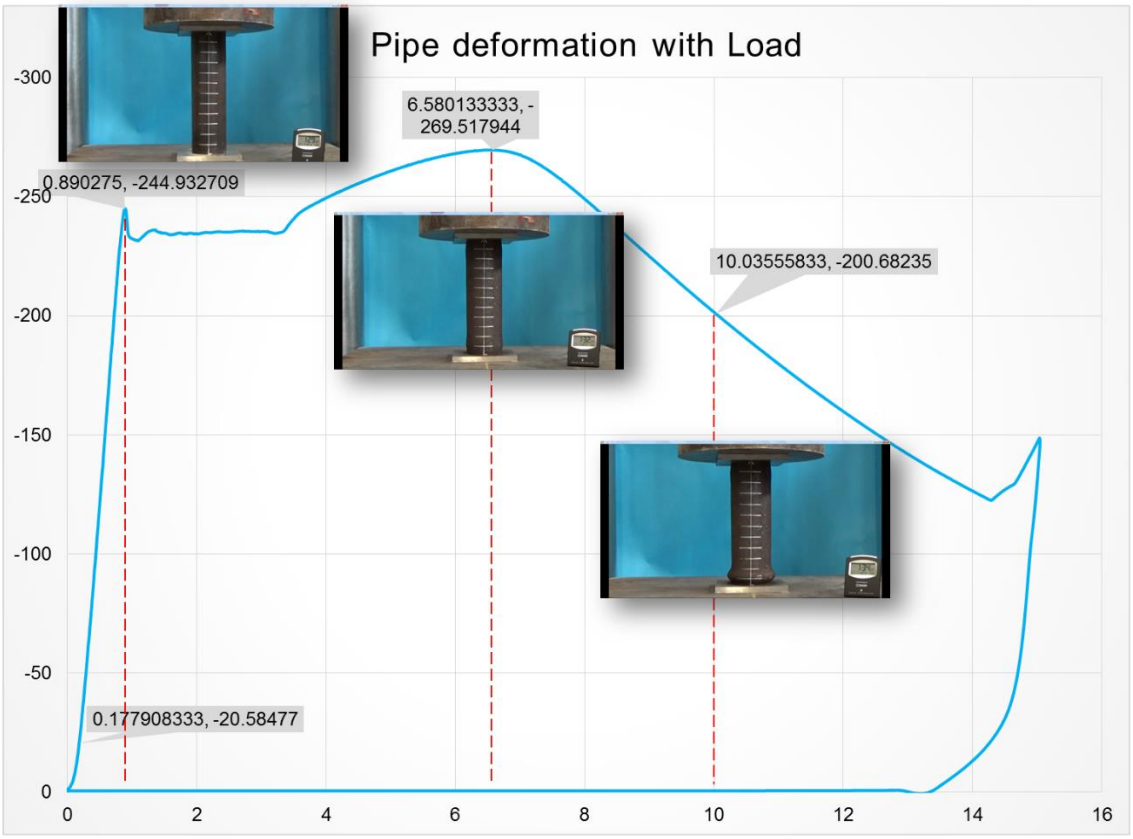

Figure 35 Pipe deformation when the load increases

From figure 36, we can see that even though P110 is a strong steel, but since the diameter is small, it is easier to buckle laterally without holding much load.

In figures 37-39, J55 base pipe and N8L2 slotted liner and N16L1 slotted liner are compared at yield point, peak strength and 10% axial strain point. As we can see in figure 39, N16L1 slotted liner tends to open much wider at a weaker level, which reduce its strength tremendously, whereas the N8L2 slotted liner deforms more uniformly. The larger base pipe area in between the slots provide better support for N8L2. This phenomena explains why the N8L2 design is stronger than N16L1.

In figures 37 and 40-42, the pipes all showed local buckling instead of lateral buckling as shown in figure 36, which illustrates that bigger diameter pipes tends to have local buckling rather than lateral buckling.

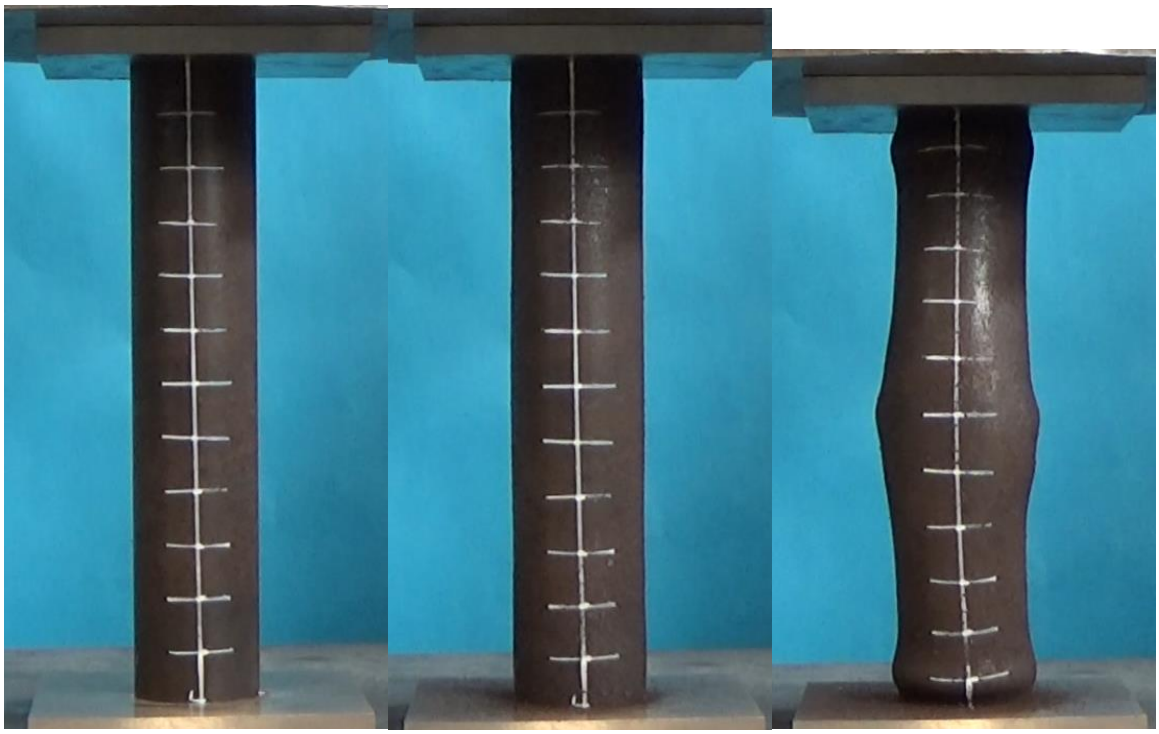

Figure 36 2 3/8" P110 under compression at yield point, peak strength, 10% axial strain

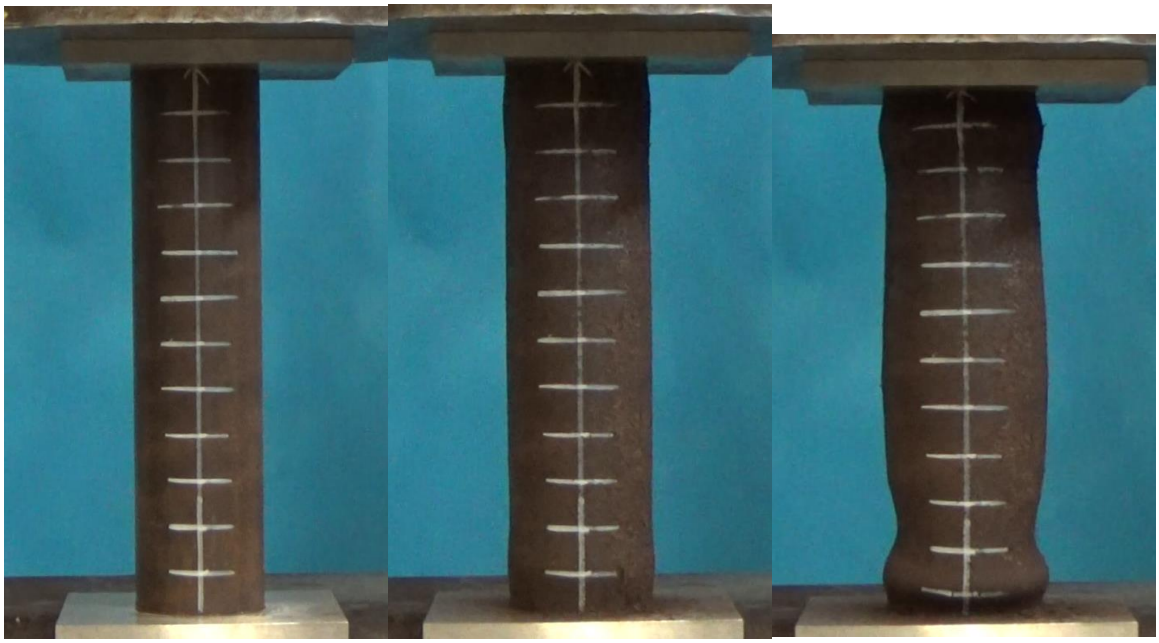

Figure 37 2 7/8” J55 under compression at yield point, peak strength, 10% axial strain

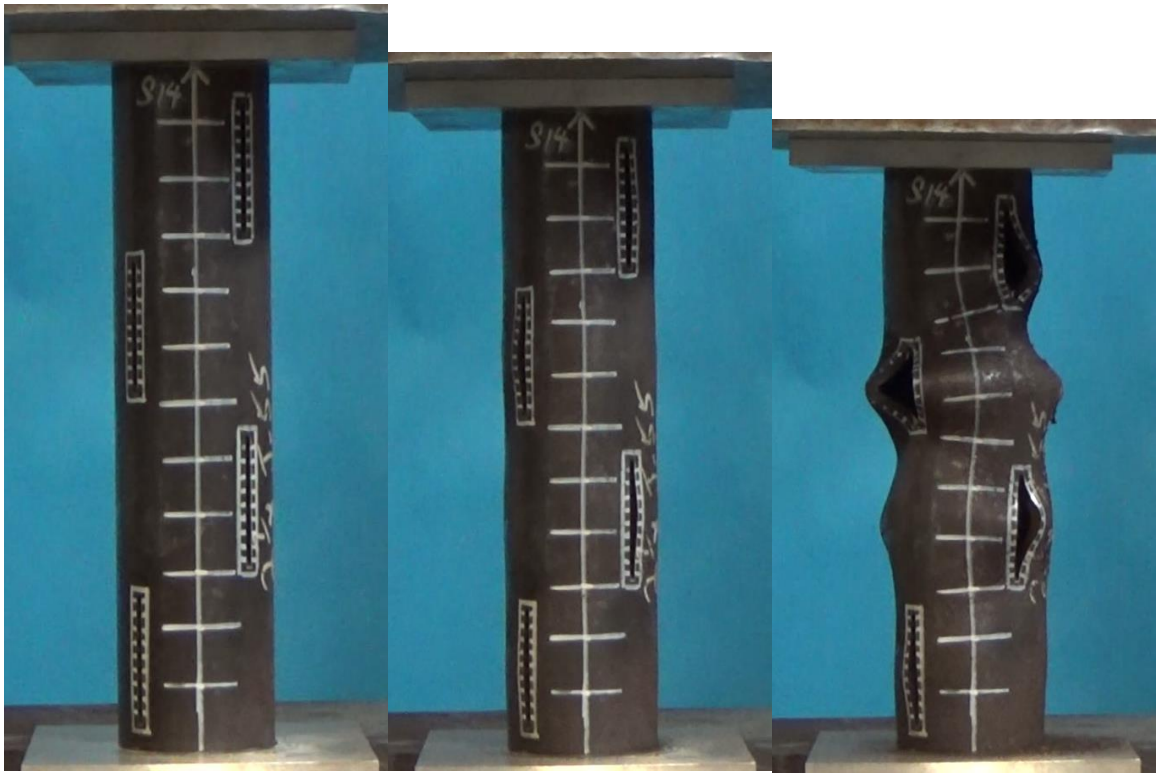

Figure 38 2 7/8" J55 N8L2 slotted liners under compression at yield point, peak strength, 10% axial strain

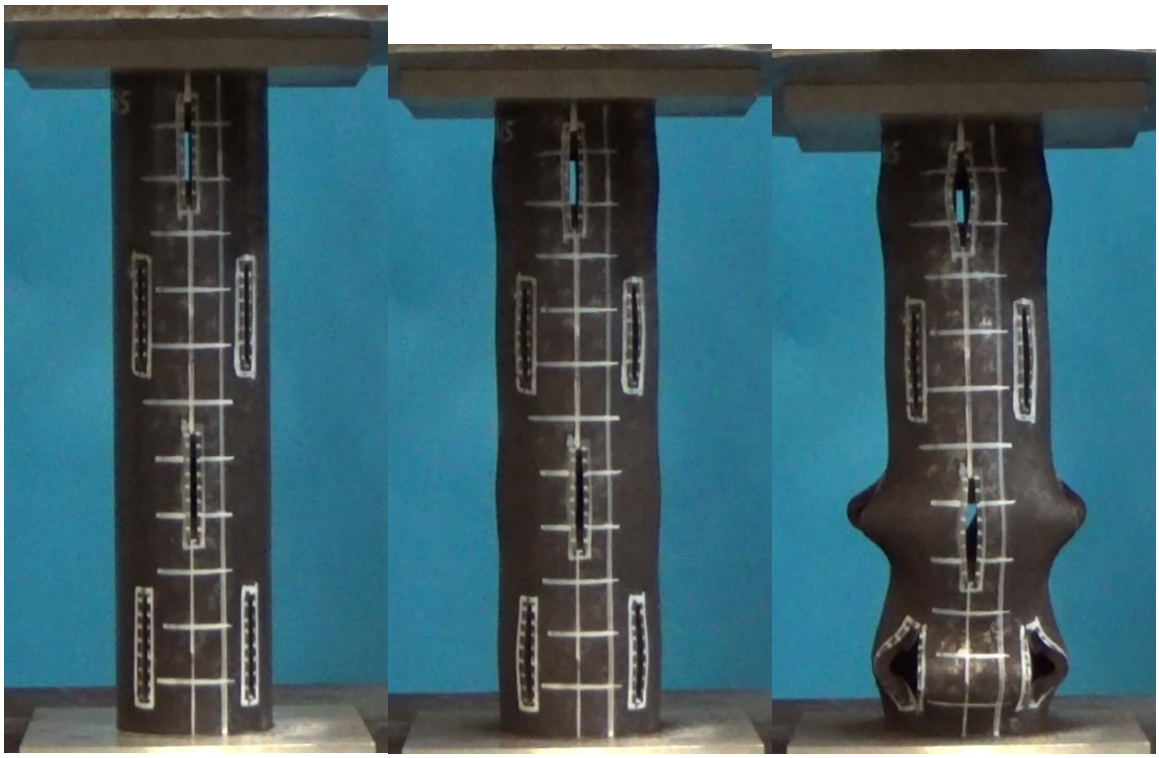

Figure 39 2 7/8” J55 N16L1 slotted liners under compression at yield point, peak strength, 10% axial strain

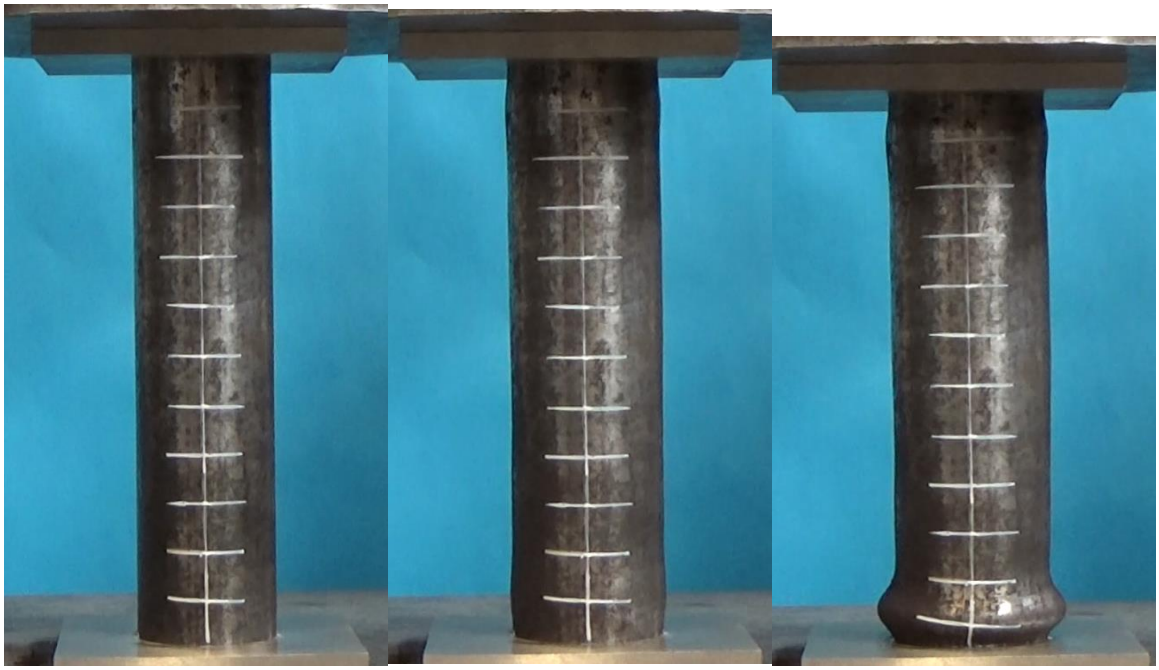

Figure 40 2 7/8" light L80 at yield point, peak strength, 10% axial strain

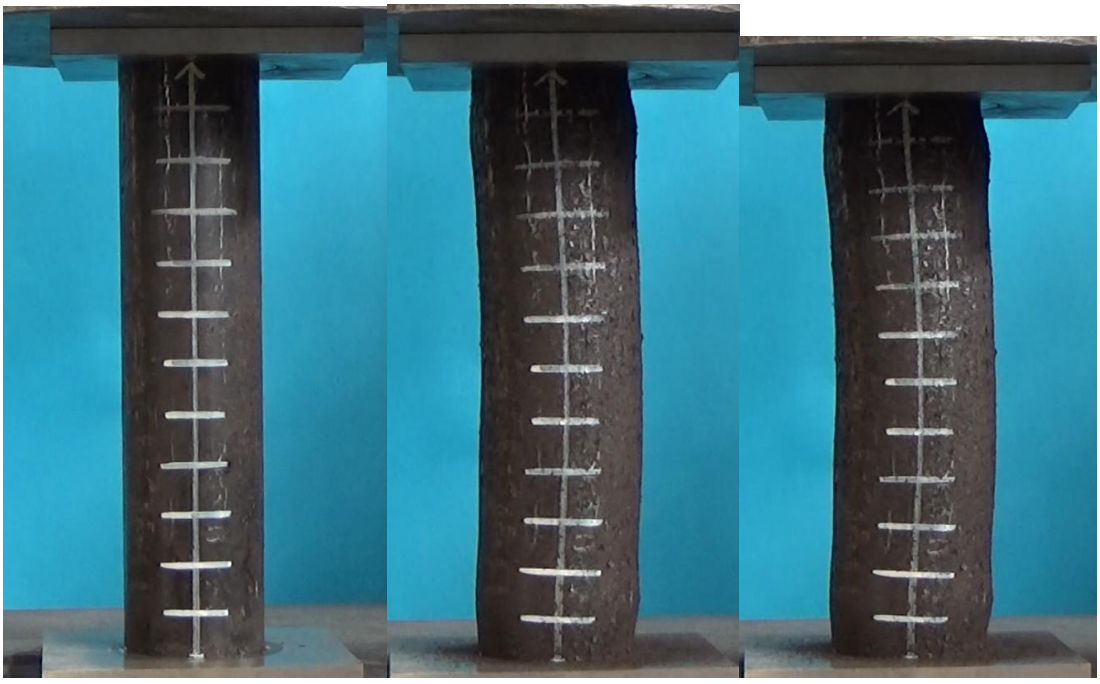

Figure 41 2 7/8" heavy L80 at yield point, peak strength, 10% axial strain

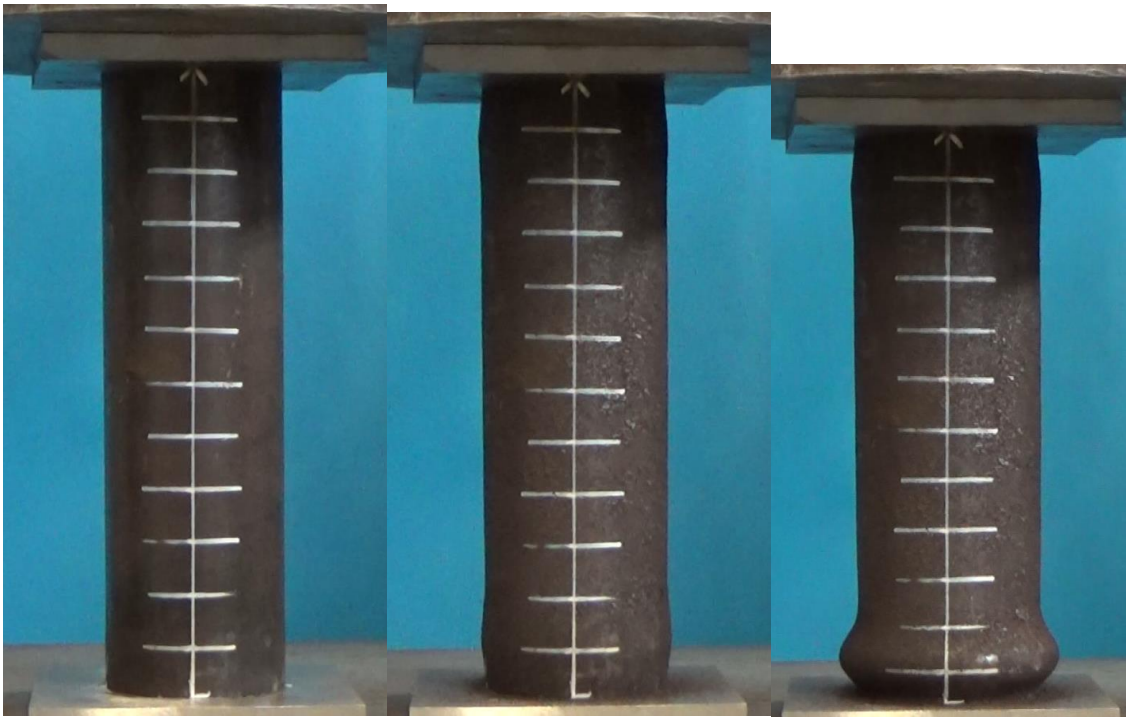

Figure 42 3 1/2" L80 at yield point, peak strength, 10% axial strain

2.2.2 Line Load Collapse Test

Line load collapse test are performed to simulate the situation where horizontal section is under geotectonic load. A sketch is shown in figure 43.

In line load collapse test, we can see the simulation result matched well with the experimental results. The boundary conditions are displacement control at rate of 0.24 in/min, and fix the bottom edge on x, y, z directions. Line load was applied on top edge of the slotted liner sample, with restricted movements in x and y direction because of the friction between slotted liner and plate. As we can see from the picture, the slots on top and bottom surfaces become narrower, while the slots on both sides become larger. Which will cause more sand to flow into the wellbore from both sides.

In this section, six different samples are tested as shown in figure 44, they all have same OD of 2 7/8”, difference is the material grades and slot distribution. Experimental apparatus is shown in figure 45. Record camera is used to record the whole process.

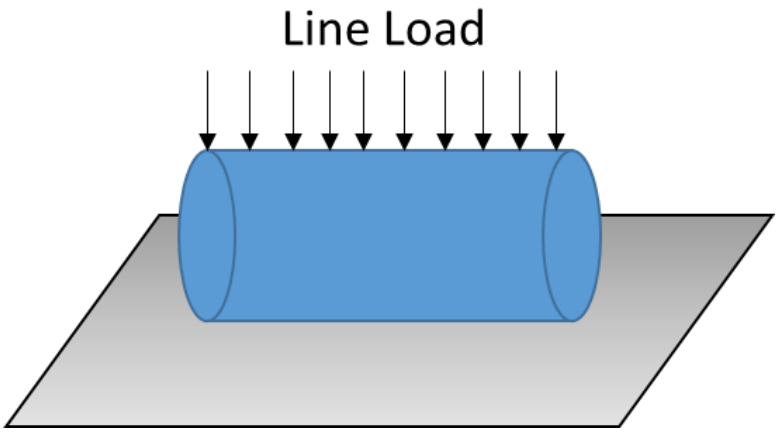

Figure 43 Sketch for line load test

Figure 44 Samples used for line load test

Figure 45 Experimental setup for line load test

Table 1 Line Load Collapse Test Samples

Grade	OD (inch)	Thickness(inch)	D/t	Slot Number/ft	Slot Legnth (ID,inch)	Slot Width (inch)	Sample No.
J55	2.875	0.217	13.249	8	1	0.125	L1
J55	2.875	0.217	13.249	16	2	0.125	L2
L80L	2.875	0.217	13.249	8	1	0.125	L3
L80L	2.875	0.217	13.249	16	2	0.125	L4
L80H	2.875	0.309	9.304	8	1	0.125	L5
L80H	2.875	0.309	9.304	16	2	0.125	L6

From figures 46-48, the deformed slotted liners after line load collapse test are shown. All the samples show similar deformation type, with slots on the load direction closing, and slots on the horizontal direction opening.

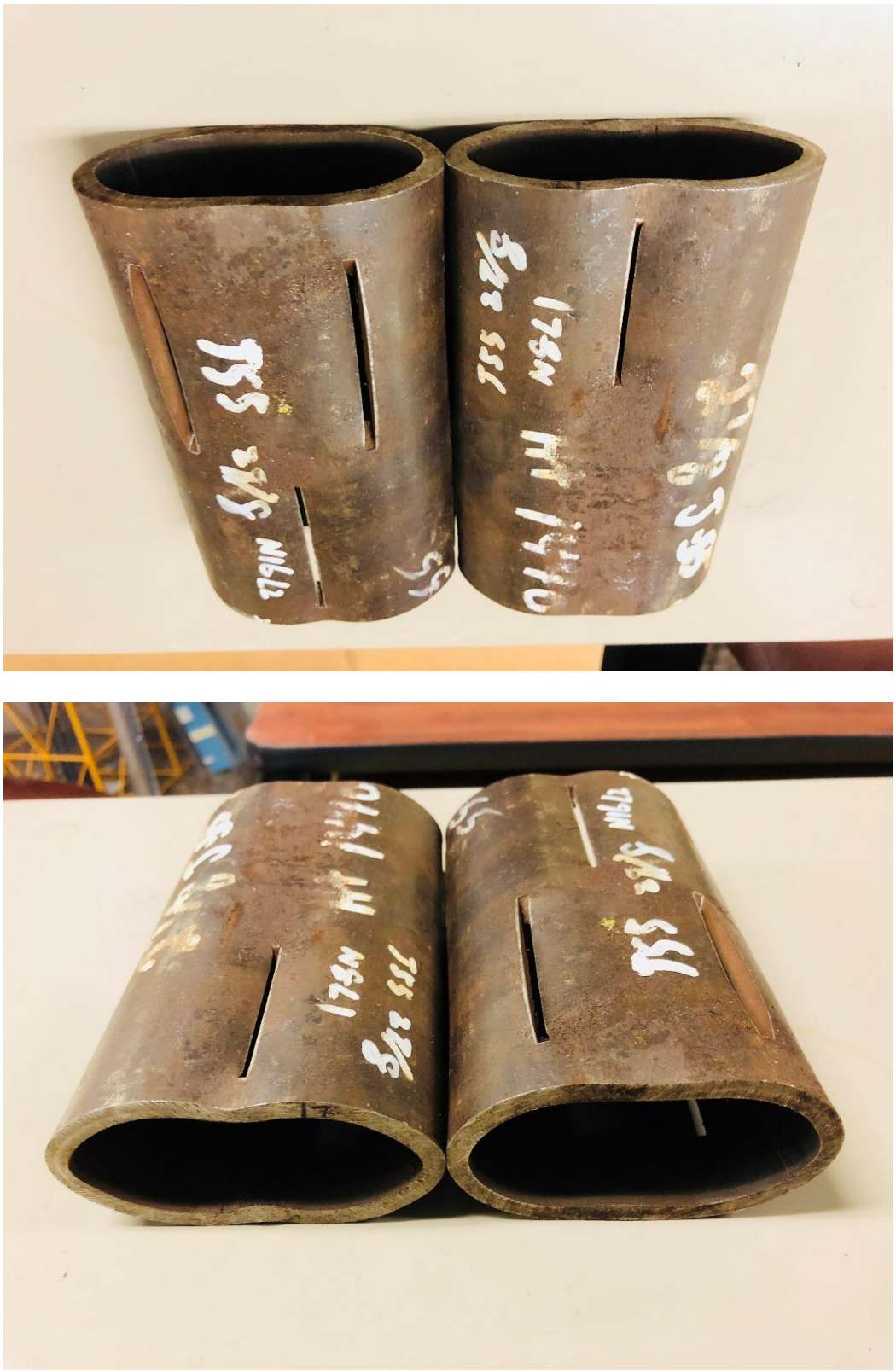

Figure 46 2 7/8" J55 samples after line load test

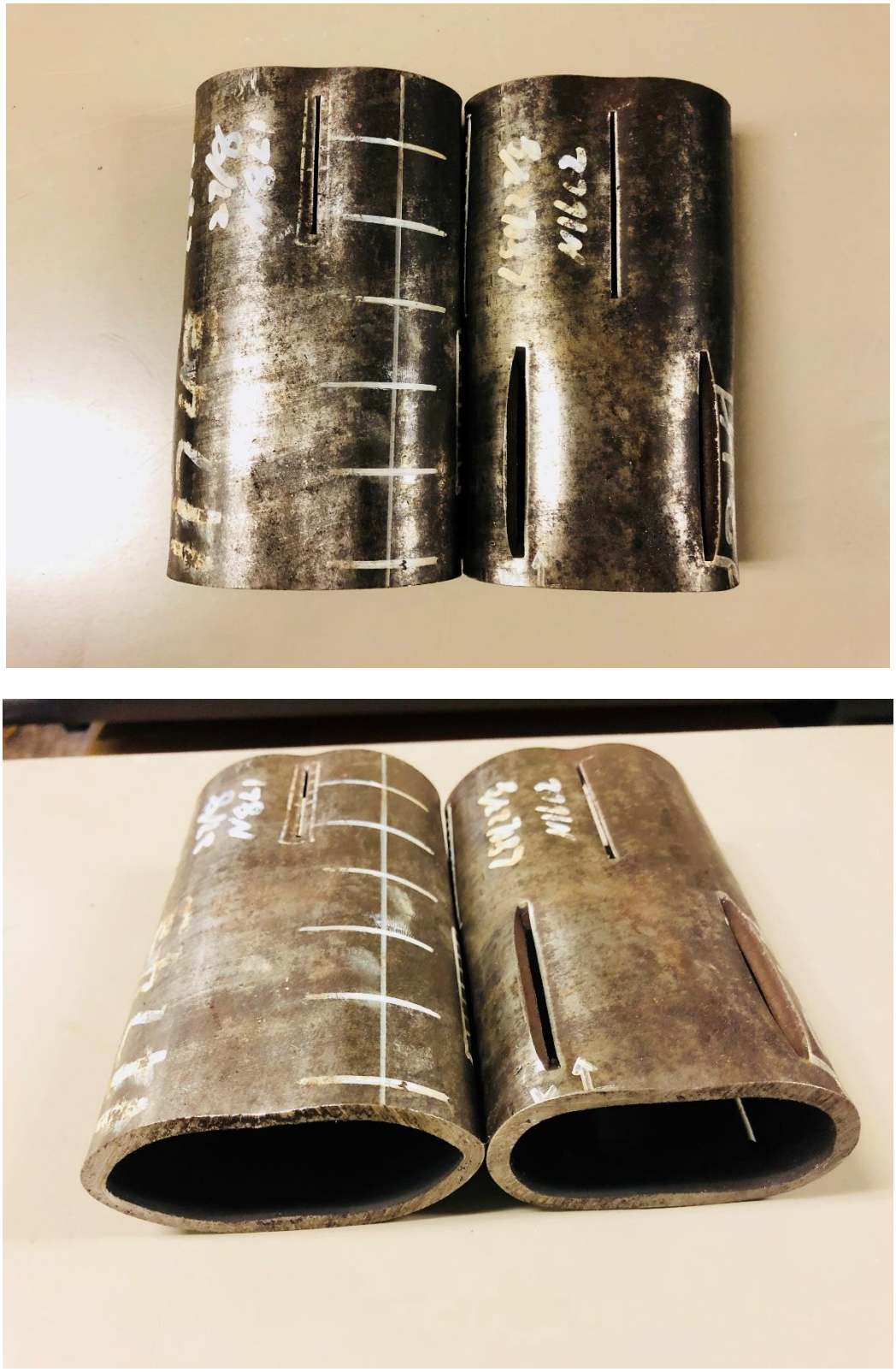

Figure 47 2 7/8" thin wall L80 samples after line load test

Figure 48 2 7/8" L80 thick wall samples after line load test

From figures 49 and 50, we compared deformed slots on different directions with the original slots. We can tell that on the side which is 90 degrees from the loading direction, the slot opened wider because of plastic deformation. Under this circumstance, bigger and more sand can flow into the wellbore, the functionality of sand control will be reduced. On the other hand, with wider opening, the structure is less stable than the original slotted liners, stability issue may occur suddenly if crack initiates at the ends of the slots.

On the contrary, figure 50 shows the closing of slots. The width of slots reduces tremendously, which will influence the oil/gas production. OFA (Open Flow Area) will become so small that the profit for the well is lower than expectation.

Figure 49 Slot opening on the side of the load comparing with original slot

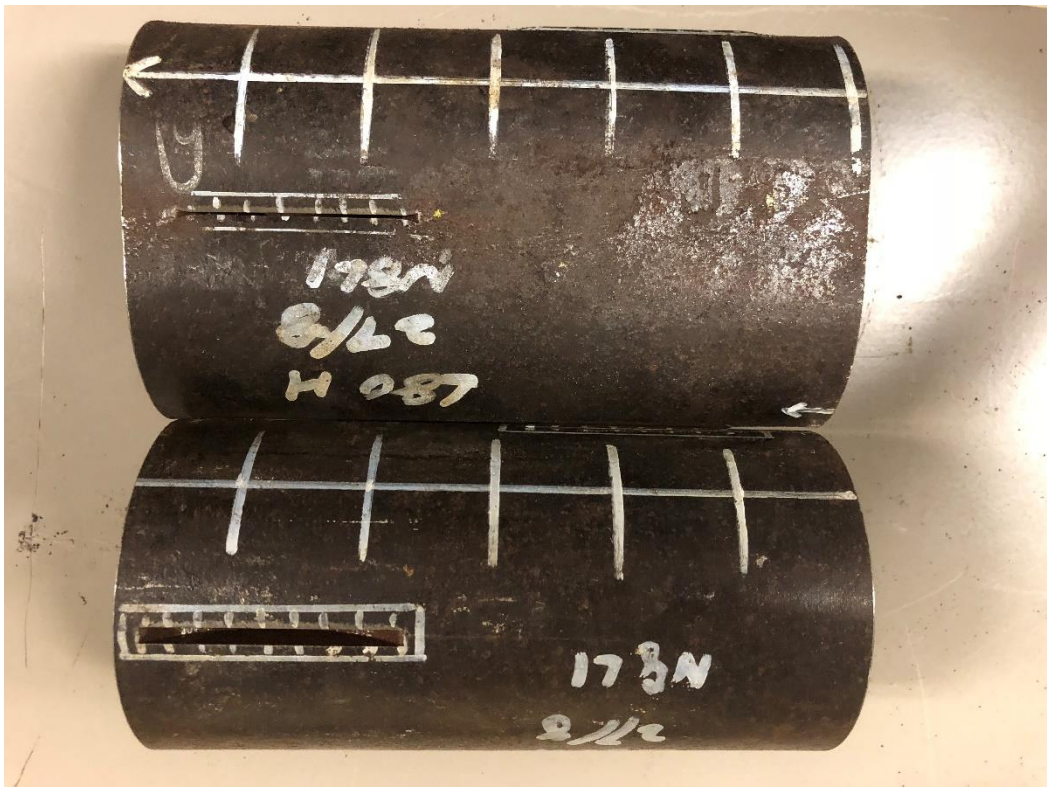

Figure 50 Slot closing under the load on the loading direction comparing with original slot

According to (Chartier, 2016), the slot width change is measured at the axial mid-level length of the slots on the OD of the liner. He indicated that higher initial levels of plastic twist increase the tendency for the slots to open under compressive axial strain.

In line load collapse test, we can see the simulation result matched well with the experimental results in figures 46- 48. The boundary conditions are displacement control at rate of 0.24 in/min, and fix the bottom edge on x, y, z directions. Line load was applied on top edge of the slotted liner sample, with restricted movements in x and y direction because of the friction between slotted liner and plate. As we can see from the picture, the slots on top and bottom

surfaces become narrower, while the slots on both sides become larger. Which will cause more sand to flow into the wellbore from both sides. Also, the collapse will cause stability issue.

Figure 51 Experiment: slot deformation after line load collapse test. Load direction on the left, horizontal cross-section on the right.

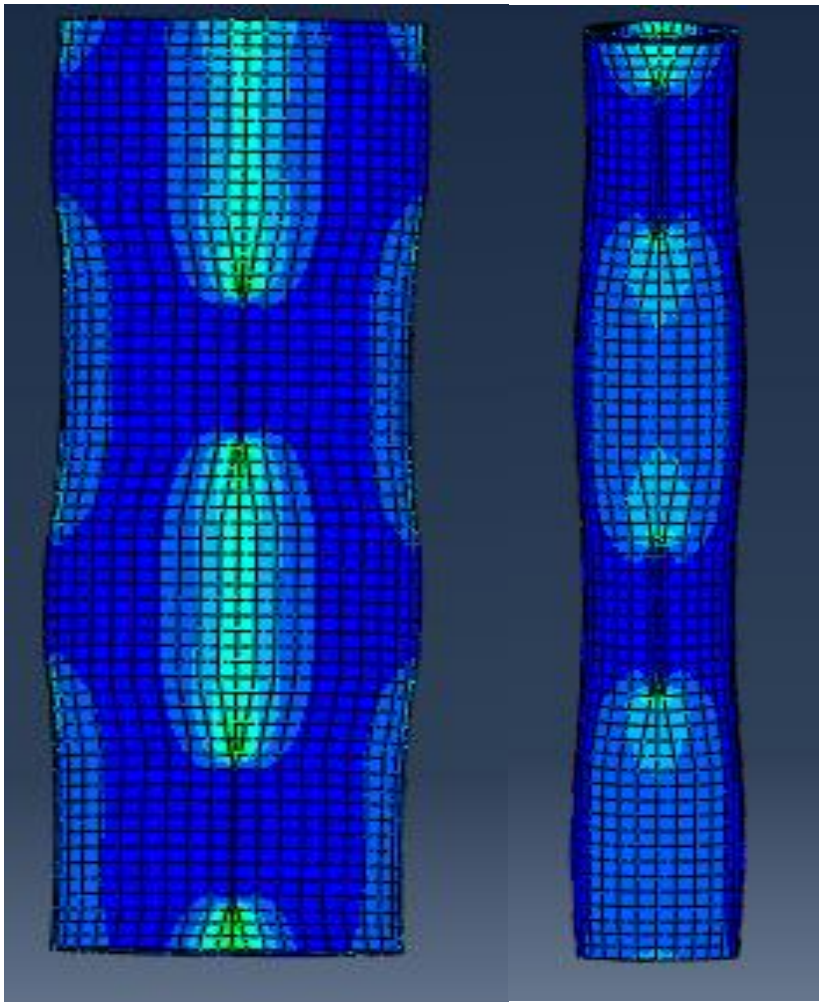

Figure 52 Slot deformation after line load collapse test

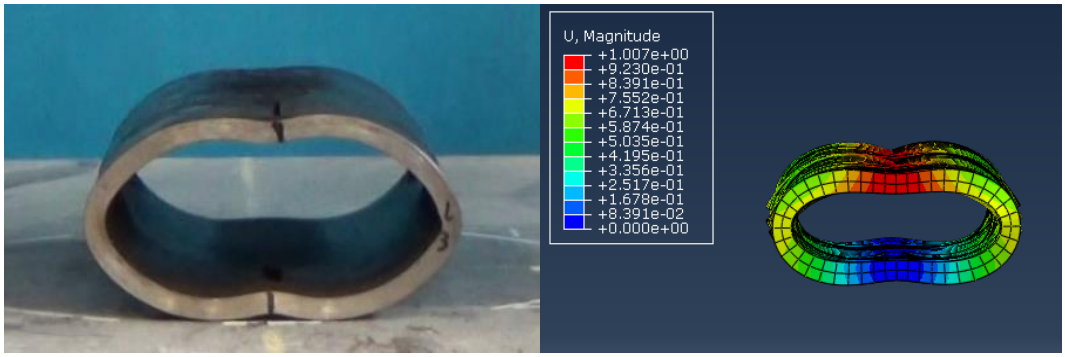

Figure 53 Deformation on load direction: experiment vs. simulation

So, it is really important to keep the integrity of the slotted liners to ensure wellbore stability and efficient production rate.

2.2.3 Triaxial Collapse Test

External pressure is exerted on the liner in horizontal wells by formation loading, which is a function of the weight of the overburden, formation horizontal stresses and the fluid pressure. Which can be obtained from the Geo3D finite element code after input the formation properties.

In the initial experiment, confining pressure applied by oil kept increasing. And the strain also increases. Before reaching 3000 psi, strain is linearly proportional to confining pressure Pc.

Figure 54 shows the triaxial load frame – GCTS RTX – 1500, it has standard 1,500 kN Load capacity and 1,750 kN/mm stiffness. The control panel in figure 55 can automatically control the flow rate and confining pressure.

Figure 56 showed out sample design to fix in the load cell. Supporting rod in between the top and bottom spacers is used to prevent axial compression to the sample. Top and bottom spacers are designed to align the sample in the center of the load cell.

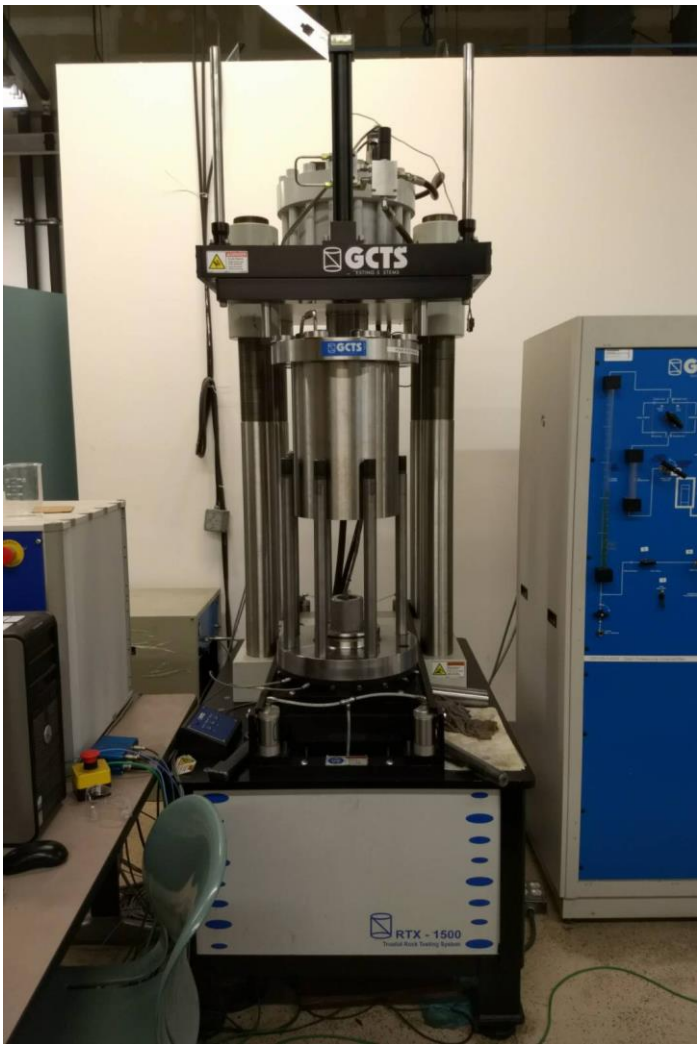

Figure 54 GCTS RTX - 1500 Triaxial Load Frame

Figure 55 Control Panel for GCTS Triaxial Load Frame

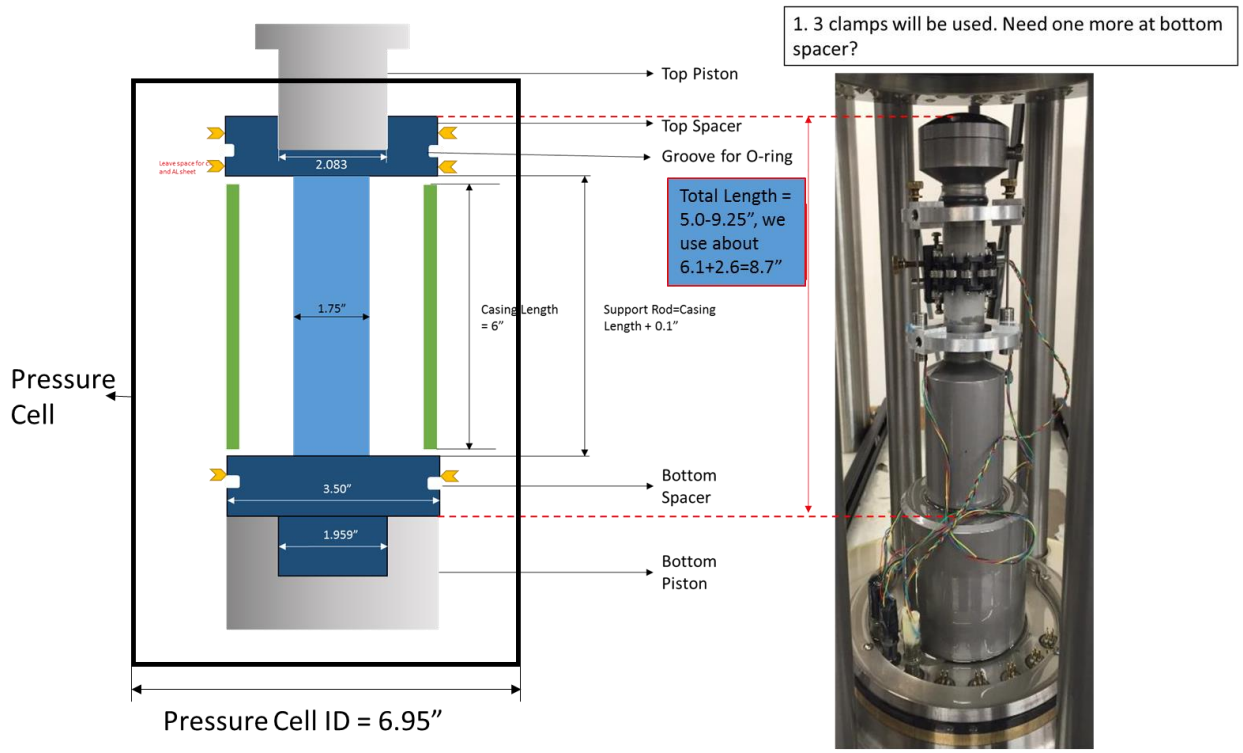

Figure 56 Triaxial Collapse Equipment and Sample Setup

As shown in Figure 57, the slotted liner was assembled with the top and bottom spacers by epoxy glue. Steel plates were placed on top of slots to prevent oil from penetrating inside the pipe. Rubber tape was placed on steel plates to keep them in place. Then, heat shrinkage tube and clamps were used to seal the whole sample. Finally, the radial strain gauge was put around the slotted liner to get the deformation through the recording system. Due to load frame under maintenance, the triaxial collapse test will be carried out once the repair process is finished.

Figure 57 Sample for Triaxial Collapse Test

Table 2 Triaxial Collapse Test Samples

Sample Name	OD (in)	Material	Slot Number	Slot Length
C1	2.875	L80_light	8	1
C2	2.875	L80_light	16	2
C3	2.875	L80_heavy	8	1
C4	2.875	L80_heavy	16	2
C5	2.875	J55	8	1
C6	3.5	L80	8	1
Spare	2.785	J55	8	1

3. RESULTS*

3.1 Axial Compression Test

All detailed results are summarized in Table 3. Steel grades, pipe diameter, thickness, D/T, length of pipe, density of slots, length of slots are considered. The D/T ratio ranges from 9.3 to 13.8. Slot patterns are N8L2 and L16L1. The 1ft base pipe of 2 7/8" heavy L80 has the highest peak strength which is 279.5×10^3 lbs. Strain at its peak strength is 9.8%. Effects of steel grade and slot density, slot pattern will be discussed in detail.

Table 3 All results for compression tests

No.	Grade	OD (inch)	Thickness(inch)	D/T	Weight (lb/ft)	Length of Samples (ft)	Slot Number/ft	Slot Legnth (ID,inch)	Slot Width (inch)	Sample No.	Yield Strength(10^3lb)	Max Strength(10^3lb)	Strain % at Max Strength
1	N80	2 3/8	0.19	12.5	4.7	1'	8	2''	0.125	S12	-135.647964	-139.403191	1.861141667
2	N80	2 3/8	0.19	12.5	4.7	2'	8	2''	0.125	S32	-119.538811	-128.352097	0.889895833
3	N80	2 3/8	0.19	12.5	4.7	1'	16	2''	0.125	S1	-111.859756	-129.133797	1.625458333
4	N80	2 3/8	0.19	12.5	4.7	1'	16	1''	0.125	S7	-124.918747	-133.915962	2.502808333
5	N80	2 3/8	0.19	12.5	4.7	2'	16	1''	0.125	S33	-111.047401	-124.091064	0.788020833
6	N80	2 3/8	0.19	12.5	4.7	1'	-	-	-	S2	-128.122185	-151.92572	4.065166667
7	N80	2 3/8	0.19	12.5	4.7	2'	-	-	-	S3	-111.032074	-132.751076	0.931708333
8	P110	2 3/8	0.19	12.5	4.7	1'	8	2''	0.125	S4	-177.399948	-182.62661	1.5692
9	P110	2 3/8	0.19	12.5	4.7	1'	16	1''	0.125	S6	-171.897392	-180.986572	1.604925
10	P110	2 3/8	0.19	12.5	4.7	2'	16	1''	0.125	S5	-174.778954	-179.729721	0.8039875
11	P110	2 3/8	0.19	12.5	4.7	1'	-	-	-	S8	-187.163536	-195.700928	3.038041667
12	P110	2 3/8	0.19	12.5	4.7	2'	-	-	-	S34	-192.574127	-192.574127	0.779654167
13	J55	2 7/8	0.217	13.2	6.5	1'	8	2''	0.125	S14	-116.427338	-135.111504	2.495208333
14	J55	2 7/8	0.217	13.2	6.5	2'	8	2''	0.125	S30	-111.53788	-125.853722	1.189820833
15	J55	2 7/8	0.217	13.2	6.5	1'	16	1''	0.125	S15	-115.369743	-134.912247	2.749133333
16	J55	2 7/8	0.217	13.2	6.5	2'	16	1''	0.125	S29	-115.017212	-125.148659	1.1856375
17	J55	2 7/8	0.217	13.2	6.5	1'	-	-	-	S16	-126.850006	-153.519775	5.169833333
18	J55	2 7/8	0.217	13.2	6.5	2'	-	-	-	S31	-123.738533	-131.846756	1.242658333
19	L80_light	2 7/8	0.217	13.2	6.5	1'	8	2''	0.125	S17	-154.485405	-158.409233	0.827933333
20	L80_light	2 7/8	0.217	13.2	6.5	2'	8	2''	0.125	S22	-160.003288	-160.003288	0.537891667
21	L80_light	2 7/8	0.217	13.2	6.5	1'	16	1''	0.125	S18	-152.615456	-159.51281	2.0953
22	L80_light	2 7/8	0.217	13.2	6.5	2'	16	1''	0.125	S23	-157.183037	-161.060883	1.044991667
23	L80_light	2 7/8	0.217	13.2	6.5	1'	-	-	-	S9	-174.824936	-189.156105	5.854075
24	L80_light	2 7/8	0.217	13.2	6.5	2	-	-	-	S24	-167.299156	-167.299156	0.561458333
25	L80_heavy	2 7/8	0.309	9.3	8.44	1'	8	2''	0.125	S11	-203.487274	-226.018631	4.455941667
26	L80_heavy	2 7/8	0.309	9.3	8.44	2'	8	2''	0.125	S25	-203.410637	-203.410637	0.542070833
27	L80_heavy	2 7/8	0.309	9.3	8.44	1'	16	1''	0.125	S10	-205.403206	-233.942924	5.17135
28	L80_heavy	2 7/8	0.309	9.3	8.44	2'	16	1''	0.125	S26	-204.83609	-206.108269	0.797141667
29	L80_heavy	2 7/8	0.309	9.3	8.44	1'	-	-	-	S13B	-212.867676	-279.557426	9.7877
30	L80	3 1/2	0.254	13.8	9.3	1'	8	2''	0.125	S19	-231.26062	-231.26062	0.849983333
31	L80	3 1/2	0.254	13.8	9.3	2'	8	2''	0.125	S27	-228.67028	-228.67028	0.546254167
32	L80	3 1/2	0.254	13.8	9.3	1'	16	1''	0.125	S20	-222.493317	-229.605255	4.154975
33	L80	3 1/2	0.254	13.8	9.3	2'	16	1''	0.125	S28	-225.129639	-226.509109	0.8591
34	L80	3 1/2	0.254	13.8	9.3	1'	-	-	-	S21	-244.932709	-269.563927	6.542875

In Figure 57, steel grade effect on base pipes are shown. 3.5" OD L80 has the highest yield point, 2 7/8" OD heavy L80 has the maximum ultimate strength. 2 3/8" OD P110 shows

* Part of this dissertation is reprinted with permission from "3D Finite Element Analysis and Experimental Study of Stability of Slotted Liners." by X. Liu, N. Morita. ARMA- 2018-269 presented at 52nd US Rock Mechanics/Geomechanics Symposium, 17-20 June 2018 in Seattle, WA. Copyright 2018 by American Rock Mechanics Association.

the third highest yield strength, but as the strain increases, it can not sustain large loading capacity due to its smaller OD. If the diameter of pipes is smaller, it is easier for the pipes to buckle laterally. 2 3/8” N80 shows the lowest yield point and peak strength, which is not recommended for field application. Comparing with light 2 7/8” L80, although yield strength of 2 7/8” J55 is smaller, but after larger deformation, J55 can still hold good load capacity.

In figure 59, steel grade effect on the N8L2 slotted liners are shown. We can tell that 2 7.8” J55 maintains great loading capacity even after large deformation till 15% strain. In figure 60, similar trends remains for N16L1 type slotted liners.

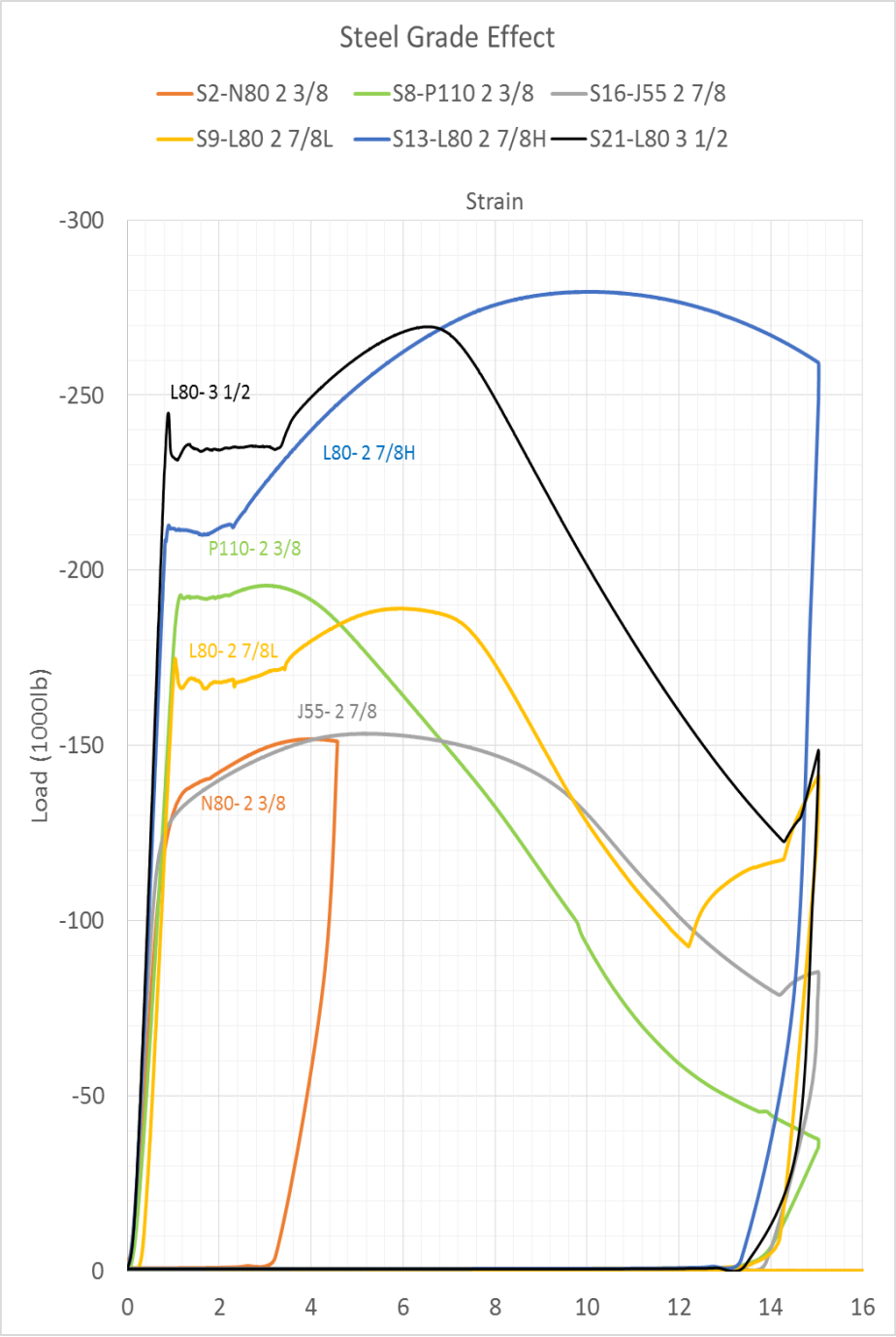

Figure 58 Steel grade effect on base pipes

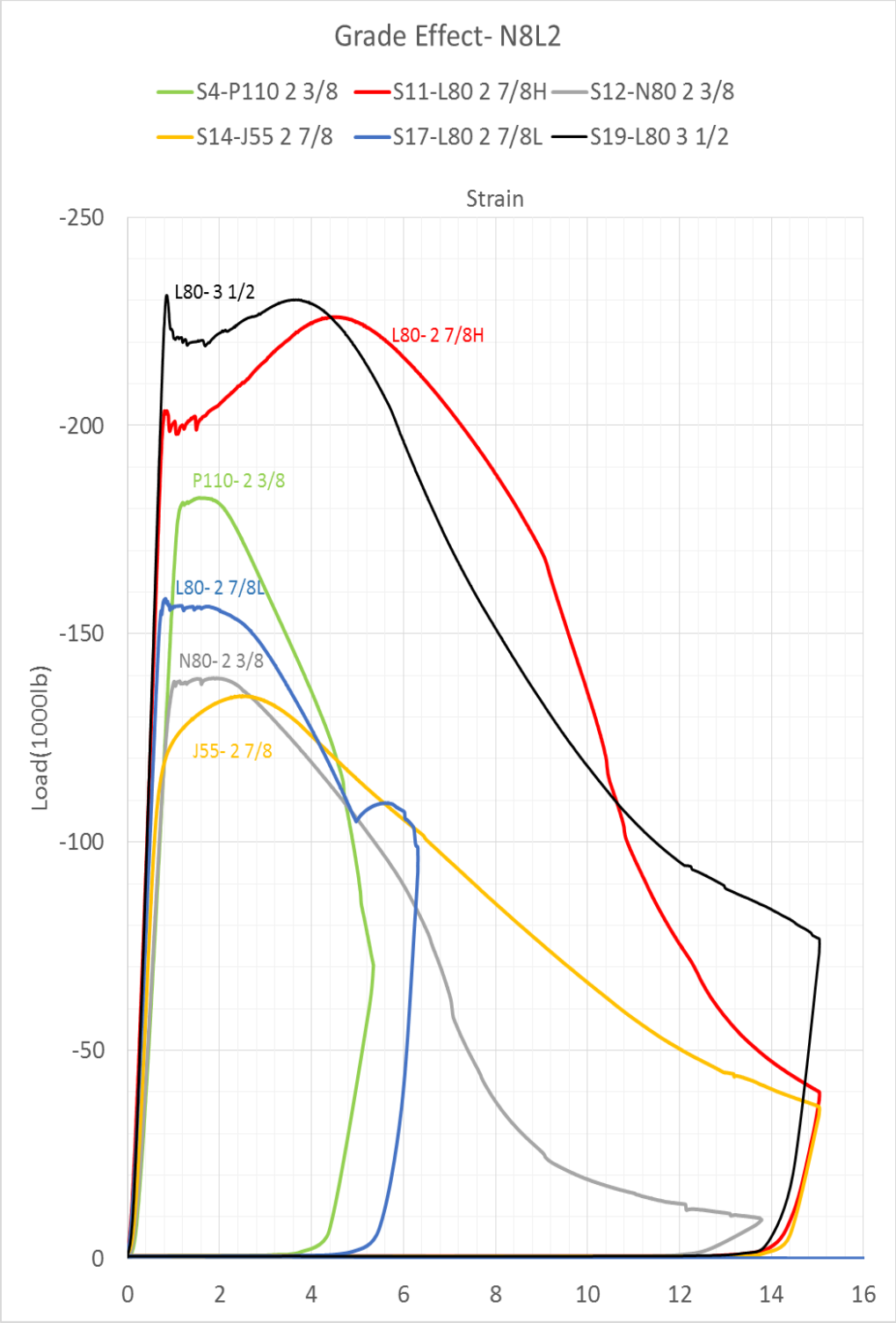

Figure 59 Steel grade effect for N8L2 slotted liners

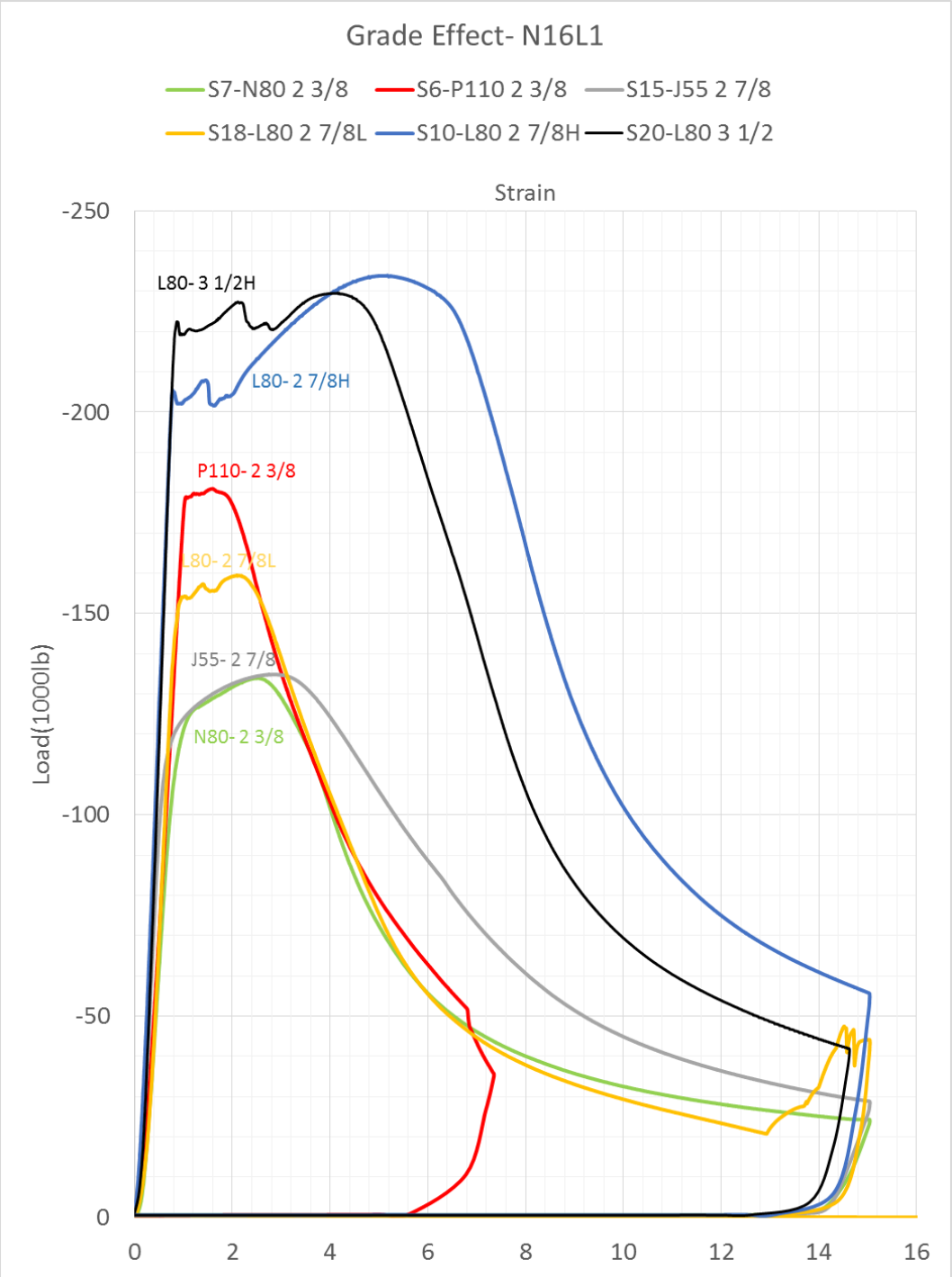

Figure 60 Grade effect for N16L1 slotted liners

From figure 61, slot pattern effect are studied. For 2 3/8” N80 steel grade, 1 ft sample of N8L2 pattern shows much higher yield and peak strength than N16L1 sample. Longer sample shows lower yield strength and maximum strength than shorter sample because longer ones tend to buckle at early stage, and lateral buckling occurs easily before local buckling. For 2 ft long slotted liner samples, N8L2 pattern also shows higher strength than N16L1 pattern.

In figures 62-65, similar trend remains for 2 3/8” P110, 2 7/8” J55, 2 7/8” light L80, 3 ½” L80. Only exception is 2 7/8” heavy L80. In figure 64, for 2 7/8” heavy L80, N8L2 pattern shows slightly lower strength than N16L1 pattern. This can be explained by due to the thicker wall, it is harder for N16L1 to find a weak level to expand like other pipes. The thick wall can help pipe maintain its original strength. So it is always important to consider the wall thickness and the ratio of diameter over wall thickness.

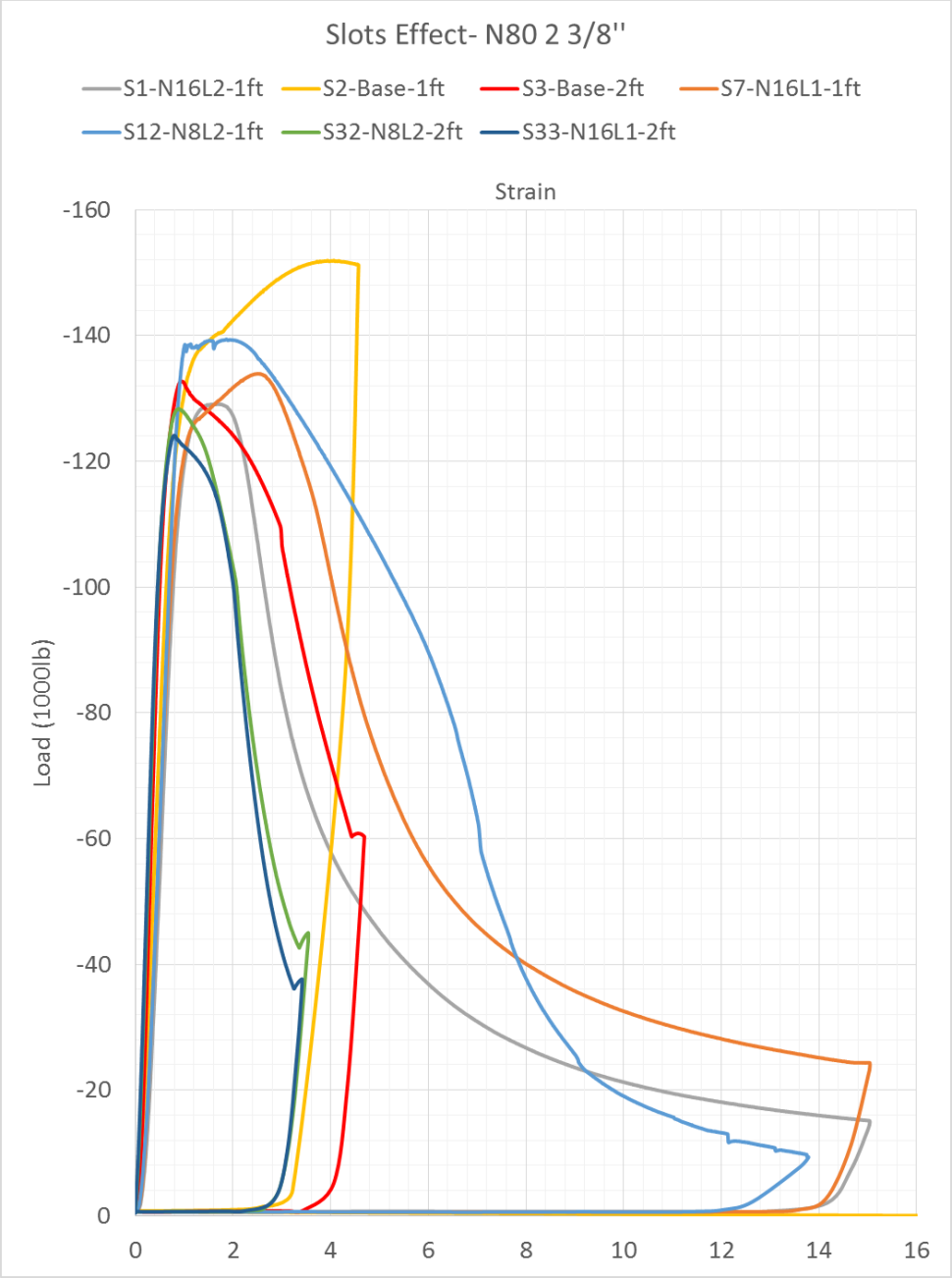

Figure 61 Slot pattern effect on 2 3/8" N80 slotted liners

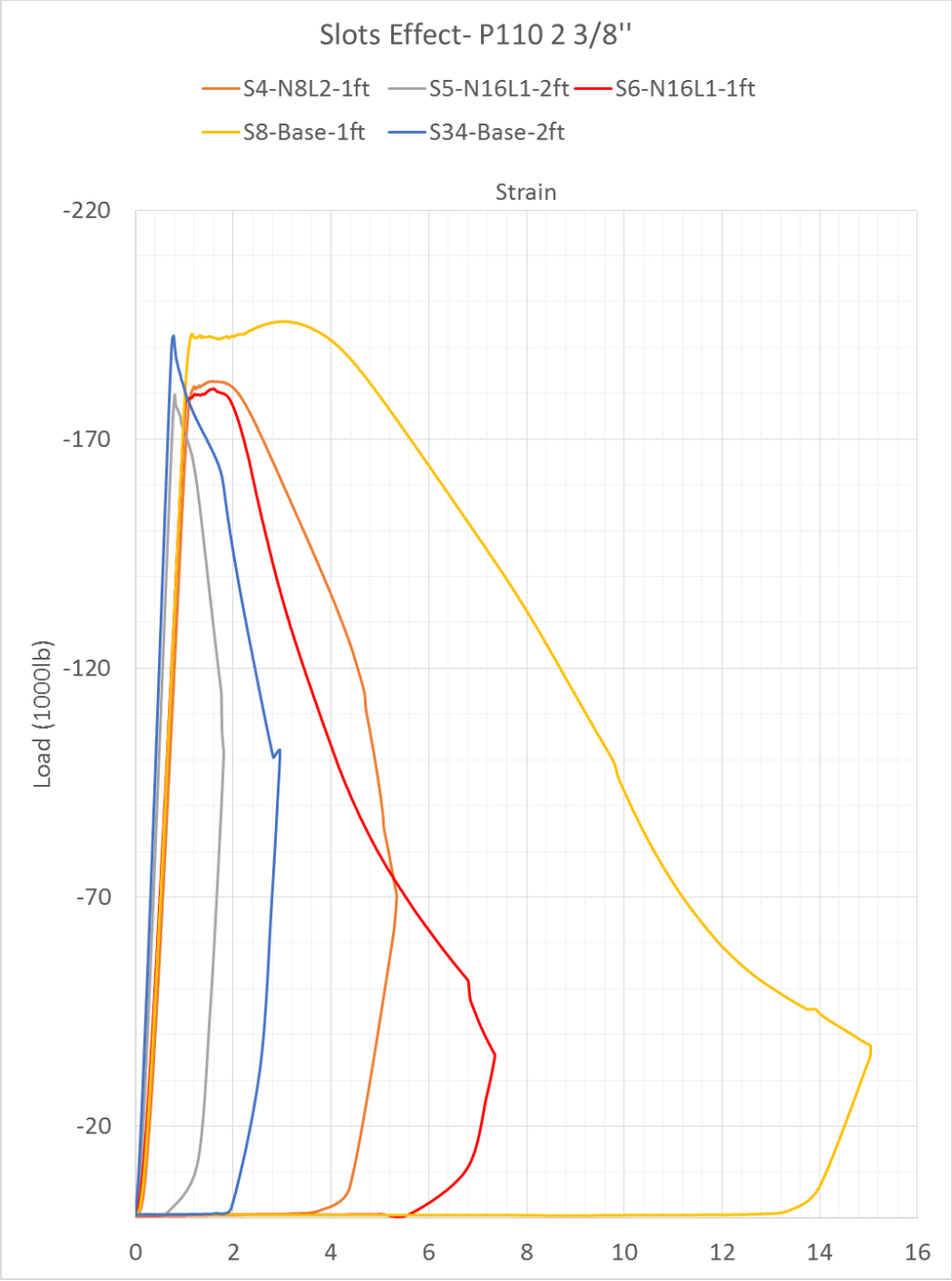

Figure 62 Slot pattern effect on 2 3/8" P110 slotted liners

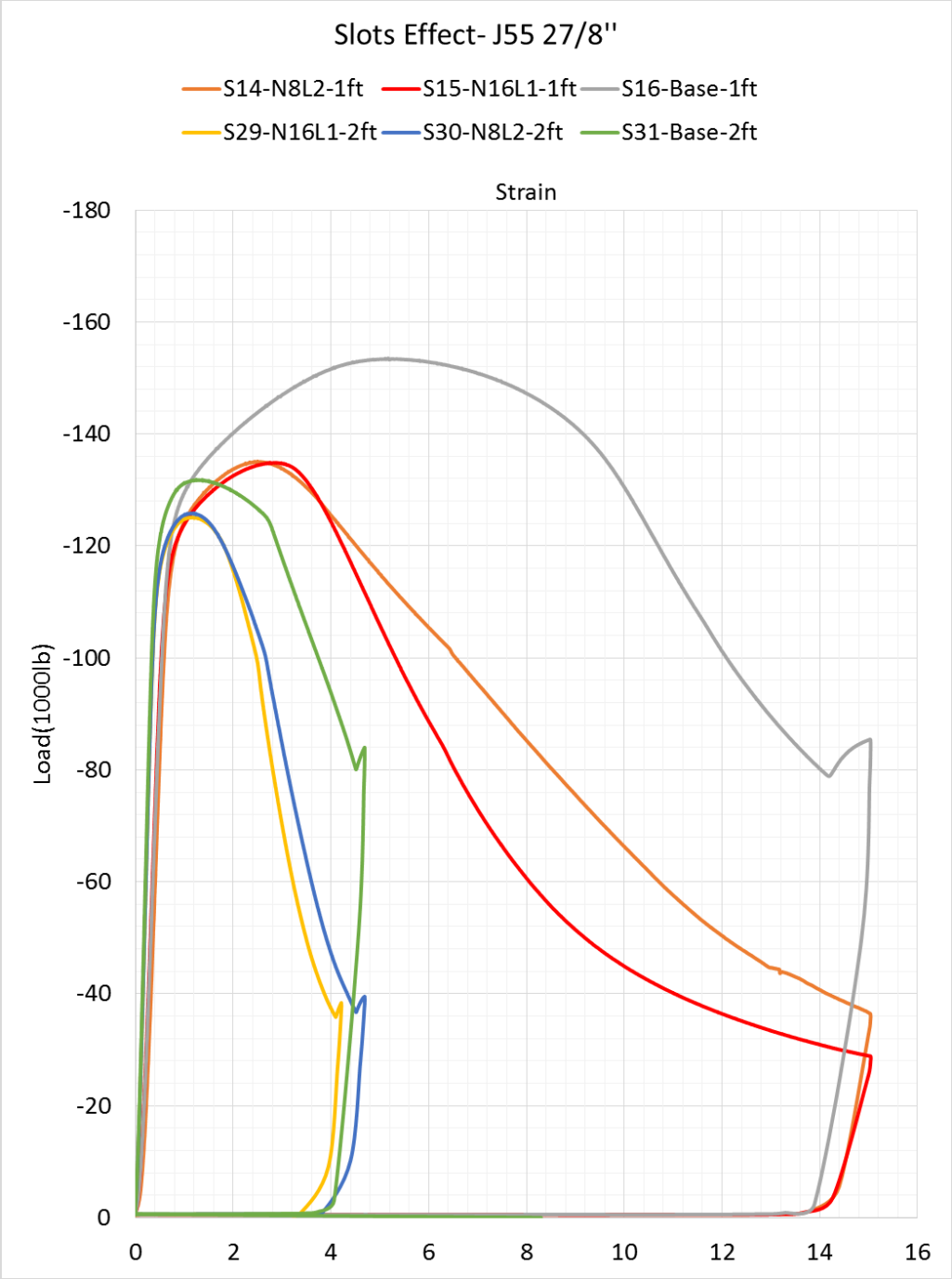

Figure 63 Slot pattern effect on 2 7/8" J55 slotted liners

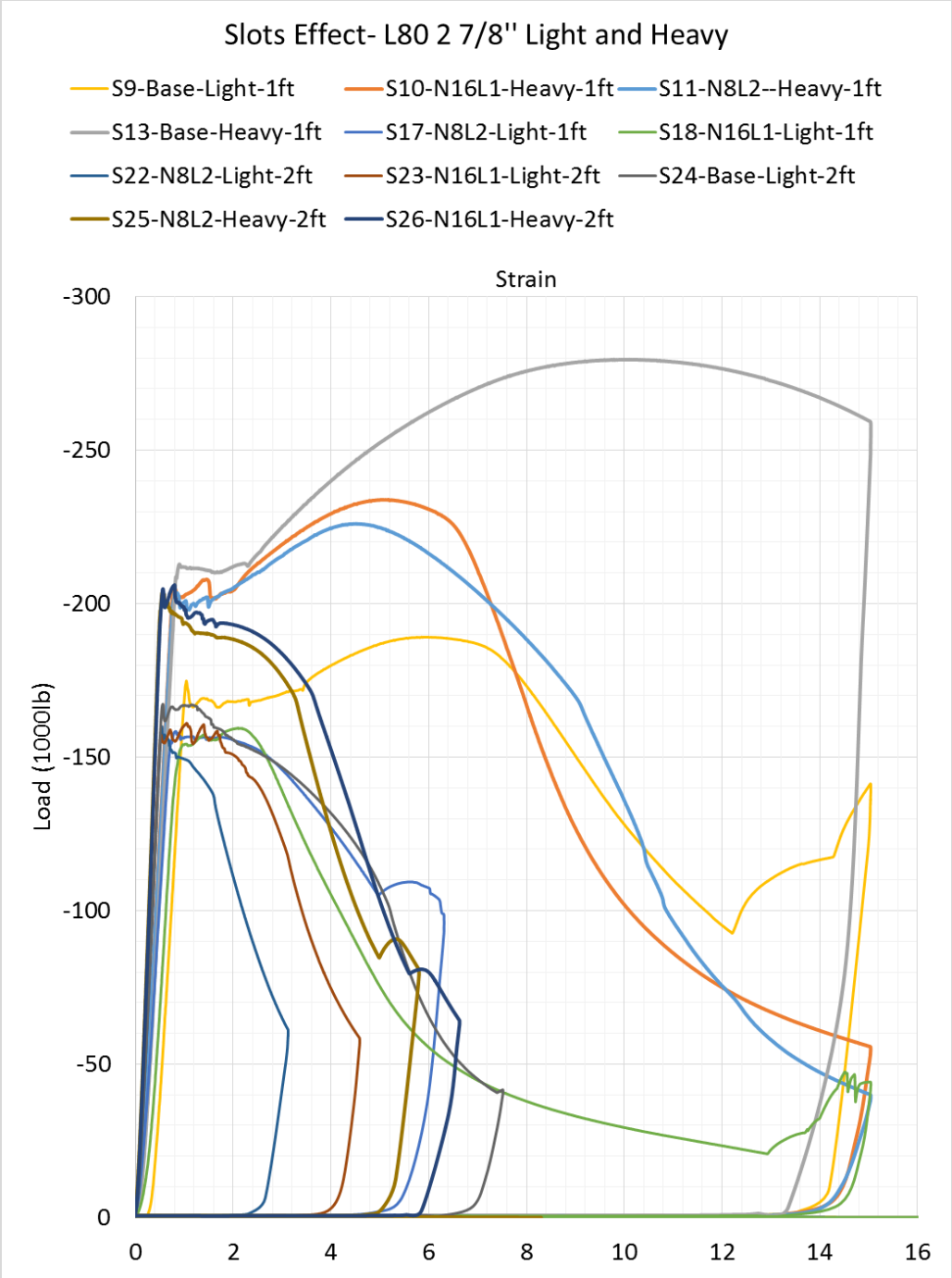

Figure 64 Slot pattern effect on 2 7/8" L80 (both light and heavy) slotted liners

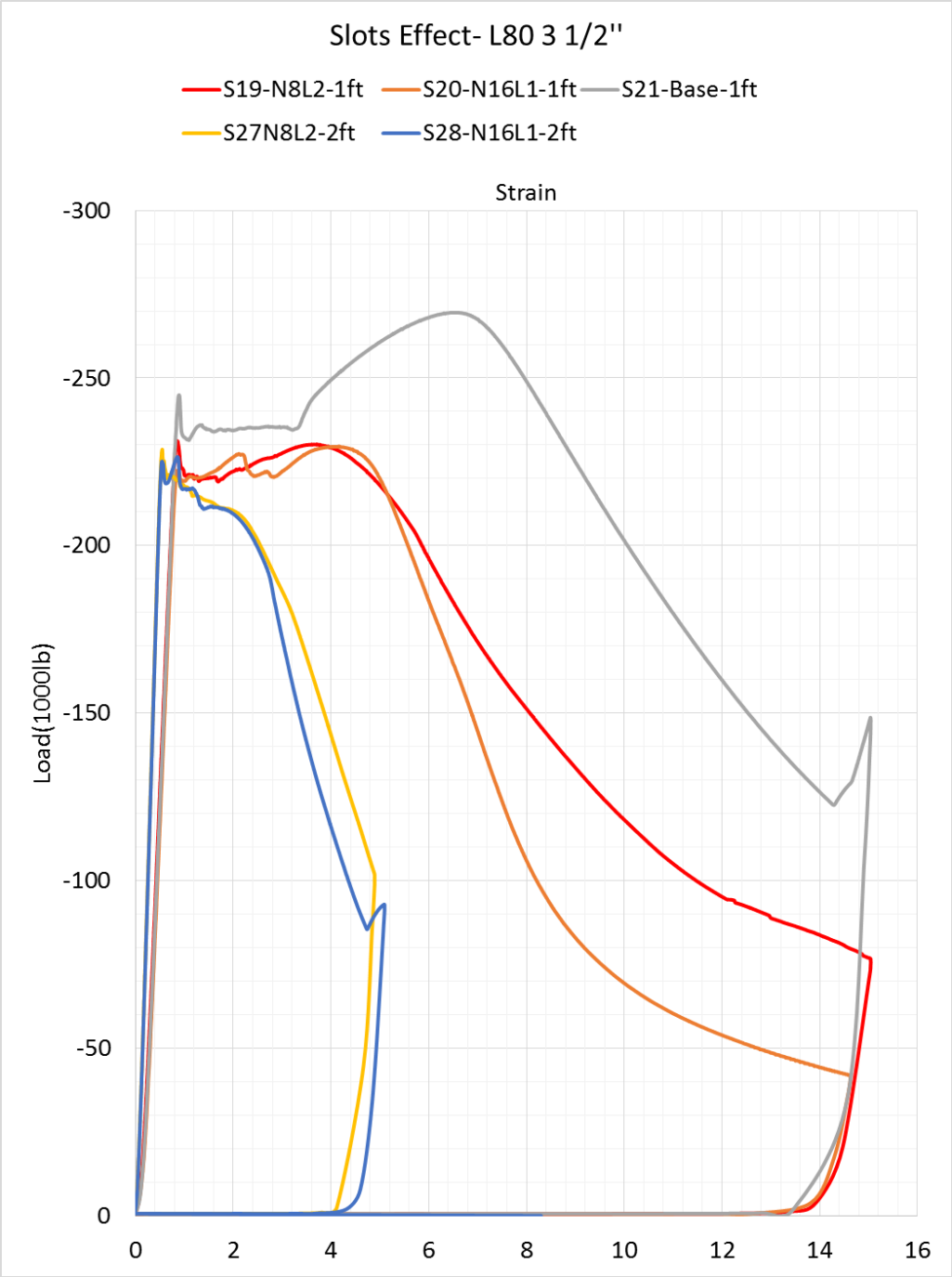

Figure 65 Slot pattern effect on 3 1/2" L80 slotted liners

In summary, we can conclude from axial compression tests:

1. Effect of slots: For all samples, the slotted liners show lower strength than base pipes.
2. Slot design while keeping the same open flow area:
    a) Same material and OD, N8L2 slot design shows stronger properties and higher strain at peak strength.
    b) N16L1 design tends to be weaker and open earlier and wider at the same overall axial strain level.
    c) For N16L1, once it find a weak level of slots, the four slots on the same level will bear from all the load till totally squashed.
3. Keeping the number of slots the same as 16, 2'' slots will reduce the strength by 15% than 1'' slots.
4. Length of pipe: Longer pipe/ slotted liners always have lateral buckling at an early stage. So the max strength and strain at max strength are both lower than shorter samples.
5. Short liners deform uniformly up to peak strength till a local buckling appears.
6. Long liners induce lateral buckling at early stage, but this phenomenon may not occur for casing installed in oil fields due to support from formation.
7. For slotted liners, the grades, the pattern and D/t ratio are the 3 most important factors.
    a) for different grades, L80 3 ½'' is the strongest, L80 2 7/8'' is the second. The point needs to pay attention is, although J55 didn't have very high yield strength, it sustained lots of load even after large deformation.
    b) for different slot pattern, N8L2 design is stronger than N16L1 for most materials except for L80 2 7/8'' heavy.

c) for Diameter/Thickness ratio, while keeping the same D/T = 13.2 for 2 7/8'' J55 and light L80, L80 has higher yield strength and peak strength, but J55 can hold up to 50% more load than light L80.

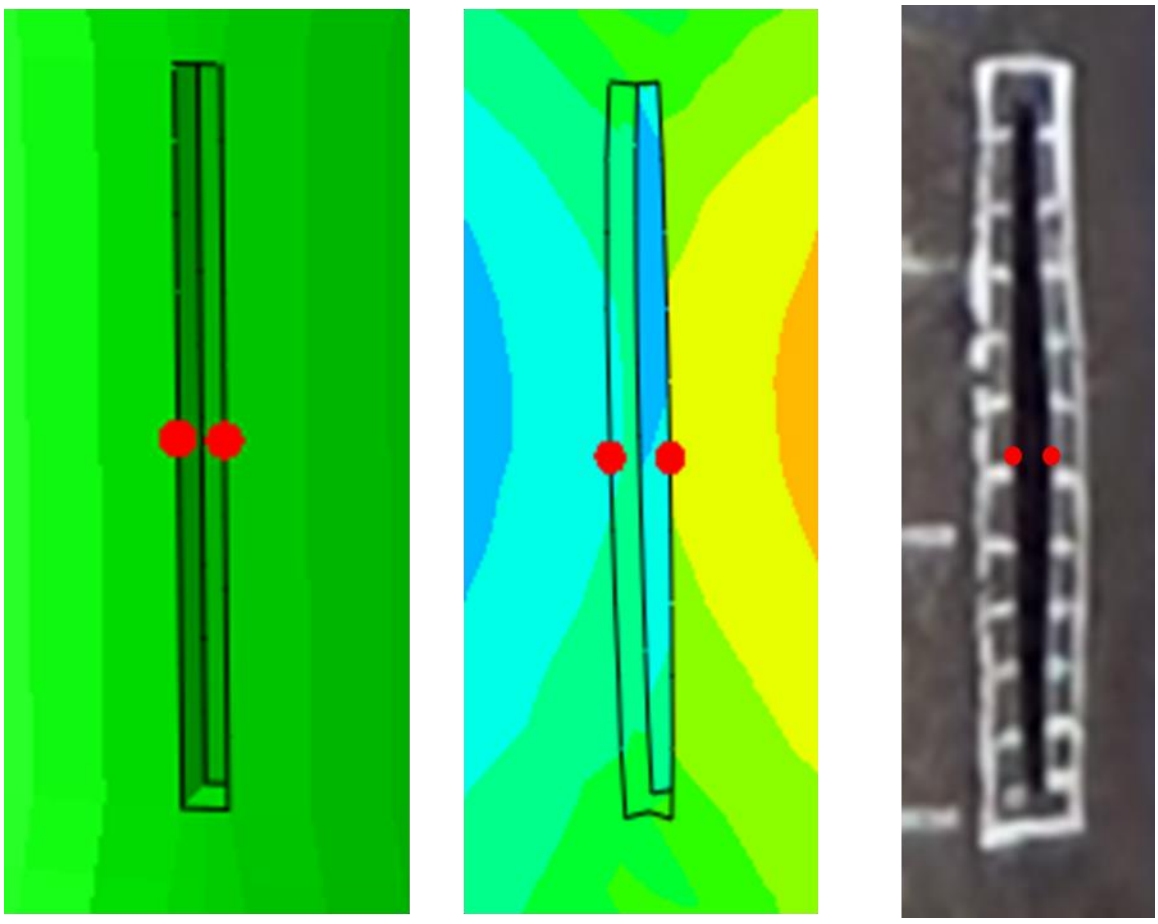

Figure 66 Comparison of slot opening. Left: original slot. Center: Simulation- at 5% axial strain, Deformed Slot under Axial Compression, Right: Experiment- at 5% axial strain

From the simulation, we can see clearly that the slots opened more widely. Especially in the center. According to stress field plot, the ends of slots are taking more stress.

For heavy L80 2 7/8'', slot N8L2 case

$$Slot\ Width\ Expand\ \% = \frac{relative\ displacement}{base\ width} = \frac{0.0146919}{0.125} = 11.75\% \qquad (7)$$

For 2 ⅞’’ heavy L80 N8L2, from experiments, maximum strength occurred at strain= 4.46%. From experiment, the slot width becomes 0.15 inch.

From simulation, at strain=4.46%, the slot width is 0.14. which is 6% error, which is in acceptable range.

Whereas for N16L1, slots tend to open even wider at the same axial strain of 4.46%. Also, because of its denser distribution of slots on one level, the slots tend to open easier once the opening starts to form.

It is obvious that the slot ends have the maximum stress, and the stress becomes smaller when moving away from the ends.

Slotted liner failure reasons:

(1) Usually the liner is bended because of the axial-compression

(2) Radial-compression collapse induced by non-uniform radial loading to liner

3.2 Line Load Collapse Test

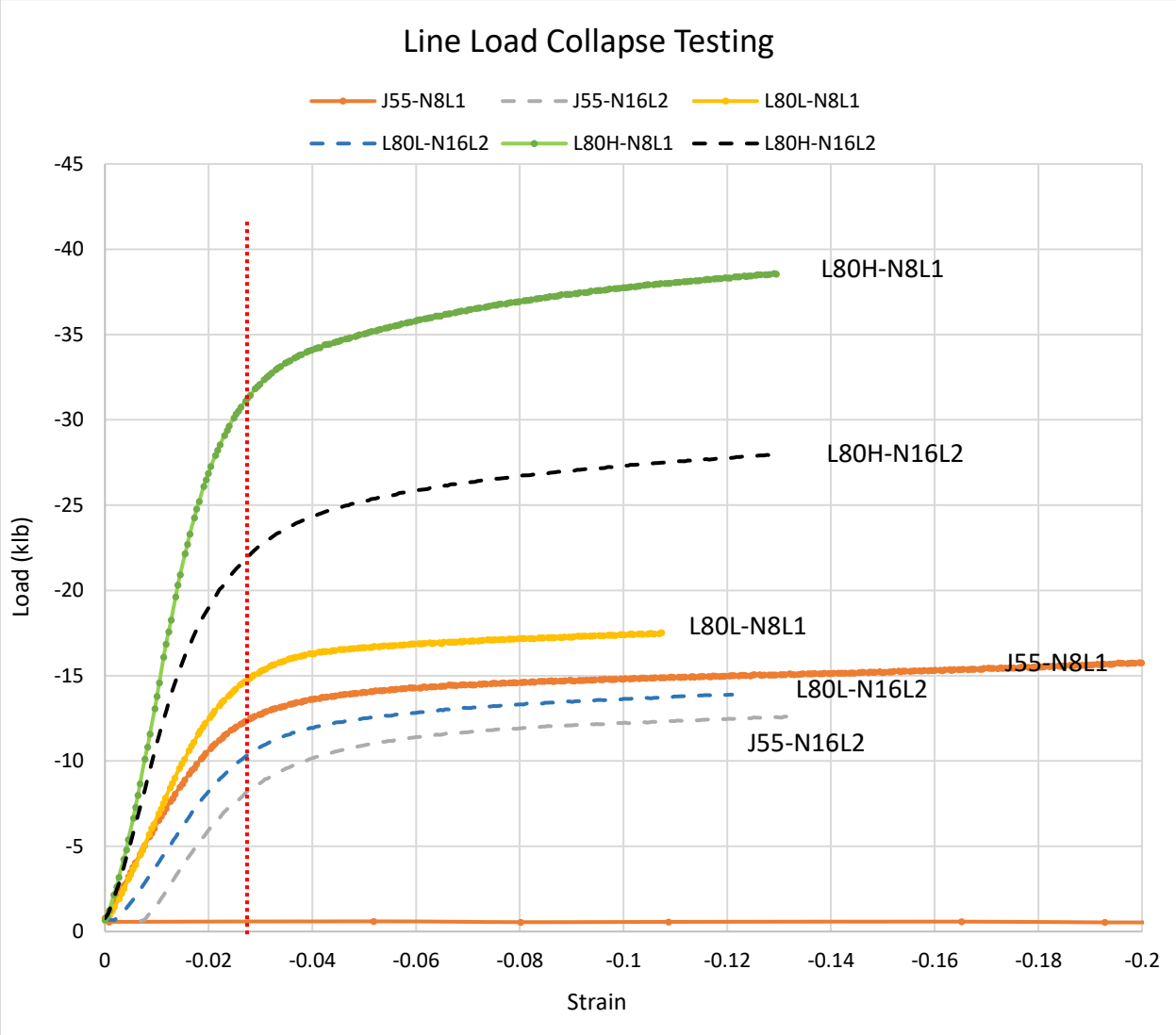

Figure 67 Results of Line Load Collapse Test

From figure 67, we can tell the curves share similar trends. And the curves deviate from linear portion at around 2% strain. The N8L1 samples have higher strength than N16L2 samples without exception. Thick wall L80H-N16L2 has higher strength than thin wall L80L-N8L1, even

though the number of slots is larger and the length is twice, the 2 7/8” thick wall slotted liner can still sustain 9000 lb more load before plastic deformation occurs.

From the experiments, it is true that the slotted liner starts to deform differently in vertical and horizontal directions.

After all, the goal of maintain productivity while having stable structural integrity can be achieved by using N8L2 slot pattern design, and J55 is great candidate for casing grade selection.

4. CONCLUSIONS

1. The work developed a finite element tool to calculate the strength and deformation of slotted liners under axial compression, tension and radial compression loads. Experiments were carried out to compare with simulation results. They showed comparable results and the model was validated.
2. With the same open flow area, N8L2 design is stronger than N16L1 case. The only exception occurs for heavy L80 2 7/8", the wall thickness effect still needs to be investigated.
3. For slotted liners, the grades, the pattern and D/t ratio are the 3 most important factors.
    a) for different grades, L80 3 ½'' is the strongest, L80 2 7/8'' is the second. The point needs to pay attention is, although J55 didn't have very high yield strength, it sustained lots of load even after large deformation.
    b) for different slot pattern, N8L2 design is stronger than N16L1 for most materials except for L80 2 7/8'' heavy.
    c) for Diameter/Thickness ratio, while keeping the same D/T = 13.2 for 2 7/8'' J55 and light L80, L80 has higher yield strength and peak strength, but J55 can hold up to 50% more load than light L80. In this case, for vertical well or part under axial compression, we can choose lower grade material such as J55.
4. Line load collapse tests showed that the slotted liners can sustain relatively large deformation without crack, but the slots will be opened or closed depending on the load direction. So it is important to avoid exceeding 2% strain at which plastic deformation begins to occur.

5. The slot width change is not significant for axial compression test, but collapse has a bigger effect on the slot width. If the slotted liners are collapsed, the hydrocarbon flow will be largely impacted, and the sand control function maybe tremendously reduced. Avoid collapse is important in the field. Higher grade pipes are recommended if the formation is easy to collapse on the vertical direction for horizontal wells.
6. Longer pipe/ slotted liners always have lateral buckling at an early stage. So the max strength and strain at max strength are both lower than shorter samples.

REFERENCES

Chartier, M. A., & Yung, V. Y. B. 2016. Impact of Installation Loads on Thermal Service Performance of Slotted Liners. Society of Petroleum Engineers. doi:10.2118/182529-MS

Furui, K., Fuh, G.-F., & Morita, N. 2012. Casing- and Screen-Failure Analysis in Highly Compacting Sandstone Fields. *SPE Drilling & Completion* **27** (02): 241-252.

George King. 2009. Sand Control Methods. http://gekengineering.com/Downloads/Free_Downloads/Sand_Control_Overview.pdf

Abbassian, F., & Parfitt, S. H. L. 1998. A simple model for collapse and post-collapse behavior of tubulars with application to perforated and slotted liners. *SPE drilling & completion*, **13**(03), 190-196.

Guo, Yonggui, Mark Blanford, Joseph Candella. 2015. Evaluating the Risk of Casing Failure Caused by High-Density Perforation: A 3D Finite-Element-Method Study of Compaction-Induced Casing Deformation in a Deepwater Reservoir, Gulf of Mexico. *SPE Drilling & Completion* **30** (02): 141-151.

Kumar, Avinav, Anil Kumar Srivastava, Ravi Kumar. 2010. Design optimization of slotted liner completions in horizontal wells of mumbai high field. *SPE-133321-MS. SPE Asia Pacific Oil and Gas Conference and Exhibition, 18-20 October, Brisbane, Queensland, Australia*

Liu, Xiaoda, Morita, Nobuo. 2018. 3D Finite Element Analysis and Experimental Study of Stability of Slotted Liners. ARMA- 2018-269. *52nd US Rock Mechanics/Geomechanics Symposium, 17-20 June 2018*. Seattle, WA.

Liu, Xiaoda, Morita, Nobuo. 2018. Collapse and Bending Analysis of Slotted Liners by 3D FEM under Various Reservoir Conditions. SPE-191441-MS. 2018 SPE Annual Technical Conference and Exhibition (ATCE). Dallas, TX.

Morita, Nobuo. 2014. Elastic-Plastic Behavior and Limit Load Analysis of Casings. *SPE-170524-MS. IADC/SPE Asia Pacific Drilling Technology Conference, 25-27 August, Bangkok, Thailand*

Morita, Nobuo, Sogo Shiozawa. 2014. Stability Analysis of Casings during Plastic Deformation. *SPE-170303-MS. SPE Deepwater Drilling and Completions Conference, 10-11 September, Galveston, Texas, USA*

Michael F. Morea. 1997. Advanced Reservoir Characterization in the Antelope Shale to Establish the Viability of C02 Enhanced Oil Recovery in California's Monterey Formation Siliceous Shales. *Chevron*. https://www.osti.gov/scitech/servlets/purl/1474

Placido, Joao Carlos Ribeiro, Ilson P Pasqualino, Carlos Eduardo Fonseca. 2005. Strength analyses of liners for horizontal wells. Society of Petroleum Engineers. *SPE-96870-MS. SPE Annual Technical Conference and Exhibition, 9-12 October, Dallas, Texas*

Spivak, D., & Horne, R. N. 1983. Unsteady-State Pressure Response Due to Production With a Slotted Liner Completion. *Journal of Petroleum Technology* **35** (07): 1366-1372.

Xie, J. 2015. Slotted Liner Design Optimization for Sand Control in SAGD Wells. *SPE-178457-MS. SPE Thermal Well Integrity and Design Symposium, 23-25 November, Banff, Alberta, Canada*